2018

Reliable and Efficient Transmission in Wireless Body Area Networks

Hongyun Zhang
University of Wollongong

UNIVERSITY
OF WOLLONGONG
AUSTRALIA

Reliable and Efficient Transmission in Wireless Body Area Networks

Hongyun Zhang

This thesis is presented as required for the conferral of the degree:

Doctor of Philosophy

Supervisor:
Prof. Farzad Safaei

Co-supervisor:
Dr. Le Chung Tran

The University of Wollongong
School of Electrical, Computer and Telecommunications Engineering

March, 2018

Declaration

I, *Hongyun Zhang*, declare that this thesis is submitted in fulfilment of the requirements for the conferral of the degree *Doctor of Philosophy*, from the University of Wollongong, is wholly my own work unless otherwise referenced or acknowledged. This document has not been submitted for qualifications at any other academic institution.

Hongyun Zhang

July 10, 2018

Abstract

As one of the most practical and promising technologies, Wireless Boby Area Networks (WBANs) play a vital role in a variety of application areas, including ubiquitous healthcare, medical, sport, and entertainment. Meanwhile, the multiple application scenarios also result in stringent and various Quality of Service (QoS) requirements in terms of data rate, reliability, energy consumption, delay, etc. Besides, due to the complicated deployment environments and peculiar channel characteristics, the design of WBAN systems is more challenging than other Wireless Sensor Networks (WSNs). Among many transmission challenges in the context of WBANs, transmission reliability and energy efficiency are the two key challenges. This thesis focuses on investigating high transmission reliability and energy-efficient transmission schemes for WBAN systems.

In order to capture the channel information variation in the real dynamic WBAN scenarios, we build a wearable wireless transceiver from easily-assembled commercial hardware modules. The measurements are conducted by test subjects wearing multiple wireless transceivers in dynamic scenarios. This thesis mainly focuses on two typical dynamic scenarios: walking and daily scenarios. Based on the channel gain datasets collected from these two scenarios, we analyze the on-body channel characteristics, including body shadowing effect, cross-correlation, autocorrelation, and transmission outage. Moreover, to improve the authenticity of our evaluation works, these channel datasets are imported into our simulation model to represent the channel variation.

Motivated by the significant cross-correlation feature of on-body channels in the walking scenarios, we propose a novel cooperation-based Network Coding (NC) scheme, namely A3NC. In A3NC, we explore the combination of the Aggregative Allocation (AA) mechanism in the MAC (Medium Access Control) layer and the Analog Network Coding (ANC) technique in the physical (PHY) layer. By comprehensive theoretical analyses and comparisons from the perspectives of data rate, energy efficiency, and throughput balance, we explore the upper bounds of A3NC in terms of data rate and energy efficiency. Simulation results confirm that A3NC achieves a better performance in terms of data rate, energy efficiency, and throughput balance, compared to the conventional approaches.

Extending from monotone walking scenarios to daily scenarios with mixed activities, we explore the Dynamic Slot Scheduling (DSS) method to improve the transmission reliability. DSS method optimizes the duration or order of time slots of different sensor

nodes. This method does not require extra hardware or software overhead on the sensor side. Motivated by the significant temporal autocorrelation of on-body channels within a time span of 500 ms, we propose a new DSS method, named DSS-TA, which applies a Temporal Autocorrelation Model (TAM) to predict the channel condition for future time slots. The performance evaluation results confirm the great potential of DSS methods (up to 52% reduction of packet loss ratio over the static scheduling method) in daily WBAN scenarios. Further, compared to the classical Markov model-based DSS methods, the newly proposed method is more effective in the prediction of channel conditions and hence achieves a better performance in terms of Packet Loss Ratio (PLR).

Lastly, we jointly consider Transmission Power Control (TPC), DSS and two-hop Cooperative Communication (CC) mechanism to achieve a better trade-off between transmission reliability and energy consumption. Motivated by the significant autocorrelation characteristic of on-body channels in the daily WBAN scenarios, we propose an autocorrelation-based adaptive transmission (AAT) scheme which uses a TAM to predict channel conditions. Then, the estimated channel conditions are used to optimize the transmission power level and the transmission order of all sensor nodes for the next superframe. Simulation results demonstrate that the proposed method can effectively reduce the PLR and increase the energy efficiency. Moreover, we also discuss the effectiveness of NC technology for two-hop transmissions. Two types of cooperative mechanisms are compared, namely the non-NC mechanism we proposed for AAT and the NC cooperative mechanism.

Acknowledgments

First of all, I would like to express my most sincere gratitude to my supervisors, Prof. Farzad Safaei and Dr. Le Chung Tran for their constant guidance, patience, and encouragement. I have learned to not only knowledge and skills, but also principles of conduct either as a researcher or person and the attitude to confront difficulties, which will help me throughout my entire career and life. It is my pleasure to be their student and it was wonderful working with them during the last three and a half years.

I am thankful to my friends and colleagues I have met here, Fuchun Guo, Rongmao Chen, Jianjia Zhang, Yan Zhao, Hao Zhang, Ke Lin, Linping Chan, Pei Tai, Zewei Ding, Pengyu Huo, Neng Zhang, Jin Cui, Tairan Huang, etc. at UOW. I am fortunate to meet them during my Ph.D. life in Wollongong. Many thanks for their support and kindness.

It is an honor for me to study in the School of Electrical, Computer and Telecommunications Engineering, University of Wollongong. I sincerely thank all the staff in the university for their kindness and valued assistance. I also take this opportunity to thank the China Scholarship Council (CSC) and the University of Wollongong for their financial support to my study.

Last but not least, I would like to express my warmest thanks and love to my family back home. It is never easy to study while being apart from family, but their love and support have always inspired me to go beyond what I could imagine. And I want to thank my girlfriend Miao Wang, who is so supportive of my work and choice. I am so lucky to meet such an amazing girl. Words cannot express my gratitude to her, I could never have reached this point without her.

List of Notations

The following notations are used throughout this thesis. Some special notations will be defined when they are first used.

x	Scalar symbol (lowercase letter);
$\bar{G}$	Average or mean value;
$\mathbf{K}$	Vector (bold-uppercase letter);
$a_{i,j}$	i-th row and j-th column component of a matrix;

List of Abbreviations

The following abbreviations are used throughout this thesis. Some special abbreviations will be defined when they are first used.

AA	Aggregative Allocation;
Ack	Acknowledgment;
ADC	Adaptive Duty Cycle;
ANC	Analog Network Coding;
B-Ack	Block Acknowledgment;
BAN	Body Area Network;
BER	Bit Error Ratio;
BO	Beacon Order;
CAP	Contention Access Phase;
CC	Cooperative Communication;
cf.	confer;
CSMA/CA	Carrier Sense Multiple Access with Collision Avoidance;
DC	Duty Cycling;
DNC	Digital Network Coding;
DSS	Dynamic Slot Scheduling;
DTP	Direct Transmission Phase;
e.g.	exempli gratia;
EAP	Exclusive Access Phases;
ECG	Electrocardiography;
EEG	Electroencephalography;
etc.	et cetera;
FEC	Forward Error Correction;
FM-UWB	Frequency Modulated Ultra-Wide Band;
G-Ack	Group Acknowledgment;
HBC	Human Body Communication;
i.e.	id est;
I-Ack	Immediate Acknowledgment;
IEEE	Institute of Electrical and Electronics Engineers;

IR-UWB	Impulse Radio Ultra-Wide Band;
ISI	Inter-Symbol Interference (ISI);
ISM	Industrial, Scientific and Medical;
L-Ack	Block Acknowledgment Later;
LQI	Link Quality Indication;
MAC	Medium Access Control;
MAP	Managed Access Phases;
N-Ack	No Acknowledgment;
NB	Narrow Band;
NC	Network Coding;
NID	Node Identifier;
OP	Opportunistic Scheduling;
PCB	Printed Circuit Board;
PDR	Packet Delivery Ratio;
PID	Pair Identifier;
PLR	Packet Loss Ratio;
PPCC	Pearson Product-moment Correlation Coefficient;
PSDU	Physical Layer Service Data Unit;
pSIFS	Short Interframe Separation Time;
QoS	Quality of Service;
RAP	Random Access Phases;
RLNC	Random Linear Network Coding;
RSSI	Received Signal Strength Indicator;
RTP	Relay Transmission Phase;
SAR	Specific Absorption Rate;
SDI	Scheduled Downlink Interval;
SNR	Signal-to-Noise Ratio;
SO	Superframe Order;
SRI	Scheduled Relay Interval;
SUI	Scheduled Uplink Interval;
TAM	Temporal Autocorrelation Model;
TDMA	Time-Division Multiple Access;
TPC	Transmission Power Control;
UWB	Ultra-Wide Band;
VSA	Vector Signal Analyzer;
WBAN	Wireless Body Area Network;
WSN	Wireless Sensor Network;
WSS	Wide Sense Stationary;
XOR	eXclusive-OR;

Contents

List of Figures

List of Tables

Chapter 1

Introduction

1.1 Background and Objectives

As one of the most promising technologies for the next generation of wireless personal networks, Wireless Body Area Network (WBAN) has been one of the hottest research topics in wireless communication. WBAN is composed of bio-medical sensor nodes that can be worn on or placed in the human body to measure certain physiological parameters of the human body [1]. The applications of WBANs span a wide area, such as remote medical system, ubiquitous healthcare, sport, fitness, entertainment, and military. Meanwhile, the variety of application areas also requires an excellent support of Quality of Service (QoS) in terms of data rate, reliability, energy consumption, delay, etc. Besides, due to the complicated deployment environments and peculiar channel characteristics, ensuring the transmission reliability in the context of WBAN systems seems to be more challenging than other Wireless Sensor Networks (WSNs). Moreover, limited by the size of battery and Specific Absorption Rate (SAR), the power consumption and transmission power are stringently restricted. All these factors lead to many transmission challenges, including transmission reliability and energy efficiency.

Many research works (including our first conference paper [2] and the works of IEEE 802.15.6 working group [3]) focused on modeling the WBAN channel by providing an analytical formula. However, due to the complexity of environment and the existence of human body, it may not be possible or accurate to use mathematical models to characterize WBAN channels, especially in dynamic WBAN scenarios that are the focus of this thesis. Accordingly, the WBAN channel characterization and modeling work are important to support the reseach work with high feasibility. Besides, considering the dynamic feature of wireless channels in WBANs and the heterogeneous QoS requirement of various applications, the conventional static design for the transmission system is suboptimal. In recent years, many adaptive transmission schemes have been proposed to meet the transmission challenges in WBANs. These adaptive methods optimize key transmission

parameters, e.g., transmission power level, duty cycle, slot scheduling, in accordance with the real-time channel state or application requirement. Besides, as a promising technology which makes use of the intrinsic broadcast nature of wireless networks, Network Coding (NC) [2] technology also attracts much attention. NC technology enables nodes to code or mix packets (or symbols) before forwarding. In recent years, many NC methods have been proposed for WBAN systems. However, the applications of NC in WBANs are still an emerging area and most existing works consider the expansions of conventional NC schemes designed for general WSNs, which may not be optimized for the unique challenges and specific characteristics of WBANs.

Aiming at meeting the transmission reliability and energy efficiency challenges in the context of WBANs, the primary research objectives are listed as follows.

• In order to collect on-body channel data in real dynamic WBAN scenarios, we aim to design and deploy portable wireless transceivers on human body to collect on-body channel data. Based on these real datasets collected from experiments, we investigate the characteristics of on-body channels.

• By considering multiple dynamic transmission method (including transmission power control, dynamic slot scheduling and two-hop cooperation communication), we aim to explore the adaptive transmission mechanisms for dynamic WBAN scenarios to achieve a better trade-off between transmission reliability and energy efficiency.

• Investigate the application of network coding technology and relay cooperation in dynamic WBAN scenarios.

• Based on the channel datasets and existing discrete event simulation system, we aim to design and implement better performance evaluation platform, which could be used to evaluate newly proposed schemes or methods.

1.2 Research Approaches

The research approaches of this thesis are summarized in Figure 1.1. As shown in Figure 1.1, this research begins with the literature reviews of the area of interests, including WBAN, IEEE 802.15.6, on-body channel characteristics, adaptive transmission designs and applications of NC in WBANs. As a result, the main open research problems and research objectives are identified.

Meanwhile, to investigate the characteristics of on-body channels in the real dynamic WBAN scenarios, we construct a self-contained wireless transceiver from easily-assembled and widely available commercial hardware modules. Numerous measurements are carried out in two typical dynamic scenarios, i.e., walking scenarios and daily life scenarios. These channel datasets gathered from measurements are utilized to analyze the on-body channel characteristics. Moreover, these channel datasets are imported into our simulation model to represent the channel variation to improve the authenticity of the performance evaluation

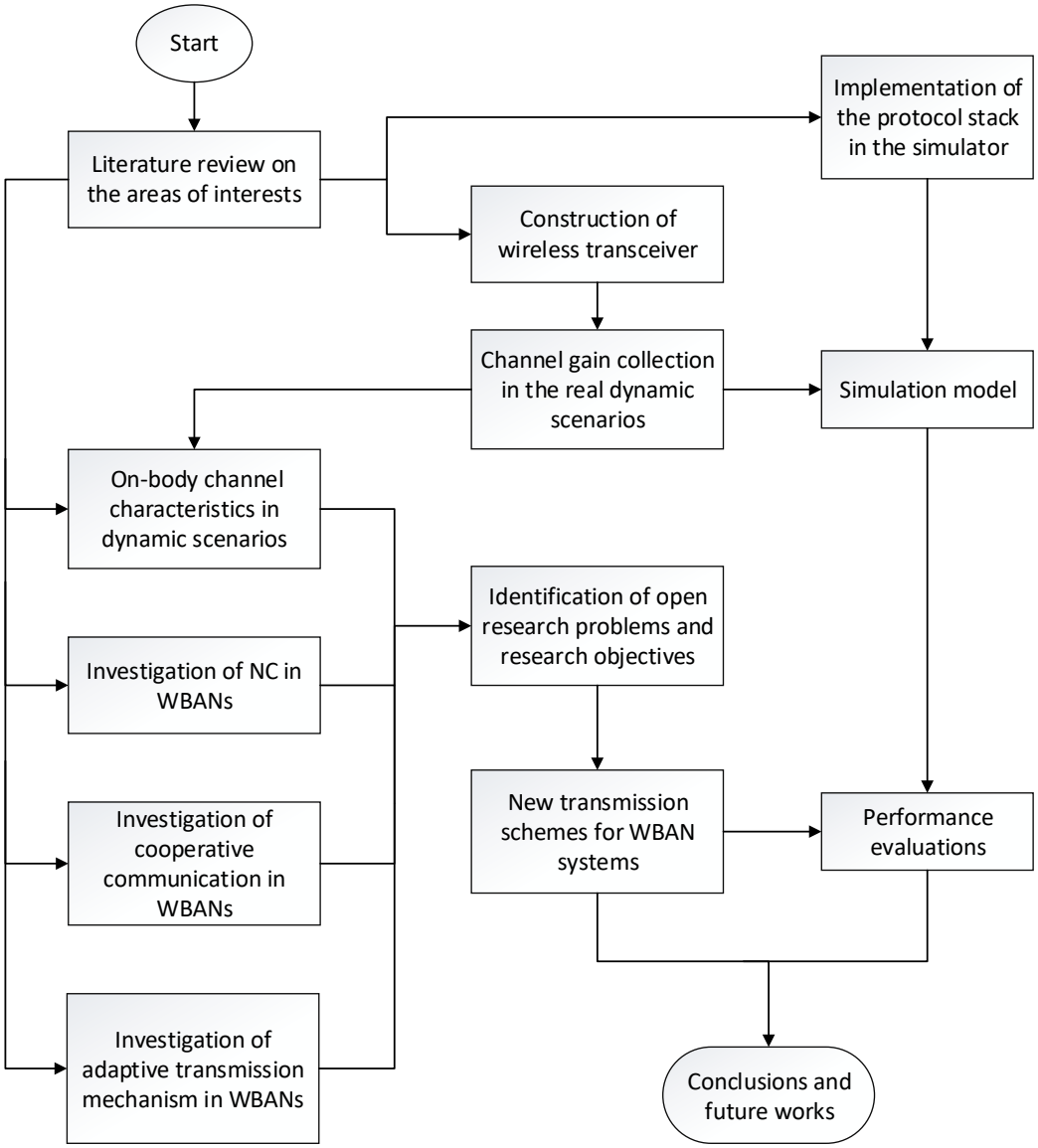

Figure 1.1: Research approaches.

works.

The lower half part of Figure 1.1 illustrates the design procedures of new transmission schemes and the method of performance evaluations. Motivated by both the literature review over the related research topics and the analysis results based on real channel datasets, we design three transmission schemes for either walking or daily activities scenarios. Then, the performances of the new schemes are evaluated on the performance evaluation platform which combines real channel datasets and the protocol stack.

1.3 Outline of the Thesis

This thesis consists of seven chapters which are outlined as follows:

In Chapter 1, we first introduce the research background and the objectives of this thesis. Then the research approaches are illustrated, followed by the outline and key contributions of the thesis.

In Chapter 2, the background knowledge relevant to the research topics is discussed, including WBAN systems, IEEE 802.15.6 standard protocol, on-body channel characteristics, adaptive transmission design and applications of NC in WBANs. This background knowledge is essential to understand the state of art and the issues related to this thesis.

In Chapter 3, a customized wireless transceiver is constructed. By deploying multiple portable transceivers on human body in walking and daily scenarios, we collect the original on-body channel datasets. Based on these datasets, on-body channel characteristics are investigated, including body shadowing effect, cross-correlation, autocorrelation, and transmission outage.

In Chapter 4, motivated by the significant cross-correlation of on-body channels in walking scenarios, we propose a novel cross-layer scheme A3NC, which explores the combination of the Aggregative Allocation (AA) mechanism in the MAC layer and the Analog Network Coding (ANC) technique in the PHY layer. Besides the performance evaluation based on the simulation model, we also provide comprehensive theoretical analyses from the perspectives of upload data rate, energy efficiency, and throughput balance.

In Chapter 5, the Dynamic Slot Scheduling (DSS) mechanism in the dynamic daily life scenarios is investigated. Considering the significant temporal autocorrelation, we propose a new DSS method, which applies a temporal autocorrelation model to predict the channel quality for future time slots. In addition, we discuss the throughput fairness problem of the DSS mechanism in the WBAN daily scenarios.

In Chapter 6, we jointly consider transmission power control, dynamic slot scheduling and two-hop cooperative mechanism to design a practical adaptive transmission protocol for WBAN systems. Besides, we provide the performance evaluation when NC technology is used in the two-hop cooperative transmission.

In Chapter 7, the conclusions of this thesis are presented, and possible future works are discussed.

1.4 Contributions of the Thesis

The main contributions of this thesis are summarized as follows.

1. A customized portable wireless transceiver is built and utilized to collect the original WBAN channel data in dynamic scenarios. We analyze the channel characteristics based on these channel datasets. This channel characterization not only facilitates the design of more optimal transmission schemes but also improves the authenticity of our performance evaluation works.

2. Development of a novel cooperation-based network coding scheme, namely A3NC, for walking scenarios, which explores the combination of the AA mechanism and the ANC technique. The mathematical model and performance evaluation results confirm that A3NC achieves a better performance in terms of data rate, energy efficiency, and throughput balance.

3. Development of a novel DSS mechanism for daily scenarios with mixed activities. A temporal autocorrelation model is utilized to optimize the slot scheduling. The new method jointly takes the latest and historical channel conditions into consideration, achieving a more accurate prediction of channel conditions. Simulation results show that, compared to conventional DSS methods, the new method provides a much better transmission reliability.

4. Development of an adaptive transmission scheme which jointly optimizes the transmission power control and slot scheduling to achieve a better performance in terms of packet loss ratio and energy efficiency. Besides, we provide the performance evaluation when NC technology is used in the two-hop cooperative transmission for the practical WBAN systems.

1.5 Publications

This thesis is based on the following papers, which have been published or submitted for publication.

Journal Papers

1. Hongyun Zhang, Farzad Safaei, and Le Chung Tran, "A novel cooperation-based network coding scheme for walking scenarios in WBANs," *Wireless Communications*

and Mobile Computing, vol. 2017, pp. 1-20, Sep. 2017.

2. Hongyun Zhang, Farzad Safaei, and Le Chung Tran, "Channel autocorrelation based dynamic slot scheduling for body area networks," *under review in EURASIP Journal on Wireless Communications and Networking*, 2018.

Conference Papers

1. Hongyun Zhang, Farzad Safaei, and Le Chung Tran, "Joint analog network coding and channel allocation in the walking scenario for WBAN," *in Proc. IEEE Symposium on Computers and Communication (ISCC)*, pp. 604-609, Jun. 2016.

2. Hongyun Zhang, Farzad Safaei, and Le Chung Tran, "Measurement-based characterizations of on-body channel in the human walking scenario," *in Proc. IEEE Vehicular Technology Conference (VTC Spring)*, pp. 1-5, Jun. 2017.

3. Hongyun Zhang, Farzad Safaei, and Le Chung Tran, "Autocorrelation Based transmission power control in WBANs", *Accepted by IEEE International Symposium on Medical Information and Communication Technology*, 2018

Chapter 2

Literature Review

In this chapter, the basic understanding of background information is provided to make this thesis self-contained. Specifically, Section 2.1 reviews the concept of WBAN, including the applications, communication architecture, and challenges. Section 2.2 overviews the IEEE 805.15.6 standard protocol, especially the detail in the MAC sublayer. Then, we review the key adaptive transmission methods in the context of WBANs in Section 2.3. The research works incorporating network coding into WBANs are reviewed in Section 2.4. Lastly, Section 2.5 provides a brief summary of this chapter.

2.1 Wireless Body Area Networks

2.1.1 Overview

With the developments and technological advancements in Micro-Electro-Mechanical Systems (MEMS) technology and integrated circuits, an increasing number of applications are beginning to benefit from the WBANs technology [3]. As defined by IEEE (Institute of Electrical and Electronics Engineers), WBANs are networks of low power devices operating in or around the human body to serve a variety of applications including medical, consumer electronics, personal entertainment and others [4].

Initially, WBAN technology was mainly driven by the need for more efficient and real-time health monitoring systems due to the aging society and the rapid increasing of healthcare expenditure. Whereas, with the promise of being cost-effective and unobtrusive and facilitating continuous monitoring, the applications of WBANs span a wide area. Figure 2.1 shows a series of key applications which will benefit from the introduction of WBANs.

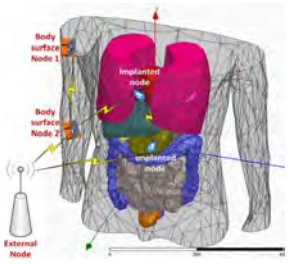

(a) Medical & Healthcare

(b) Sports & Fitness

(c) Lifestyle & Entertainment

(d) Military & Profession

Figure 2.1: Key applications of WBAN.

2.1.2 Architecture

Generally, the communication architecture of WBANs can be divided into three tiers as follows [3], [5], [6]:

• **Tier-1:** Intra-WBAN communication is the communication between the sensors (or actuators) and the hub in a space of 2 to 5 meters surrounding the human body.

• **Tier-2:** Inter-WBAN communication is between the hub and one or more access points. This communication interconnects the WBAN with several networks to facilitate the transmission of data to the user.

• **Tier-3:** Beyond-WBAN communication is the connection between Tier-2 and the remote server via the internet. The function of the remote server depends on what application scenarios the system is designed for. For example, in a medical or healthcare application, a database is one of the most important components of Tier-3.

Figure 2.2 illustrates these communication tiers of WBANs. Because the human body affects the radio wave propagation, radio channels in Tier-1 exhibit the most unique and peculiar feature in comparison with other WSN systems. Accordingly, Tier-1 is considered as the most challenging component in a WBAN system. This thesis focuses on this tier, and in the following chapters, the term "WBAN" refers to the Tier-1 component if not specified otherwise. The node in Tier-1 is defined as an independent device that is deployed on/in/around the human body. Based on the functionality, these nodes can be classified as follows:

1. **Hub:** It is also called coordinator, personal device or aggregator in some other research works. In this thesis, we use the term "hub", which is also the one used

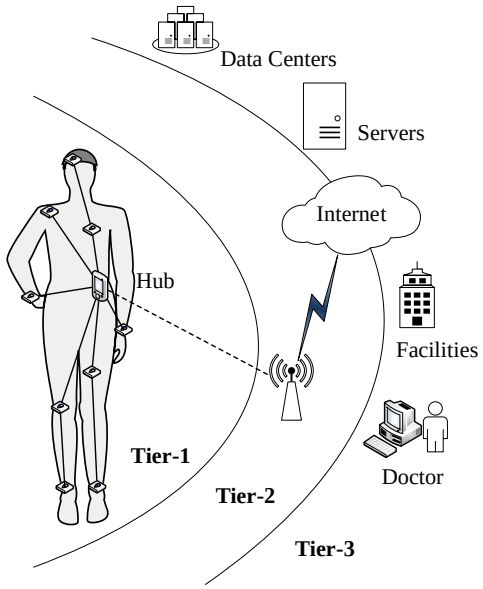

Figure 2.2: The communication architecture of WBAN.

by the IEEE. The hub is in charge of collecting all the information acquired by the sensors and actuators nodes, then handling interaction with other devices, e.g., remote medical center, application serves and cloud database.

2. **Sensor:** Sensor nodes in WBANs measure certain internal and external parameters of the human body and then upload this data to the hub. Specifically, the sensors can be classified into three categories: physiological sensors, biokinetic sensors, and ambient sensors. Physiological sensors are used to measure the physiological sign of the human body, including body temperature, heart rate, blood pressure, blood glucose level, blood oxygen level, Electrocardiography (ECG), and Electroencephalography (EEG). The kinetic indicators resulting from the human movements are measured by biokinetic sensors. At last, the ambient sensors are in charge of the measurement of ambient environmental parameters, such as light, sound and pressure level.

3. **Actuator:** It is the device that acts according to the data received from the sensors nodes or the interaction with the hub. For example, a diabetic may wear an actuator with a reservoir and an integrated pump. The actuator provides the correct dose of insulin to give based on glucose level measurements.

4. **Relay:** The intermediate node that assists the cooperative communication is called a relay node. If the channel from a sensor or actuator node to the hub is experiencing a severe fading, the relay node is essential for the channel. Note that, a relay node may also be a sensor or an actuator node.

2.1.3 Challenges

The development of WBANs is of great importance for healthcare applications, emergency services, sports and consumer entertainment. However, due to the complicated communication environments, the presence of the human body tissue and the peculiarity of WBAN channels, WBANs still face many particular transmission challenges, which are summarized as follows.

• **Transmission Reliability**

On one hand, transmission reliability is vitally important for healthcare or medical WBAN systems. Loss of emergency signal could lead to a fatal consequence. On the other hand, due to the presence of the human body, the wireless channels in WBAN exhibit significant peculiarity in comparison with other WSN channels. There is a large number of factors contributing to the severe signal attenuation (over 100 dB has been observed) of WBAN channels. These factors include diffraction, reflection, energy absorption, antenna losses, shadowing by the body tissue, and body posture [7], [8]. The deep fading effect in WBANs might last from 10 ms to 300 ms [9], [10], which is longer than cellular networks.

Moreover, unlike other longer-range networks where the distance between the transmitter and receiver dominates the signal attenuation, the strength of a WBAN signal is mostly affected by the physical location and orientation of the nodes in relation to each other as well as the human body, which can "shadow" or attenuate the signal [11].

• **Energy Efficiency**

To ensure the comfortable and unobtrusive deployment of wireless devices in/on the human body, WBAN sensor or actuator nodes are required to have a small size, which obviously limits the battery capacity. Meanwhile, in many WBAN applications, changing or replacing of the battery is infeasible. For example, a pacemaker or a glucose monitor would require a lifetime lasting more than 5 years [6]. Generally, the energy consumption of a sensor or actuator can be divided into three domains: sensing or actuating, wireless communication, and data processing, in which the wireless communication is the most power consuming component. Therefore, designing energy-efficient communication protocol is extremely important for reducing the energy usage.

• **Heterogeneous QoS Requirements**

As mentioned before, WBANs enable a wide application area, which also leads to different WBAN systems having totally different QoS (Quality of Service) requirements in terms of data rate, latency, packet loss ratio, etc. For example, the video stream application requires up to 10 Mb/s data rate, while some healthcare applications may only require a guarantee

of 1Kb/s data rate. Providing the heterogeneous QoS support is challenging due to the highly resource-constrained nature of WBAN systems and unreliable wireless links [5].

• **Security**

In WBAN systems, information obtained by sensors is subject to privacy considerations and the action performed by the actuator may be vital for the well-being of the individual. Therefore, the security issues are of a high priority in the context of WBAN. However, constrained by the resource in terms of power, memory, and computational capability, as well as inherent security vulnerabilities, the security specifications proposed for other networks may not be applicable to WBANs.

• **Managing Coexistence**

The coexistence issue in the context of WBANs can be classified into two categories. The first one is the scheduling for a large number of devices in a single WBAN network, and the second type is the interference mitigation with other wireless networks, including Wi-Fi (802.11), Bluetooth and IEEE 802.15.4 networks. The interference becomes more complicated when multiple people wearing WBANs come into the range of each other.

In WBAN systems, transmission reliability and energy efficiency are certainly two of the most important challenges. In fact, boosting the transmission power could significantly increase the Packets Deliver Ratio (PDR), and hence improve the transmission reliability. There is a trade-off between reliability and power consumption for wireless nodes in WBANs, especially for the sensor and actuator nodes. In this thesis, we mainly focus on these two challenges, i.e., transmission reliability and energy efficiency, from the perspective of communication protocols.

2.2 IEEE 802.15.6 WBAN Standard Protocol

To address the above challenges, the IEEE 802.15 Task Group (TG) 6 was set up in 2008 to introduce a new standard for WBANs. Then, in February 2012, the approved version of the IEEE 802.15.6 standard was released [4]. The aim of IEEE 802.15.6 standard is to develop a communication standard for low power devices and operation on, in or around the human body (but not limited to humans) to serve a variety of applications including medical, consumer electronics and personal entertainment.

In fact, there are a number of existing standards that seem to be appropriate for WBANs, such as Bluetooth LE [12] and the IEEE 802.15.4 standard [13]. For some WBAN applications, these existing standards may indeed be suitable, but they are not flexible enough to cover the wide range of WBAN applications, nor can they meet WBANs' tough reliability and energy efficiency requirements [11], [14]–[16]. IEEE 802.15.6 standard

specifies new physical (PHY) layer and Medium Access Control (MAC) layer for WBANs to support flexible, high reliability, low power, lightweight designs of communication protocols.

2.2.1 PHY Layer of IEEE 802.15.6

The PHY layer is responsible for the following tasks: activation and deactivation of the radio transceivers, clear channel assessment within the current channel and data transmission and reception. Specifically, the IEEE 802.15.6 standard defines three different PHY layers, i.e., Human Body Communication (HBC) PHY, Ultra-Wide Band (UWB) PHY and Narrow Band (NB) PHY.

Firstly, the HBC PHY solution uses the human body as a communication medium. This PHY layer employs electrodes in contact with the body for transmitting or receiving the signal through the body by means of electromagnetic coupling. The band frequency of operation is centered at 21 MHz. However, its effectiveness depends on the size of the coil, and the data rate is low.

Secondly, UWB PHY is used for the communication between on-body devices and the communication between on-body and off-body devices, especially for the WBAN application with a high data rate requirement. Based on the operation frequency band, UWB PHY is divided into a low (3.25-4.75 GHz) band and a high (6.6-10.25 GHz) band. Two different types of UWB technologies are included in the IEEE 802.15.6 standard, namely impulse radio UWB (IR-UWB) and frequency modulated UWB (FM-UWB).

Thirdly, NB PHY is designed for the communication of wearable and implantable wireless devices. Multiple possible operation frequency bands are provided to meet various requirements from different applications. As summarized in [4], there are seven available frequency bands for NB PHY. Table 2.1 lists the data rates and the receiver sensitivities corresponding to the seven frequency bands. Note that parameters listed in the table are the lowest requirements for the compliant wireless device when PLR (Packet Loss Ratio) is less than or equal to 10% and the Physical Layer Service Data Unit (PSDU) is of 255 octets in an additive white Gaussian noise environment. An IEEE 802.15.6-compliant device shall be able to support the transmission and reception in at least one of the listed optional frequency bands. Compared to UWB and HBC PHY, NB PHY is better suited to most WBAN applications, not only because of its mature technology, but also the resolvable multipath and the Inter-Symbol Interference (ISI) can be neglected [17], [18]. The works of this thesis are conducted on the basis of the NB PHY technology.

2.2.2 MAC Layer of IEEE 802.15.6

The primary task of MAC layer protocols is to organize the access time to the shared medium between nodes. Unlike the PHY layer, the IEEE 802.15.6 working group only

Table 2.1: Available frequency bands for NB PHY and the corresponding data rates and receiver sensitivities.

Frequency band (MHz)	Data rate (kbps)	Receiver sensitivity (dBm)
402 to 405	79.5	-95
	151.8	-92
	303.6	-89
	455.4	-83
420 to 450	79.5	-90
	151.8	-87
	187.5	-84
863 to 870 902 to 928 950 to 958	101.2	-94
	202.4	-91
	404.8	-87
	607.1	-82
2360 to 2400 2400 to 2483.5	121.4	-92
	242.9	-90
	485.7	-87
	971.4	-83

defines one MAC layer on top of three PHY layers. Therefore, to meet the flexibility requirement of BAN protocols, multiple access modes and various transmission phases are provided in the MAC layer. More specifically, the hub could decide whether to operate through one of the following three access modes:

1. **Beacon mode with beacon periods (superframes)**

   In this access mode, the hub divides the time axis (or medium) into superframes of the same size. By sending beacon packets, the beginning of an active superframe is defined. The hub shall also organize applicable access phases in each active superframe, and the structure of one superframe in this mode is illustrated in Figure 2.3. As depicted in Figure 2.3, a superframe is divided into Exclusive Access Phases (i.e., EAP1 and EAP2), Random Access Phases (i.e., RAP1 and RAP2), Managed Access Phases (MAP) and a Contention Access Phase (CAP). The length of any access phase may be set to zero, but the RAP1 shall not be ended before the guaranteed earliest time as communicated in connection assignment frames sent to nodes that are still connected with it. Besides, to provide a non-zero length CAP, the hub shall transmit a preceding B2 frame. The hub shall not transmit a B2 frame if the CAP that follows has a zero length unless it needs to announce B2-aided time-sharing information and/or provide group acknowledgment. Specifically, in EAP, RAP, and CAP periods, nodes contend for the channel allocation using either CSMA/CA (Carrier Sense Multiple Access with Collision Avoidance) or slotted Aloha access procedure. EAP1 and EAP2 are utilized for high priority traffic, such as reporting emergency events. CAP, RAP1 and RAP2 are only used for regular

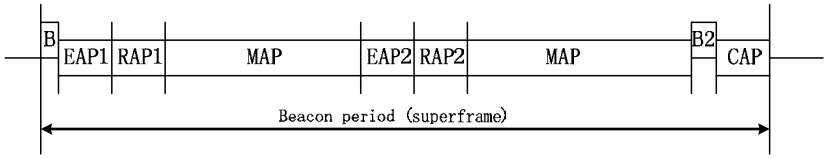

Figure 2.3: Superframe structure in the beacon mode with beacon periods.

traffic. In MAP periods, scheduled, unscheduled and improvised access methods are possible. The scheduled access procedure is generally used for applications that involve periodic monitoring.

2. **Non-beacon mode with superframes**

   In this mode, a hub may have only one MAP (Managed Access Phase) in a superframe, and it may organize the access to the medium as explained above for the MAP phase in the beacon-enabled access mode.

3. **Non-beacon mode without superframes**

   In this mode, only unscheduled polled allocations and/or posted allocations are provided by the hub. A node may treat any time interval as a portion of EAP1 or RAP1 and performs CSMA/CA mechanism to obtain a contented allocation, which also means each node has to establish its own time schedule independently [3].

As the beacon mode with superframes provides the most abundant options in terms of access phases, it is considered as a universal mode for most WBAN applications, especially for healthcare applications. In this thesis, we also focus on the beacon mode with superframes.

Next, a brief introduction of frame (or packet) acknowledgments is provided, as it is a key procedure to the transmission. Upon receiving a packet, a recipient shall acknowledge a received packet according to the *Ack Policy field* in the MAC header of the packet. Four different acknowledgments policies are defined, and they are No Acknowledgment (N-Ack), Immediate Acknowledgment (I-Ack), Group Acknowledgment (G-Ack), and Block Acknowledgment Later & Block Acknowledgment (L-Ack & B-Ack).

• **N-Ack:** A frame with the *Ack Policy field* set to N-Ack indicates that the current frame does not require an acknowledgment from the recipient, either immediately or later. A frame with an N-Ack can be transmitted by either the hub or a node, and most control packets adopt the N-Ack policy.

• **I-Ack:** Upon receiving a frame with the I-Ack request, a recipient shall send an I-Ack frame after the end of the received frame with a given interframe spacing (e.g. pSIFS = 75 μs). Management type frames are always transmitted with an I-Ack request.

• **G-Ack:** The packets with G-Acks are applicable to data frames sent to a hub. The key advantage of G-ACK policy is that the hub could acknowledge data frames with G-Ack

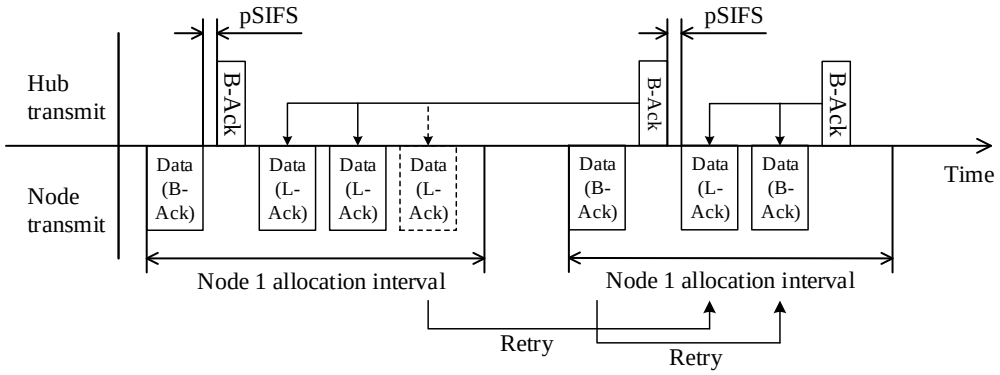

Figure 2.4: An example of L-Ack & B-Ack [4].

requests from multiple nodes together through multicast of one B2 frame. A B2 frame contains a set of Node Identifiers (NIDs) to indicate nodes from which the hub has received a frame with G-Ack requests since the last transmitted B2 frame. A node may retry the frame with the G-Ack request upon failing to receive the expected B2 frame, or if its NID does not appear in a received B2 frame. A detailed example of G-ACK can be found in Figure 61 in the standard document [4].

• **L-Ack & B-Ack:** Both node and hub can transmit the frame with L-Ack or B-Ack request. L-Ack & B-Ack policy is defined to support the block transmission, in which the source shall send frames of the same subtype in the order of non-decreasing sequence numbers. In a block of frames, except for the last frame being set with the B-Ack request, the other frames before it contains the L-Ack request. The receiver does not send an acknowledgment frame after receiving a frame with L-Ack requests. Instead, the block of frames is acknowledged by a B-Ack frame pSIFS (e.g., 75 μs) after the reception of the last frame with a B-Ack request. To illustrate the block transmission scheme, we provide an instance in Figure 2.4. In Figure 2.4, Node 1 transmits data frames to the hub in the manner of block transmission. The sender retransmits the data frames from the oldest lost one (represented by a dashed rectangle), after receiving the B-Ack. Note that a block transmission may span more than one allocation interval.

Besides, some other aspects related to the BAN transmission are specified in the IEEE 802.15.6 standard document [4], including transmission security, clock synchronization, power management, interference mitigation, etc.

2.3 Adaptive Transmission Design in WBANs

Considering the dynamic of the wireless channel in WBANs and the heterogeneous QoS requirements of various applications, the conventional static design for the transmission system is suboptimal. In recent years, many dynamic schemes which optimize key trans-

mission parameters in accordance with the real-time channel condition or application requirements have been proposed to meet the transmission challenges in WBANs. The adaptive transmission design for WBANs can be categorized into three main topics, namely Transmission Power Control (TPC), Adaptive Duty Cycling (ADC) and Dynamic Slot Scheduling (DSS), based on the regulating transmission parameters.

2.3.1 Transmission Power Control

Generally, powerful devices like cellphones or smartphones are well suited for a hub. The sensor and actuator nodes, however, are assumed to have a limited energy supply and a limited processing power. Therefore, reducing the energy consumption of the sensor or actuator node is considered as the main approach to increase the lifetime of WBAN systems. Meanwhile, wireless communication is often a major power consumer in the sensor and actuator nodes. Transmission Power Control (TPC) methods refer to the adaptive method which optimizes the transmission power (Tx Power) based on the change of channel conditions or QoS requirements. TPC is considered as an effective approach to improve the energy efficiency [19]. As a classical research topic, TPC has been extensively explored in the context of cellular networks and WSNs. Although the WBANs are usually considered to originally emerge from the field of WSNs, these WSNs-specific TPC methods are not suitable for WBANs. First, most WSNs-specific methods estimate the channel quality by utilizing control frames and then adjust the transmission power based on the estimated result. Whereas the channels in WBANs vary much more frequently than WSNs, the extra energy cost from the control frames certainly degrades the system lifetime. Second, many existing TPC methods require the transmitting node to stay in active state to track the real-time channel condition so as to optimize the Tx power. However, in WBANs, the transmitter is usually acted by the sensor or actuator node, which is expected to be in the sleep mode for most of the time to save energy.

Except for the motivation from the perspective of energy consumption, there are two other aspects that may benefit from the TPC technology. First, in WBANs, the wireless device is in close proximity to, or inside, a human body. To avoid the negative impact of electromagnetic radiation on the human body (e.g., temperature rise), the Tx power should be restricted to comply with the limitation of Specific Absorption Rate (SAR) of local regulatory bodies (the limitation of Federal Communications Commission is 1.6 W/Kg). Note that SAR is defined to measure the amount of power absorbed by the tissue. The second aspect that may benefit from TPC is the interference mitigation. In WBAN systems, multiple wireless devices are located in a space within 2-5 meters, and interference problem gets severe when several WBANs crowd in a small area. Reducing Tx power could significantly mitigate the signal interference to other nodes or other WBANs.

Among numbers of TPC methods proposed for WBANs, adjusting the Tx power based

on the channel condition to achieve a better trade-off between energy consumption and transmission reliability is considered as one of the major categories. In such approaches, predicting the future channel quality is the key part. The work of [20] is considered as the first work designing a TPC method for WBAN systems. Reference [20] firstly investigates the potential benefits of adaptive TPC for energy saving in body-wearable sensor devices used for medical monitoring, and then proposes a practical TPC method that adapts the Tx power according to the feedback RSSI (Received Signal Strength Indicator) values obtained from the sensor node. Specifically, the hub jointly considers the latest feedback RSSI value and previous average RSSI to estimate the new average RSSI (denoted as $\bar{R}$), and the new transmission level is configured based on the comparison between the new average RSSI and two pre-defined thresholds T_H and T_L. If $\bar{R}$ drops below the lower threshold T_L, then the transmission power is doubled. In contrast, if $\bar{R}$ is above the upper threshold T_H, then the transmission power is reduced by a small fixed constant. Based on different weighting configurations between the latest RSSI and previous $\bar{R}$, three TPC schemes, namely Conservative, Balance and Aggressive schemes, are designed for different applications with the different requirement in terms of data packet loss and energy consumption. Similarly, the TPC schemes proposed in [21]–[27] also utilize the comparison between historical RSSI record(s) and RSSI threshold(s) to reduce the power consumption while maintaining a high packet delivery ratio. In [28], the autocorrelation characteristics of on-body channels are taken into account to facilitate the TPC. The hub utilizes a correlation model to predict the future RSSI value, and then the transmission power level is adjusted based the predicted value.

There are some works exploring the relay-aided TPC method in WBAN, which aim at a higher transmission reliability or a lower energy consumption [29], [30]. The authors of [31], [32] try to use artificial neural network technology to optimize the TPC method in WBANs. Trained with RSSI values measured in human subjects, a channel quality estimation model is built to predict the on-body channel quality variations. Instead of using RSSI as the only indicator to estimate channel quality, the work of [33] explores the combination of RSSI and LQI (Link Quality Indication), which may have a better performance in the environment with interference.

With regard to the interference mitigation, game theory is widely used for the TPC methods [34]–[37]. In these game theory based TPC schemes, the power control problem is modeled as a non-cooperative game, in which the cost function is designed based on both QoS requirement and energy constraint. Besides, in [38] the relay selection problem is jointly considered with TPC to further improve the transmission performance in terms of energy efficiency, delay, and jitter.

Another group of TPC methods is adjusting the transmission power level based on the change of human posture or motion [39]–[43]. This category of TPC methods is novel because the presence and movement of the human body are taken into account. However,

in the dynamic scenarios, most of these work only consider the walking case which exhibits significant periodicity. The effectiveness in other complicated dynamic scenarios is not assessed. Besides, these works presume an effective activity recognition algorithm has been deployed, which also affects the feasibility.

2.3.2 Adaptive Duty Cycling

Duty cycle is calculated as the fraction of the time that a system is in an "active" state, which includes the transmitting (Tx), receiving (Rx) and listening states. Hence, reducing the duty cycle could significantly prolong the lifetime of a wireless system. Adaptive Duty Cycling (ADC) technology, which adjusts the duty cycle according to the traffic or other QoS requirements, has been extensively discussed in the context of WSNs, especially based on the IEEE 802.15.4 standard. Essentially, the superframe structure defines the duty cycle of nodes in IEEE 502.15.4, so adapting the duty cycle is changing the structure of superframe. Two key factors determining the superframe structure are Beacon Order (BO) and Superframe Order (SO). In existing literature, the efforts mainly focus on changing BO [44], [45] , changing SO [46]–[49] or changing both BO and SO [50]. Taking the work in [48] as an example, the coordinator calculates the number of received packets in each superframe to adjust the active period. If the amount of received packets is above a threshold, the value of SO is incremented by 1 unit to augment the duty cycle. On the other hand, if a significant traffic reduction is detected, SO should be decremented. Besides, if no relevant traffic change is detected, SO remains unchanged. Reference [51] provides a comprehensive survey for the ADC schemes in IEEE 802.15.4-based networks.

In recent years, there are some works exploring the tailored ADC schemes for WBAN systems. In [52], the authors propose a dynamic duty cycle algorithm, namely D-MAC, for WBAN systems. In D-MAC, the packet received ratio and packet delay are taken into consideration to adjust both BO and SO simultaneously. In [53], the authors propose a new ADC scheme for resource-constrained WBAN systems. The new ADC scheme allows the sensor nodes to adapt the duty cycle according to the traffic. The dynamic adaptation of duty cycle avoids the extra energy waste from idle listening, overhearing, collisions and unnecessary wake-up beacon transmissions. In [14], the network traffic load, delay-reliability factor, and superframe duration are taken into account to assist the effective duty cycle adaptation. Besides, ADC is combined with Network Coding (NC) technique, which could improve the energy efficiency of these nodes located in the bottleneck zone [54].

2.3.3 Dynamic Slot Scheduling

Generally, the MAC protocols can be classified into contention-based and schedule-based protocols. In the case of contention-based protocols, several nodes compete for the same

resource by using contention-based methods such as CSMA/CA or slotted Aloha. While the schedule-based protocols aim to reserve a resource for each node by using schedule-based methods such as TDMA (Time Division Multiple Access) or polling method. Due to the advantages in collision-free and energy efficiency, the schedule-based methods, especially TDMA, are put forth as the most appropriate MAC solutions in the context of WBAN systems [55], [56]. However, considering the high volatility of on-body channels, a simple static TDMA allocation may lead to significant waste. Specifically, if a time slot is assigned to a particular sensor node with a bad channel to the hub (coordinator or sink), the data packets from this sensor are prone to be lost. However, at the same time, the slot cannot be used by any other nodes that may have a good link, which not only wastes the energy but also decreases the throughput. Ideally, we would like to allocate a transmission slot to a node only when the state of its link to the hub allows a successful data transfer. The core idea of DSS method is scheduling the time slots according to the channel conditions, rather than a fixed schedule. It is worth noting that all the additional controls are added to the hub and there will be no increase in sensors' complexity, which is a big advantage for resource-constrained WBAN systems.

The core idea of DSS is usually referred to as "opportunistic scheduling" in the context of cellular networks [57]. However, traditional opportunistic scheduling approaches are not compatible with WBAN systems as they require that the slave nodes are continuously available for communication. This requirement is unacceptable for the energy-constrained sensors, which are in the sleep mode most of the time [11]. Besides, most opportunistic scheduling methods for cellular networks do not consider the peculiarities of WBAN channels, e.g., high variation and predominant shadowing from the body.

Recently, some DSS works are proposed in the context of WBANs. In [58], [59], the authors use a two-state ("good" or "bad") Gilbert model [60] to describe the variation of on-body channels. Based on the Markov channel model, a DSS scheme, named *Flipping*, is proposed to maximize the expected number of successful transmissions in a TDMA round. The *Flipping* scheme schedules all "bad" links of the previous superframe last and preserves the order in time in which they are observed while schedules all "good" links first but reversing the order in which they are observed in the previous superframe. The rationale behind *Flipping* method is that all "bad" links are given the longest time to recover (i.e., getting out of the outage), while the flipped ordering of the good links takes advantage of the most recently observed "good" links to ensure a high probability of success in the next transmissions round [11]. Some other research works are also based on the assumption of the two-state Markov channel model. To tackle the dynamic fluctuation of on-body channels, [61] presents a novel transition matrix estimation method. In [62], the authors focus on adapting the slot order to improve the effectiveness of retransmission. The node with the worst channel condition is scheduled to occupy the first time slot to get the highest chance of discovering a relaying node and the best channel is scheduled

at the last. In [63]–[65], the authors propose a *Flipping*-like scheduling approach which also adopts a Gilbert model to describe on-body channels. Besides, the QoS requirements, including energy efficiency, data rate, and packet reception rate, are taken into account to optimize not only the slot order but also the slot number. The main limitation of these Markov model based schemes is that the condition of on-body channels is limited to only two states, "good" and "bad", which are insufficient to describe the on-body channel states in the complex WBAN application scenarios.

With regard to the slot number, adaptively allocating the slot number based on the data priority is of interest [66]–[69]. In such schemes, the sensor node with a high priority is allocated with additional time slots to guarantee transmission reliability.

Similar to some TPC works exploring the motion feature of the human body, there are some works trying to utilize the channel fluctuation feature to facilitate the time slot scheduling in WBANs [70]–[73]. For instance, the authors of [73] and [70] apply Fast Fourier Transform (FFT) to the RSSI time-series and identify the dominant frequency, to find the transmission window. However, most of these works seem to be effective only in periodic movement patterns, such as walking, jogging and running, which may not be applicable in general.

Instead of improving the transmission reliability or supporting QoS requirements, the work in [74] adaptively allocates the time slots based on the number of BANs or sensors that exist in a nearby area, to mitigate the potential interference.

2.3.4 Other Adaptive Designs

Apart from TPC, ADC and DSS schemes, some researchers explore dynamic tuning of other parameters. For example, references [75], [76] try to combine the contention-based and the TDMA approaches by adaptively modifying the MAC frame structure. In [75], non-interfering sources use CSMA/CA to communicate with the relays. Whilst a flexible TDMA approach is adopted when interference is detected. The LPDQ (Low-Power Distributed Queuing) scheme proposed in [76] switches between Aloha and TDMA according to the traffic scale. In [77], a dynamic backoff scheduling algorithm is proposed for low data rate WBAN applications. The algorithm works on CSMA/CA, and the backoff length for each node is configured based on its past successful trials in accessing the channel and also its data rate. The works in [78]–[80] discuss the packet (or frame) size adaptation for WBANs.

Last but not least, some works try to jointly optimize multiple key parameters in MAC or PHY layers, including transmission power, slot order/duration, transmit rate, modulation, and space-time-frequency coding, etc [81]–[87]. For example, in [84]–[87], the authors propose to adaptively change the modulation, transmit power, and space-time-frequency coding to allow the better channel carry more information.

2.4 Applications of Network Coding in WBANs

Network Coding (NC) was initiated at the turn of the millennium in a seminal paper by Ahlswede, Cai, and Yeun [2]. NC has been proved to improve throughput, reliability, manageability, and support of QoS in wired or wireless environment [88]–[91]. The core notion of network coding is to allow and encourage mixing of data at intermediate network nodes, instead of simply storing and forwarding in the traditional network. More specifically, based on the deployment protocol layer of NC technology, NC can be categorized as either digital network coding (DNC) or Analog Network Coding (ANC). In DNC, the NC technology is performed above the data link layer. The encoding operation is completed on digital bit [88], [89]. In ANC, the mixing or coding operation is done over physical signals in the wireless channel itself [90], [92].

Considering the tremendous potential of NC technology in the context of wireless transmission, exploring the applications of NC in WBANs attracts many researchers' attention. However, most existing works explore the combination of NC and WBAN from the perspective of conventional wireless network coding. In this thesis, all existing "WBAN+NC" schemes are categorized into the following three groups.

2.4.1 MP-based Scheme

In [93], Marinkovic and Popovici propose to use NC in the context of WBANs to achieve a better transmission reliability, and the scheme proposed in [93] is called MP scheme based on the names of the authors. All MP-based schemes only consider a two-hop star topology for data streaming from sensor or actuator nodes to the hub. Upon receiving the data packets from sensor or actuator nodes, the dedicated relay nodes perform XOR (eXclusive-OR) coding to these packets and transmit redundant packets to the hub. By this approach, the transmission reliability is improved. Figure 2.5 depicts a typical network topology of MP-based schemes.

In [94], an Unequally Error Protection (UEP) concept is introduced to support the different priority requirement of different application data. For a medical application, maximal XOR coding is performed to provide the best transmission reliability. Whereas, only partial packets are XORed in non-medical applications since it has a lower reliability requirement. In [95], [96], Byrne and Manada try to analyze the robustness of the MP scheme from the perspective of graph theory and linear algebra. Graph representations are used to describe the encoding and decoding of the packet in the hub side, and hence to explore the optimal ratio between the number of native and XORed packets sent by the relay node. The authors of [97] propose to concatenate the XOR encoding and BCH (Bose-Chaudhuri-Hocquenghem) encoding to counteract communication error and reduce energy consumption. In [98], the QoS requirement is taken into account, and an adaptive coding scheme is proposed to support various QoS requirements in terms of reliability,

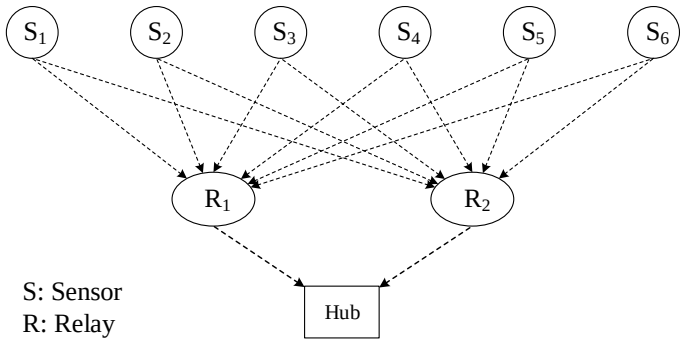

Figure 2.5: The typical network topology of MP-based scheme [93], [98].

energy efficiency, and delay. The direct transmission from the sensor node to the hub (i.e., one-hop transmission) is neglected in the MP-based scheme.

However, unlike massive WSNs, one-hop transmission is considered as an important component for WBAN systems. Moreover, MP-based schemes are not adaptive to the channel condition, which impedes its potential to improve the transmission reliability in the WBANs with complex wireless channels variations.

2.4.2 Cluster-based Scheme

Another important category in the "WBAN+NC" area focuses on the cluster-based network architecture, in which the intermediate relay nodes are divided into multiple cooperative clusters to facilitate the cooperative communication [99]. Instead of forwarding original packets between consecutive clusters, the NC packets are utilized to reduce the packet retransmission time in the cluster-based schemes. Figure 2.6 depicts a typical network topology of cluster-based schemes when a single source node is considered. Based on the cluster network topology, [100]–[102] use cooperative network coding and cooperative diversity coding to combat packet loss and reduce latency. In [103], a cloud coordinator is added to the cluster-based network to manage the encoding and retransmission at the relay nodes. Similarly, the work in [104] also employs a cloud resource for the relay coordination. The control packets are coordinated by the controller in the cloud, while all data related operations take place locally at the off-cloud nodes.

However, there exist some drawbacks for cluster-based schemes. First, as stated in [98], it is very difficult to make a clustering algorithm adaptive to the dynamic channel condition. Moreover, the network scale of WBAN is relatively smaller than other WSNs. Maximal two-hop transmission is sufficient for most on-body channel transmissions. Thus, the feasibility of cluster-based schemes is questionable in the context of WBAN systems.

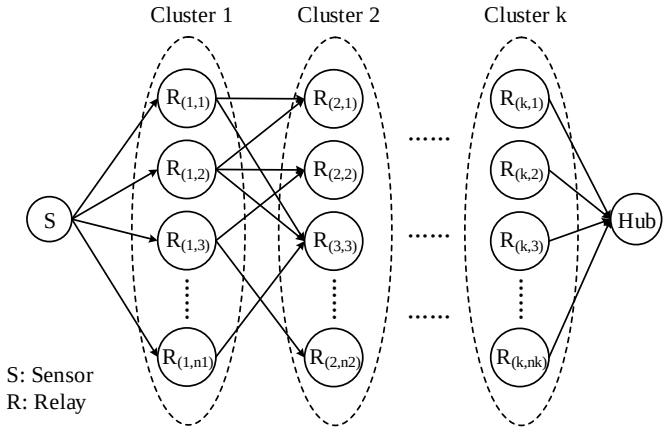

Figure 2.6: The typical network topology of cluster-based scheme [100]–[102].

2.4.3 CARQ-NC

Both MP-based and cluster-based schemes mainly focus on exploring the spatial diversity provided by the relay cooperation to improve the transmission reliability in WBAN systems. Whereas, the CARQ-NC (Combined ARQ and Network Coding) scheme proposed in [105] tries to leverage random linear network coding (RLNC) in the source node without the assistance of relay nodes. Specifically, TDMA (Time Division Multiple Access) scheduling is used to allocate the wireless channel to individual nodes within the network. Each sensor node linearly combines its data packets before taking turns to send the ensuing mixtures to the hub. Unlike the MP-based or cluster-based schemes, CARQ-NC is designed on the basis of a one-hop star network topology, and only source coding is performed. CARQ-NC reduces the sensors' time slot of sending packets by encoding redundant packets. In this way, the sleep time of sensor nodes is increased and hence the energy consumption is reduced. In [106], the authors explore the strategic use of network coding in the wireless packet erasure relay channel from the perspective of both throughput and energy metrics. A fluid flow model is used to describe the case where coding is applied at both the source and the relay, and Markov chain models are proposed to describe packet evolution if coding is only applied at the relay nodes.

In fact, CARQ-NC is similar to the Forward Error Correction (FEC) technology, except the redundant information (or check information) is added in the packet level. Besides, there is no closed-form answer for the redundant packet number of each sensor.

Apart from these three typical groups of the "WBAN+NC" schemes, there exist some other works which provide new methods to the harnessing of NC in the WBAN systems. In [107], the authors propose a practical NC approach, namely DF-NC, for WBANs using decode-and-forward relays. Only one linear combination of packets is sent to the destination. Energy usage at the relay node is minimized compared to existing cooperative

schemes without NC, such as Maximum Ratio Combining (MRC), Selection Combining (SC) and Switched Combining (SwC). DF-NC scheme achieves a near-optimal outage probability performance while maximizing the energy efficiency of WBANs by fixing the average number of transmissions per node. In [108], researchers in MIT propose a Joint Channel-Network Coding (JCNC) scheme, which jointly considers the RLNC and FEC according to the variation of channel conditions. In [109], the relay first chooses d different decided symbols from the received symbols and then performs Demodulate-and-Forward operation before encoding. Then, the destination performs message-passing algorithm (MPA) to reduce the computation complexity of decoding. Note that a larger value of d means an NC symbol contains more symbols from source nodes. However, in the simulation section of [109], the author only considers the scenario with $d = 1$, thus the scheme actually degenerates into simple forwarding without coding. To improve the energy efficiency of sensor nodes in the bottleneck zone, the authors of [54], [110] propose to apply the RLNC technology in the multi-hop transmission of WBAN systems. In [111]–[113], the Cooperative Compressed Sensing (CCS) approach is jointly considered with the RLNC to further increase the energy efficiency. Besides, some research works discuss the transmission security issues in NC-enabled WBANs [114].

2.5 Chapter Summary

In this chapter, we first provide an overview of the WBAN system, including the communication architecture, application area, and main challenges. Then the standardization work developed by IEEE, i.e., IEEE 802.15.6, is introduced, especially the technical detail in the MAC layer. At last, we review the literature focusing on the adaptive transmission design and application of NC in WBAN systems. The up-to-date literature review shows that there are open and challenging problems in providing the heterogeneous transmission requirement in terms of transmission reliability, energy consumption, data rate, transmission latency and priority support etc. Thus, this thesis focuses on exploring the characteristics of WBAN channels in real dynamic scenarios and then investigates more effective transmission schemes by using these peculiar channel characteristics.

Chapter 3

Channel Data Collection and Analysis

3.1 Introduction

In WBANs, the on-body channel is considered as the most prevalent channel. However, affected by the tissue shadowing and dynamic body motion, on-body channels undergo complex temporal variations. One way to characterize the on-body propagation is through the theoretical description of electromagnetic propagation phenomena using anatomically accurate models of the human body. Limited by its large computational overhead and mobility, the anatomical channel model is intended for the detailed descriptions of specific aspects of the propagation, e.g., the influence of the body structure on the antenna patterns. Another popular approach to characterize the on-body channel propagation is based on empirical channel gain data from real human body measurements [115]–[117]. By taking the motion and posture of the human body into account, this approach seems closer to the practical WBAN systems. The works of modeling on-body channels can be categorized into two categories: small-scale fading model and large-scale fading model.

The small-scale fading models for fitting probability distributions to measured channel gains have been explored extensively in the literature [118]–[120]. In general, the best-fitting distributions to channel gains are lognormal, gamma and Weibull. The Rayleigh distribution is a poor choice for WBAN channels, though it is a good fit when various multipath in the radio channel are additive in the linear domain. For the walking scenarios, the Weibull distribution is found to be the best fit. On the other hand, with respect to the large-scale fading models, the distance between two radio devices are utilized to model WBAN channels' path loss in many works [107], [109], [121]–[123]. However, as the WBAN is a short-range communication, for the majority of deployment scenarios, the signal attenuation is significantly affected by the shadowing of body tissues instead of the distance between two devices. Considering the slow fading characteristic for NB communication, we mainly focus on the large-scale fading of on-body channels.

In this chapter, we build customized wireless transceivers to measure actual channel

gain data in two typical dynamic scenarios, i.e., walking and daily life scenarios. The on-body channel characteristics, including autocorrelation, cross-correlation, outage duration, etc., are analyzed to lay the background for our design of more efficient transmission schemes. Besides, these real on-body channel gain datasets are imported into the simulation model to support the performance evaluation, which eliminates the defect of the distance-based channel models.

The contents of this chapter were published in our paper [124] and partly in our papers [125]–[127].

3.2 Portable Wireless Transceiver

Many current works utilize a Vector Signal Analyzer (VSA) as a testbed to capture the on-body channel information in dynamic motion scenarios. However, due to the size and power requirements of VSA, it is impractical to capture real channel information in mobile scenarios. For example, instead of measuring channel data in real walking or running scenarios, the VSA-based works have to carry out the measurement on a treadmill or by simulative walking or running on the spot. Given this limitation, we build a portable wireless transceiver to collect the real on-body channel information in dynamic and mobile scenarios. The customized transceiver is self-powered and capable of collecting real-time RSSI values.

Inspired by the testbed design in [128], we construct our new wireless transceiver from easy-assembled and widely available commercial hardware modules. As illustrated in Figure 3.1, each wireless transceiver consists of one radio module, one microcontroller, one MicroSD card, and one battery. The microcontroller controls all other components. The radio module is in charge of broadcasting and receiving wireless signals, and the MicroSD card stores the information of wireless channels. The main function of these devices is to transmit and receive continuous data packets from each other, thus facilitating the analysis of on-body channel characteristics.

Based on the hardware design in Figure 3.1, all the components are chosen from the mature commercial products.

• Radio Module: The XBee series 1 is utilized as the RF front end, which works at the 2.4 GHz ISM (Industrial, Scientific and Medical) radio bands. When in operation, the XBee's output power is set to 0 dBm.

• Microcontroller: the Arduino UNO is utilized as the logical controller board. Both the XBee module and MicroSD card shield module are plugged into the control board. The Arduino UNO not only controls the transmitting and receiving of data packets but also writes the channel information to the MicroSD card. When the transceiver works as a transmitter, the sample data packets are transmitted at the frequency of 200 packets per second (i.e., transmitting one packet every 5 ms), and the transmission data rate of 250

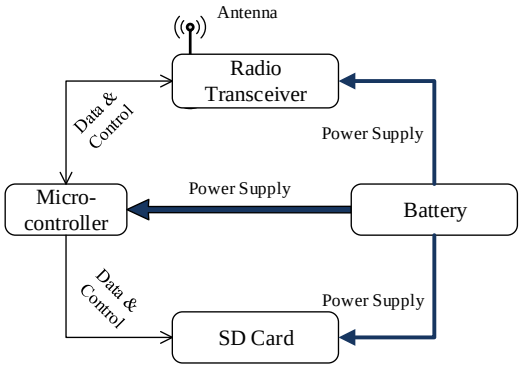

Figure 3.1: Hardware design diagram.

kbps.

• MicroSD card: The MicroSD card is used to record the channel information by receiving data from the radio. Specifically, the receivers write the receiving time, packet ID and the real-time RSSI (Received Signal Strength Indicator) value to the MicroSD card. Note that since the XBee's transmission power is 0 *dBm*, the RSSI value is actually the channel gain and equal to the inverse of the path loss.

• Battery: A power shield with two AAA batteries is plugged into the control board to supply the power.

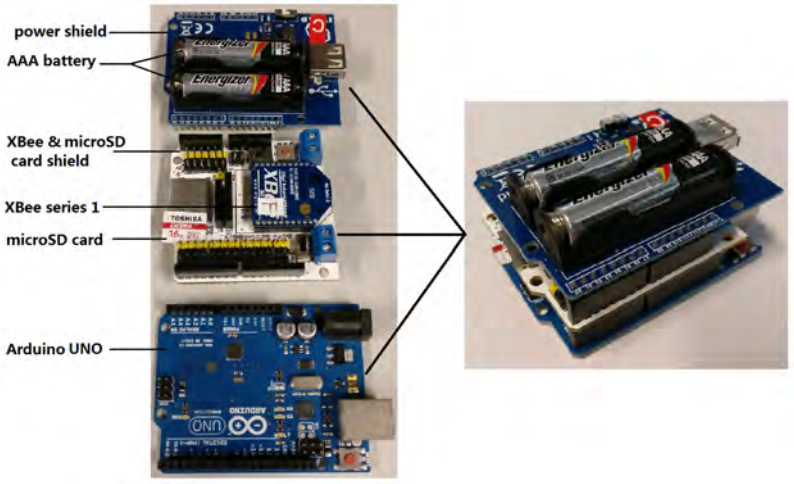

Figure 3.2: Components of the portable transceiver.

As shown in Figure 3.2, the wireless transceiver looks like a "sandwich" with three PCBs (Printed Circuit Boards) overlying each other to make the system self-contained.

3.3 Walking Scenarios

We first focus on the on-body channel characteristics in the walking scenarios, which is one of the most frequent dynamic activities for the human.

3.3.1 Measurement Setups

In our experiment, the measurements are conducted in both indoor and outdoor environments. As shown in Figure 3.3, the outdoor environment is an open oval field of about 13,000 square meters, and the indoor environment is a hallway inside a building.

Figure 3.3: Typical indoor and outdoor environments.

As the swinging motion of the upper limbs is a unique feature in the walking scenarios, in this chapter, we mainly consider the network deployment in Figure 3.4 with two sensors bound on the wrists.

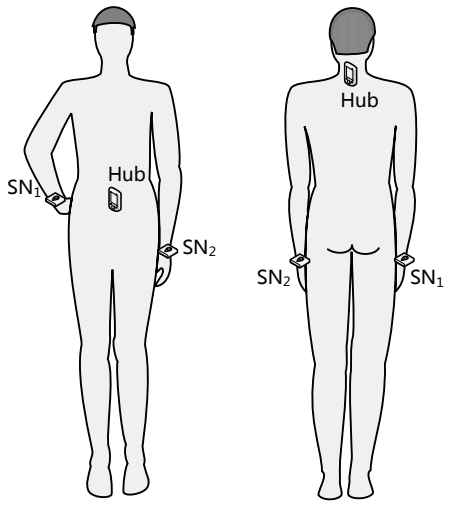

Figure 3.4: Deployment of the sensors and the hub.

As shown in Figure 3.4, we consider two locations for the hub (coordinator or gateway), i.e., on the abdomen (can be attached to the belt buckle) and on the back collar, where a subject could comfortably wear the hub that is expected to be larger than a sensor node. Two sensors (SN_1 and SN_2) are attached to the wrists. Moreover, to explore the effect of the antenna direction and the shadowing of wrists, the XBee module is rolled around the wrist in four directions: 0°, 90°, 180° and 270°, as depicted in Figure 3.5. The experiments

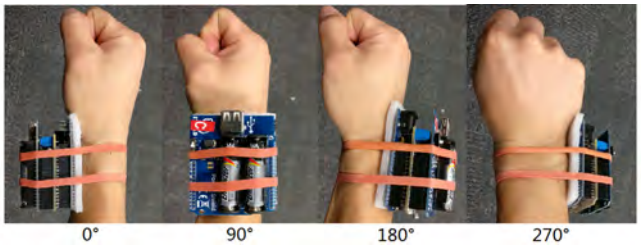

Figure 3.5: Four directions of the testbed on the wrist.

are carried out for one male subject. Consequently, there are 16 individual experimental setups (2×2×4) in total.

In each measurement, the hub node is configured to broadcast packets to two sensors continuously with the frequency of 200 Hz (200 sample packets per second). In other words, the time resolution is 5 ms, which is considered to be sufficient to capture the time variation of the on-body channels. When the XBee modules on the wrists receive the packets, the microcontroller extracts the RSSI and writes it to the MicroSD card together with the system time and the packet sequence. As each setup lasts for about 1 minute (walking one minute) and there are 16 setups, 16-minutes channel gain data, containing about 192,000 samples, is recorded.

In addition, it is necessary to explain why the downlinks (from the hub to the sensors) are utilized to capture the channel gain, instead of the uplinks (from the sensors to the hub). As demonstrated in [128] and [117], in the narrowband communication environments the on-body channels show prominent reciprocity, which means the channel profiles of downlink and uplink are approximately the same. Moreover, as the two sensors record the corresponding RSSI almost simultaneously, the downlinks are a better choice for the cross-correlation analysis.

3.3.2 Signal Attenuation and Shadowing Effect

We first analyze the RSSI data for the four different scenarios. Figures 3.6-3.9 present typical time-varying RSSI data for the two links from the hub to the two sensors. $RSSI_1$ and $RSSI_2$ refer to the RSSI of the packets received by SN_1 and SN_2, respectively. Observations that can be derived from the four figures are listed below.

1. When the hub is on the “Collar”, the channel path losses are much greater than the “Belt” cases. The main reason is that, in the “Collar” cases, the signal is affected not only by the shadowing of the torso but also the shadowing of the upper limbs

2. The comparison between the indoor and outdoor environments shows that there exist more small-scale fluctuations in the indoor environment, resulting from the reflection from surrounding objects, such as desks, wall, and roof.

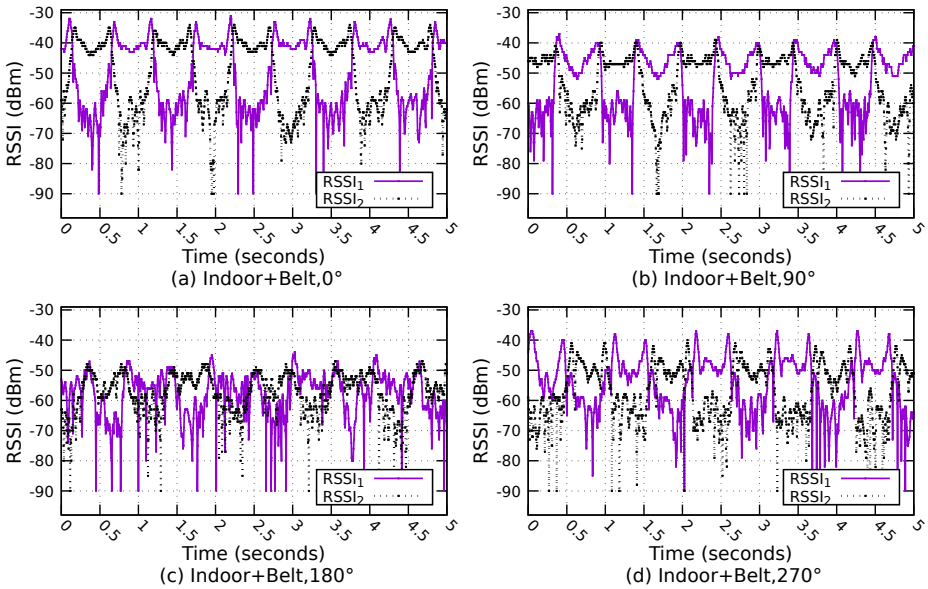

Figure 3.6: RSSI vs. time in the "Indoor+Belt" scenario.

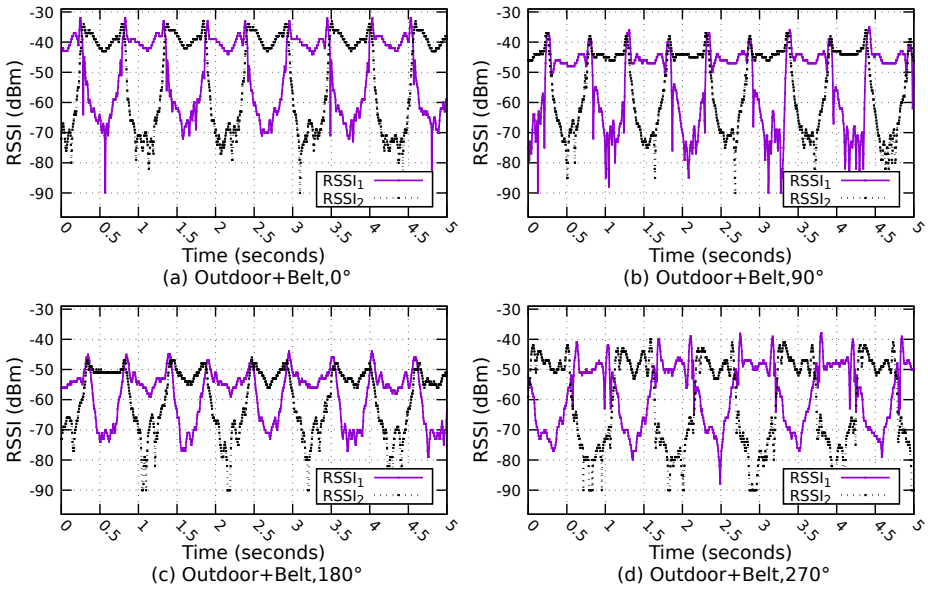

Figure 3.7: RSSI vs. time in the "Outdoor+Belt" scenario.

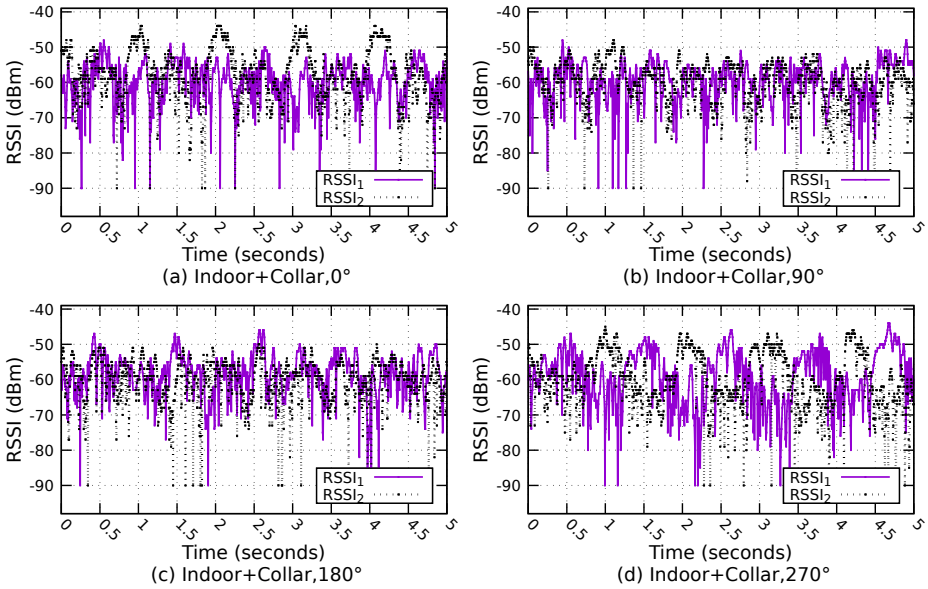

Figure 3.8: RSSI vs. time in the "Indoor+Collar" scenario.

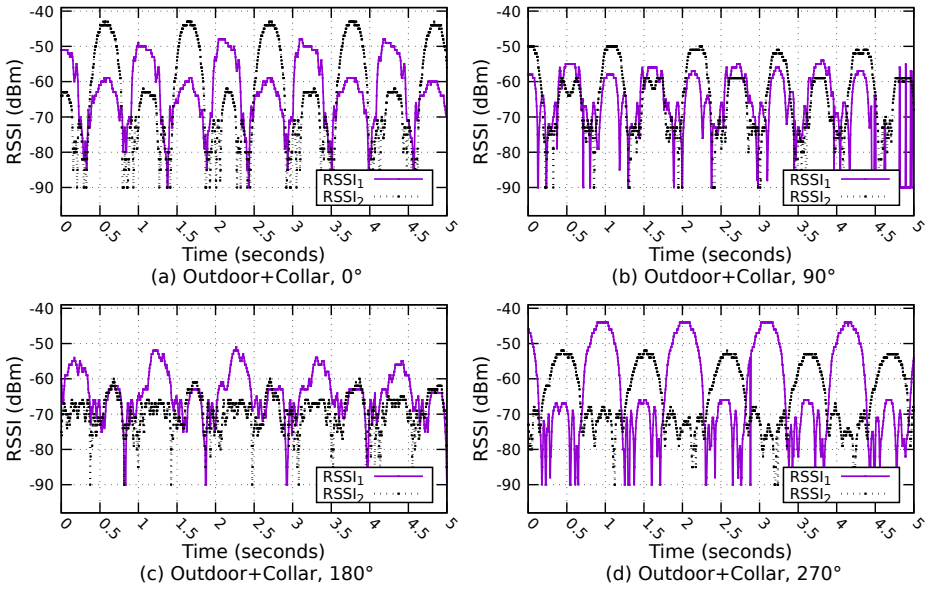

Figure 3.9: RSSI vs. time in the "Outdoor+Collar" scenario.

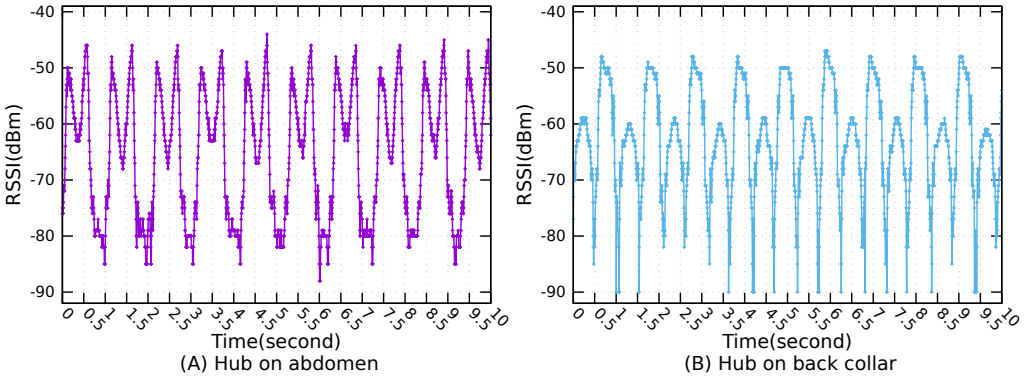

Figure 3.10: Time variation of the RSSI.

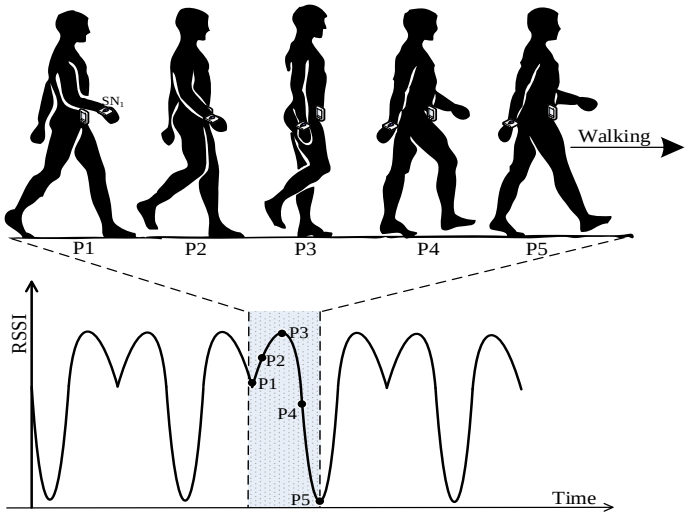

Figure 3.11: RSSI variation and corresponding walking phases when the hub is deployed on the abdomen.

3. The direction of transceivers also affects the signal attenuation. When the hub is on the abdomen, the 180° cases experience the biggest path loss. The reason is that when the transceivers are bound on the top of the wrists, the signal is not only affected by the shadowing of the torso but also the shadowing of the wrists themselves. Similarly, in the "Collar" cases, both 90° and 180° cases bring more shadowing from the upper limbs, leading to lower RSSI values.

Next, considering the influence from reflection can be neglected in the outdoor environment, two outdoor cases, i.e., "Outdoor+Belt" and "Outdoor+Collar", are picked to analyze the shadowing effect from the torso. Figure 3.10 shows the plots of a typical time variation of RSSI for the link from one sensor to the hub in the outdoor environment.

As shown in Figure 3.10, the RSSI values exhibit sharp fluctuations either for the "belt case" or the "collar case". To deepen understanding of the shadowing effect from body parts in the human walking scenarios, Figures. 3.11 and 3.12 illustrate the trend of RSSI variation and corresponding walking phases.

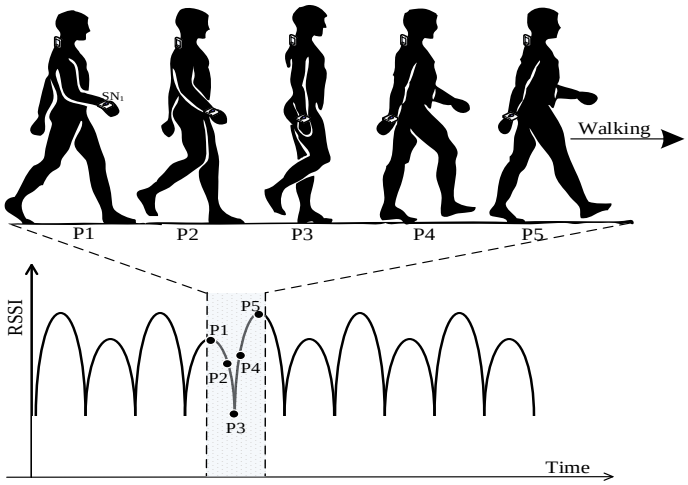

Figure 3.12: RSSI variation and corresponding walking phases when the hub is deployed on the back collar.

As shown in Figure 3.12, when the hub is placed on the back collar, the distance from the wrists to the hub remains nearly the same. However, the RSSI curve still exhibits sharp fluctuation when the person walks. Further, the signal attenuation is highly relevant to the "extent" of the body part that shadows the direct link between the transmitter and receiver. The "extent" here refers to the volume and depth of the impeding body part. On the other hand, if the shadowing from body parts can be neglected, the path loss is also affected by the distance between them, but causing a much smaller impact compared to the body's shadowing. Considering the process in Figure 3.11 as an example, when moving from $P1$ to $P3$, the links are line-of-sight. Consequently, the path loss diminishes with the decrease of the distance between the two radios. Conversely, when the arm swings behind the torso ($P3$ to $P5$), the RSSI suffers a steep drop. In other words, the absolute value of the curve's gradient for $P3$-$P5$ is much bigger than that for $P1$-$P3$, which confirms the body shadowing as the predominant factor for the signal attenuation.

3.3.3 Autocorrelation and Periodicity

In this section, we explore the periodicity by exploring the temporal autocorrelation of channel gain. Intuitively, the periodicity results from walking cycles, and can be clearly observed from Figure 3.10 for both "belt cases" and "collar cases". Whereas, the periodicity of channel quality seems to be not straightforward when the experiment is performed in the indoor environment. For example, it is hard to tell the periodicity by the curves plotted in Figure 3.8. To deepen the insight behind the periodicity, we utilize Pearson Product-moment Correlation Coefficient (PPCC) [129] to present the temporal autocorrelation of RSSI.

$$\gamma(k) = \frac{\sum_{n=1}^{N-k}(G(n)-\bar{G})(G(n+k)-\bar{G})}{\sum_{n=1}^{N}(G(n)-\bar{G})^2} \tag{3.1}$$

where $\bar{G}$ is the mean of array of N channel gain (or RSSI) values, i.e., $\{G(1), G(2)\ldots G(N)\}$. k is the shifting data points in the record sequence. As the sampling frequency in our experiment is 200 Hz, k also represents a time lag of $k \times 5$ ms.

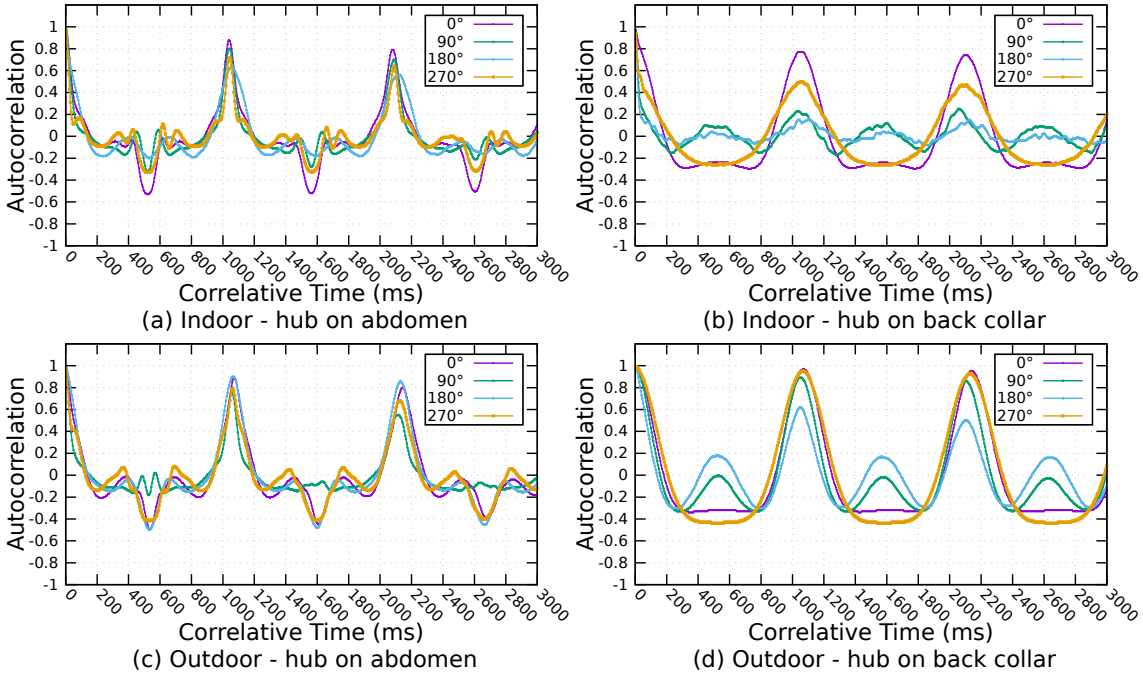

Figure 3.13: Autocorrelation vs. Time interval.

Taking the channel $SN_1 - hub$ as an example, Figure 3.13 shows the autocorrelation coefficients for different setups. The autocorrelation exhibits a clear periodicity and it is easy to extract the cycle period to be around 1050 ms. In the indoor scenarios, there are more reflections from the surrounding objects. Hence the curves experience more small deviations and the magnitude of autocorrelation coefficients is smaller. Moreover, when the radio device rolls around the wrist, i.e., 0°, 90°, 180° and 270°, the autocorrelation coefficient is affected. The differences mainly result from the change of antennas' direction and the change of shadowing from the arms. Especially for the case of 180°, since the transceivers are bound on the top of wrists and shadowed further by the wrists themselves, the autocorrelation for these cases still exhibits the periodicity but with smaller amplitudes.

3.3.4 Cross-correlation and Path Loss Discrepancy

The cross-correlation between different links is instructive for network resource allocation and the scheduling of cooperative communication. Similar to the above autocorrelation analysis, the PPCC is used to evaluate the cross-correlation between the two channels from sensors to the hub.

Table 3.1: Cross-correlation between two links.

	Indoor		**Outdoor**	
	Belt	Collar	Belt	Collar
0°	-0.45	-0.08	-0.42	-0.27
90°	0.15	0.00	0.43	0.14
180°	0.20	0.06	0.22	0.09
270°	-0.27	-0.26	-0.30	-0.44

$$\gamma_c = \frac{\sum_{n=1}^{N}(G_1(n)-\bar{G}_1)(G_2(n)-\bar{G}_2)}{\sqrt{\sum_{n=1}^{N}(G_1(n)-\bar{G}_1)^2}\sqrt{\sum_{n=1}^{N}(G_2(n)-\bar{G}_2)^2}} \tag{3.2}$$

where γ_c is the correlation coefficient between $G_1(n)$ and $G_2(n)$, which represent the channel gain time series of the link $SN_1 - hub$ and $SN_2 - hub$, respectively. $\bar{G}_1$ and $\bar{G}_2$ are the means of channel gain values. $N = 12,000$ is the number of samples in each measurement.

Table 3.1 shows the cross-correlation coefficients for different experimental setups. It is found that the walking scenarios exhibit relatively small cross-correlation coefficients, as the coefficient is generally considered to be significant when its absolute value is 0.7 or greater. Further, the cross-correlations vary dramatically with the network deployment, including the placement of the hub and sensors, surrounding environment, and the direction of transceivers. When the radio device rolls around the wrist, i.e., 0°, 90°, 180° and 270°, γ_c also varies accordingly. The differences mainly result from the change of antennas' direction and the change of shadowing from the arms. Especially for the "collar" cases, significant shadowing comes from both torso and upper limbs outweighs other effects, leading to a relatively small γ_c.

The cross-correlation between different links is considered to be an instructive parameter for the design of communication systems. However, a small absolute value of γ_c does not necessarily mean that two links are entirely independent. Taking the case of Figure 3.7(c) as an example, γ_c of the two channels is 0.22, but the two channels are obviously not independent. In this chapter, we focus on a simple but important parameter, namely the path loss discrepancy (in dB), referred to as PLD, to reflect the actual difference between two channel gains.

As shown in Figure 3.14, the probability distributions of the PLD are different for the four scenarios, but they all show a high proportion of the cases where the PLD is greater than 5 dB. Besides, the PLD medians for the four experimental setups from Figure 3.14 (a) to Figure 3.14 (d) are 15 dB, 7 dB, 21 dB and 11 dB respectively. In the outdoor environment, the PLD tends to be greater than that in the indoor environment. The main reason is that the reflections from surrounding objects in the indoor environment narrow

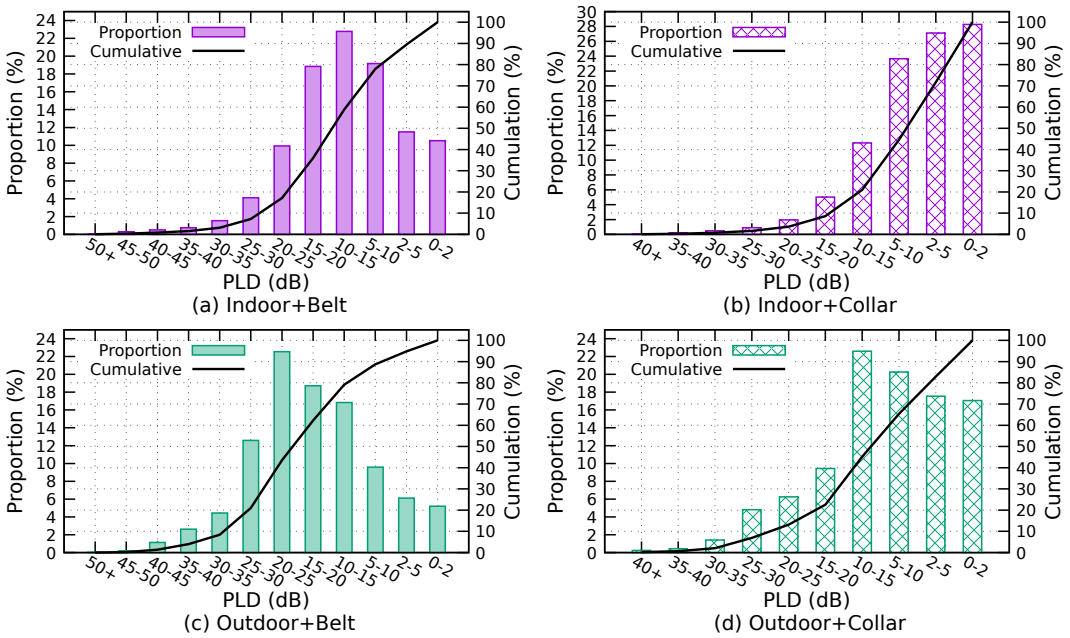

Figure 3.14: The distribution of the PLDs.

the gap between the RSSI of the two channels. Besides, the "belt" cases experience a bigger PLD than the "collar" cases, mainly because the shadowing effect is stronger in the latter.

Assuming that the environmental noise is relatively small, the PLD is the major constituent of the overall SNR (Signal-to-Noise Ratio). Meanwhile, SNR is a crucial parameter for the BER (Bit Error Ratio). The relationship between SNR and BER has been investigated intensively in the literature [130], [131]. As shown in Figure 3.15, when SNR is greater than 7 dB, the system achieves a BER of lower than 1×10^{-2} for the most low-order modulation schemes, which may be considered to be sufficient for practical implementation. Accordingly, if the two sensors located on the wrists concurrently broadcast packets to the hub on the torso in walking scenarios, the hub can restore at least one signal with a high probability. In other words, although the two sensors transmit simultaneously, the probability of packet collisions is small. Consequently, the observed PLD in walking scenarios may be sufficient to justify the rationale for simultaneous transmission from the two sensors to the hub.

3.4 Daily Life Scenarios

Instead of a monotone posture or motion, in this section, we focus on the daily life scenarios with mixed every-day activities. The channel datasets collected from these scenarios not only support the characterization of on-body channels but also facilitate the design and evaluation of new transmission protocols.

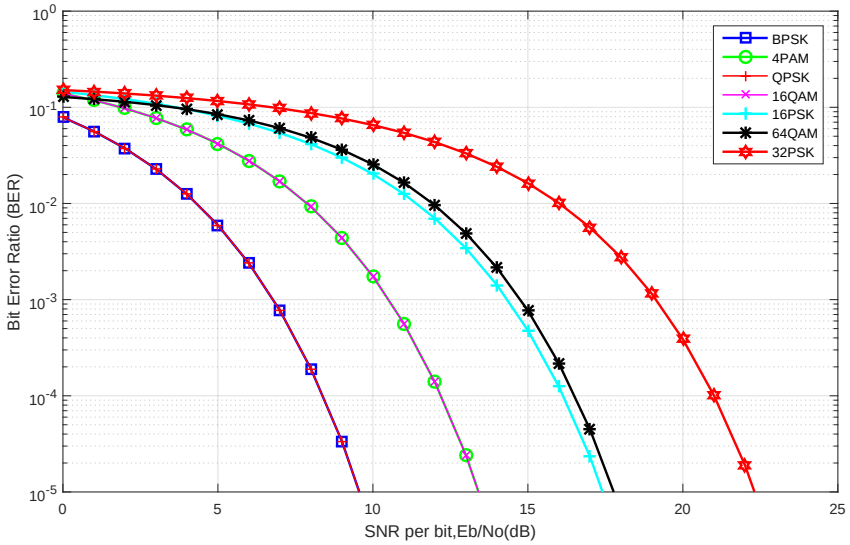

Figure 3.15: Bit error ratio vs. SNR for various modulation schemes.

3.4.1 Measurement Setups

A one-hop star topology composed of one hub and five sensors is considered. The deployment of the transceivers is depicted in Figure 3.16, where the transmitter (acting as the hub) is placed on the abdomen and five receivers (acting as sensor nodes) are mounted on limbs and head. The receiver mounted on the left wrist is named as SN_{LW}. Corresponding to the positions of the other receivers, the other four receivers are named as SN_{RW} (right wrist), SN_{LA} (left ankle), SN_{RA} (right ankle) and SN_H (head).

When the measurement begins, the transmitter continuously broadcasts sample packets to the five receivers with the transmission power of 0 dBm, and the sample packets transmission frequency is 200 Hz (i.e., sending 200 packets per second). Upon receiving the sample packet, the receivers record the packet sequence number, the timestamp, and the RSSI value into a text trace file. If the gap of sequence numbers between two successive sample packets, which a receiver receives successfully, exceeds one, some packets between these two packets have been lost due to the severe channel condition. In this case, the records of these lost packets will be added to the trace file with RSSI = -100 dBm. Taking the case in Figure 3.17 as an example, the hub broadcasts four sample packets ($Pkt_{16} - Pkt_{19}$) to the sensors nodes, but SN_{LW} only receives two packets (Pkt_{16} and Pkt_{19}) and loses two packets (Pkt_{17} and Pkt_{18}). Accordingly, after receiving Pkt_{19}, SN_{LW} will add two more data rows in the trace file with RSSI = -100 dBm, i.e., the middle two records in the data file of Figure 3.17. In addition, as the transmission power is set to 0 dBm, the RSSI value can be considered as the channel gain and the inverse of the RSSI is the path loss.

We focus on mixed activities encountered in typical daily scenarios, so the measurement environments include indoor office, gym, home, walkway, car, etc. Meanwhile, we do not limit the types of activities that the test subjects should conduct. These activities

Figure 3.16: The deployment of transceivers.

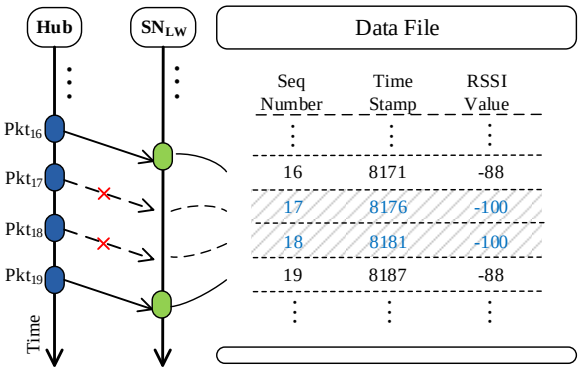

Figure 3.17: Channel data recording when packets are lost.

include standing, walking, jogging, running, sitting, driving, and many other irregular movements. Two male subjects and two female subjects are invited to conduct the measurements. Each test subject conducts four measurements on four different days. For each measurement, the test subject is required to wear 6 wireless transceivers for one hour, and the subject continues their daily life just like every other normal day. Corresponding to the five receivers, each measurement produces five trace files, each of which stores 72×10^4 records (200 packets/second $\times$ 3,600 seconds). Each trace file is a channel realization for one particular channel, e.g., from the hub to SN_{LW}. The five trace files collected from one measurement form one dataset, and we refer to each dataset as a channel dataset. Since 16 measurements are conducted, there are 16 channel datasets in total, and they are named CD_1 to CD_{16} respectively.

3.4.2 Autocorrelation

Next, these channel realizations collected from the daily scenarios are used to characterize the temporal autocorrelation of the on-body channels. As demonstrated in [116], the on-body channel may not satisfy the Wide Sense Stationary (WSS) assumption when the time window is longer than 500 ms. Hence, we focus on exploring the autocorrelation within a time lag of 500 ms. Equation (3.1) is adopted to evaluate the autocorrelation. Corresponding to the time lag from 5 ms to 500 ms, parameter k is set from 1 to 100. Besides, if whole channel realization records are considered, the record size for one link is 72×10^4, i.e., $N = 72\times10^4$.

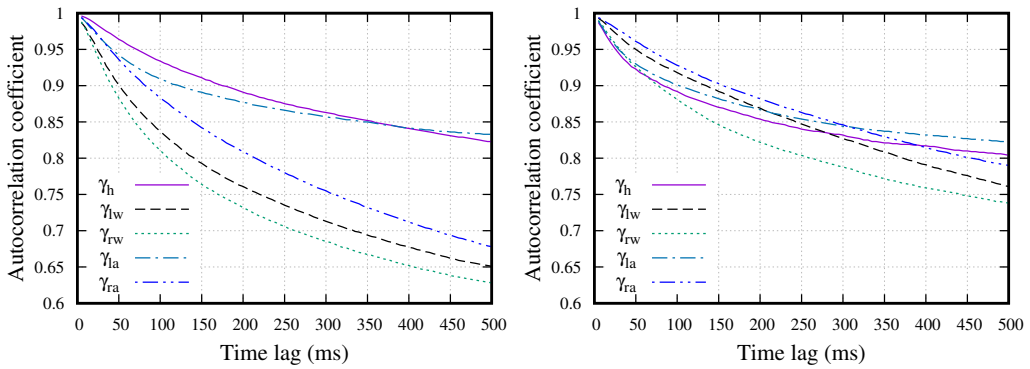

(a) Channel dataset 1 (CD_1) (b) Channel dataset 9 (CD_9)

Figure 3.18: The autocorrelation in two typical channel datasets.

First, two channel datasets are picked to show the autocorrelation variation between different links and different test subjects. Figure 3.18 shows the autocorrelation coefficients of the five on-body channels. The results displayed in Figure 3.18 (a) are calculated based on the first channel dataset performed by male subject 1, i.e., CD_1, and the results of Figure 3.18 (b) correspond to the first channel dataset from female subject 1, i.e., CD_9. Clearly, due to the variations of activities, environment, and sensor position, the autocorrelation of on-body channels varies with the change of test subject and the location of the receiver. For example, the autocorrelation coefficient of channel "SN_{RW}-Hub" (denoted as γ_{rw}) drops rapidly with the increase of time lag in CD_1. Whereas, γ_{rw} exhibits a much smoother and smaller decline in CD_9.

However, in spite of the discrepancy resulting from different test subjects and different sensor positions, all five on-body channels exhibit significant autocorrelations characteristics within a time lag of 500 ms. To have more insights into the on-body channel autocorrelation, we explore the ensemble average of autocorrelation coefficients over all 16 channel datasets. As shown in Figure 3.19, $\bar{\gamma}_h$, $\bar{\gamma}_{lw}$, $\bar{\gamma}_{rw}$, $\bar{\gamma}_{la}$, $\bar{\gamma}_{ra}$ represent the ensemble average of autocorrelation coefficient for channel "SN_H-Hub", "SN_{LW}-Hub", "SN_{RW}-Hub", "SN_{LA}-Hub" and "SN_{RA}-Hub", respectively. If the coherence time is defined as the period when the autocorrelation coefficient is above 0.7, the average coherence

times for the five on-body channels all exceed 500 ms, which is much longer than the coherence time in the monotone walking or running activity scenarios [132] (23 - 73 ms). The main reason may be because the daily scenarios are mixed with multiple activities, but most activities are relatively static, e.g., standing and sitting. More specifically, the channel between the torso and the head exhibits the most striking autocorrelation. It is mainly because the relative distance, as well as the shadowing effect in this channel, are more stable than the other four channels. Besides, the channels between the torso and two ankles show a more significant autocorrelation than the channels between the torso and two wrists. The main reason for this phenomenon may be because the movement of upper limbs is more drastic than lower limbs.

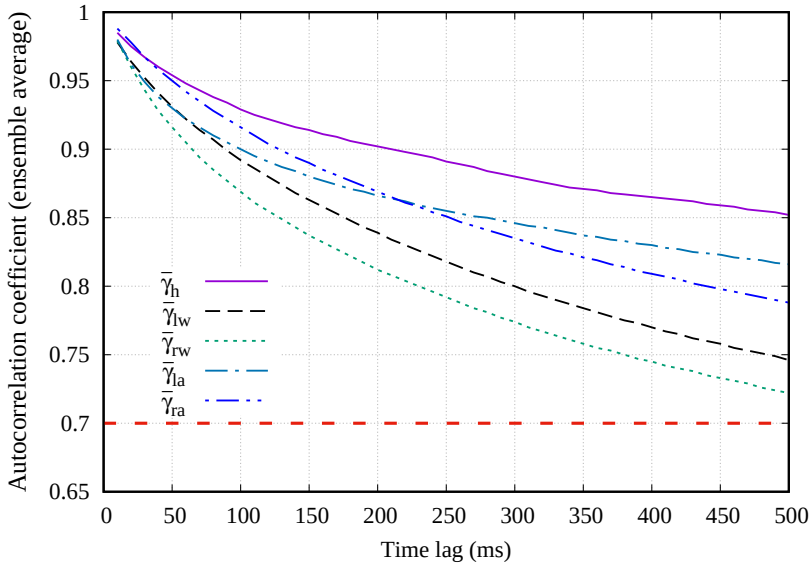

Figure 3.19: Ensemble average autocorrelation vs. time lag.

Next, instead of calculating the autocorrelation coefficient based on the whole records in one channel datasets, i.e., $N = 720,000$, we try to explore the variation of autocorrelation within a single channel dataset. Taking the channel dataset CD_1 as an example, Figure 3.20 exhibits the variation of autocorrelation when the time lag is 100 ms, i.e., k=20. In particular, we recalculate the autocorrelation coefficient based on the channel gain records in the past 2 seconds, i.e., $N = 400$. As shown in Figure 3.20, for the channel dataset collected from one test subject, the autocorrelation coefficient varies dramatically in the timeline. For example, γ_{rw} in the 4^{th} second is around 0.4, while it sharply increases in the next one second, and reaches to the maximum (around 0.9) in the 5^{th} second. The fluctuation of autocorrelation is mainly due to the variety of activities in the human daily life.

In summary, the autocorrelation of on-body channels varies with the change of test subject and the location of the receiver. However, in the daily scenarios, the on-body channels exhibit a significant autocorrelation within a time lag of 500 ms. This general characteristic

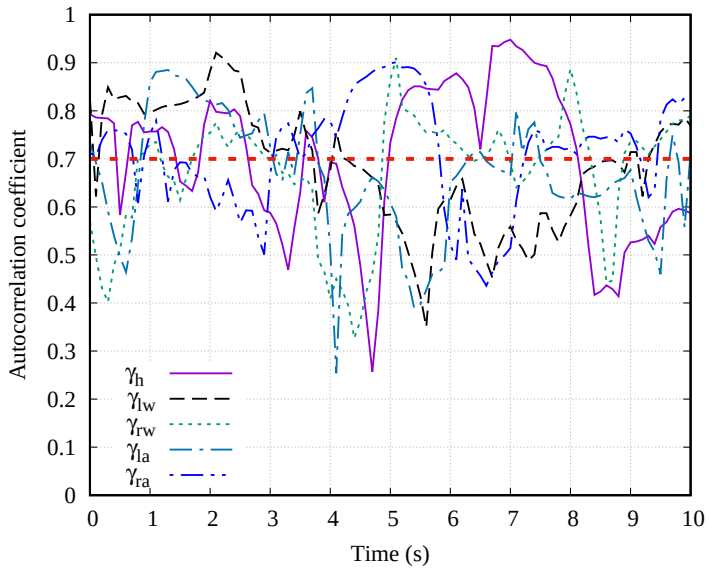

Figure 3.20: The autocorrelation variation over a time span of 10 seconds, time lag = 100 ms, CD_1.

may provide a great potential in channel condition estimation. This untapped feature has inspired us to optimize the transmission power control and TDMA slot scheduling which will be detailed in Chapter 5 and Chapter 6. In addition, due to the dynamic variation of body's shadowing effect and reflection from surrounding objects, the autocorrelation for a specific on-body channel on a certain subject fluctuates in the timeline. Accordingly, if we want to predict the channel condition by using the on-body channel autocorrelation, the autocorrelation coefficient should be kept up to date.

3.4.3 Outage Analysis

In this thesis, the "outage" refers to the event where receiver side fails to receive the packets from the transmitter because the RSSI is below the Rx sensitivity. Investigating the characteristics of outage is meaningful for designing more reliable transmission schemes. In this section, the Rx sensitivity is set to -91 dBm, -86 dBm, -81 dBm, and -76 dBm, respectively, to show the outage feature of real on-body channels in daily scenarios. Specifically, the 16 channel datasets (i.e., $CD_1, CD_2, \ldots, CD_{16}$), are used to analyze three important second-order statistics, namely *outage duration*, *outage interval* and *outage magnitude*.

• Outage Duration

When the RSSI is below the Rx sensitivity of the receiver, the corresponding link is experiencing an outage. *Outage duration* refers to the length of a period when outage occurs. First, the sum of duration corresponding to four different Rx sensitivity configurations are

Table 3.2: The sum duration of outage in different Rx sensitivity configurations.

Rx sensitivity	-91 dBm	-86 dBm	-81 dBm	-76 dBm
Sum duration of outage (ms)	14,230,995	37,962,745	91,445,735	180,699,030

presented in Table 3.2. As expected, with the increase of Rx sensitivity, on-body channels tend to experience more outage.

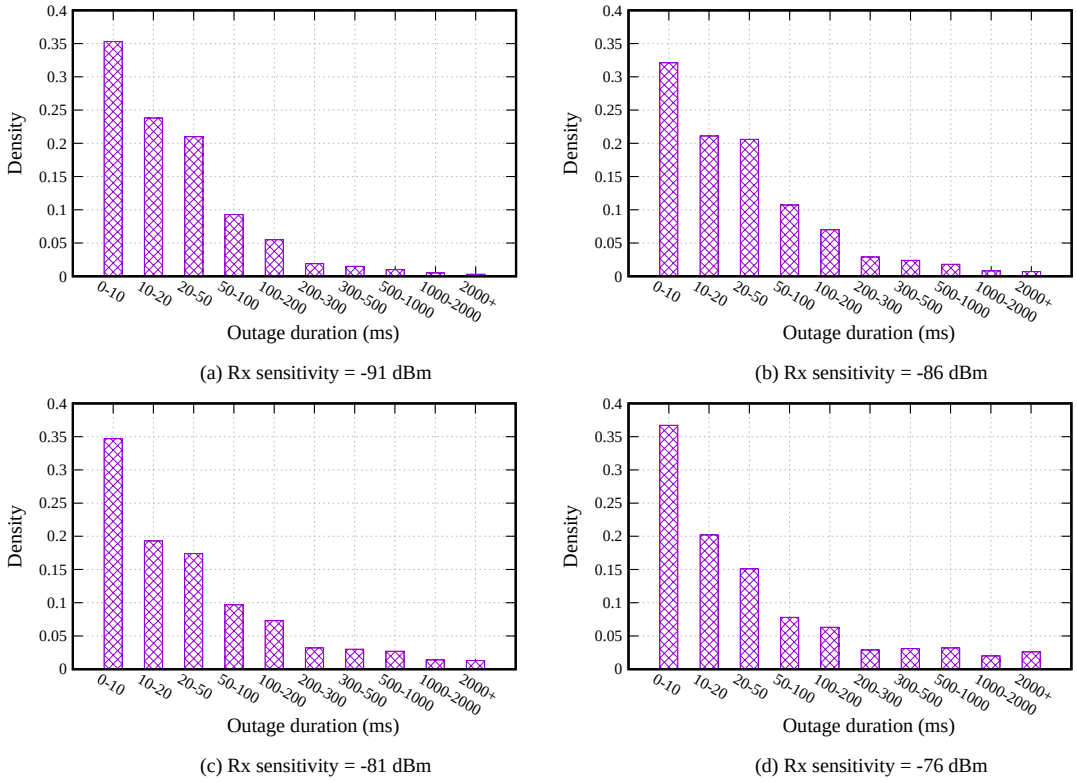

(a) Rx sensitivity = -91 dBm

(b) Rx sensitivity = -86 dBm

(c) Rx sensitivity = -81 dBm

(d) Rx sensitivity = -76 dBm

Figure 3.21: The outage duration distributions corresponding to different Rx sensitivity configurations.

Next, we present the distributions of *Outage duration*. Figure 3.21 shows the statistical result of outage duration when the Rx sensitivity is set to four different levels. We notice that the shortest outage (outage duration $\leqslant$ 10 ms) always composes the biggest portion (from 32.1% to 36.7%), regardless of the Rx sensitivity. On the other hand, if we define an outage longer than 500 ms as a "long outage", the proportion of "long outage" events exhibits a perceptible rise with the increase of Rx sensitivity, especially for the outage lasting longer than 2,000 ms.

Outage duration is crucial for the scheduling of retransmission, relay cooperation and DSS (Dynamic Slot Scheduling). For instance, given that over 60% outage duration exceed 10 ms, instead of the immediate retransmission after a packet loss, the cooperative communication assisted by the relay node might be a better choice.

• **Outage Interval**

Outage interval is defined as the interval between two neighboring outages. Figure 3.22 shows the outage interval distribution when Rx sensitivity is set to different levels. Since a higher Rx sensitivity causes more outages, the outage interval shortens with the increase of Rx sensitivity. Taking the interval longer than 2,000 ms as an example, when the Rx sensitivity is set to -91 dBm, around 9% of outage intervals are longer than 2,000 ms. The percentage drops to 1.6% when the Rx sensitivity is set to -76 dBm.

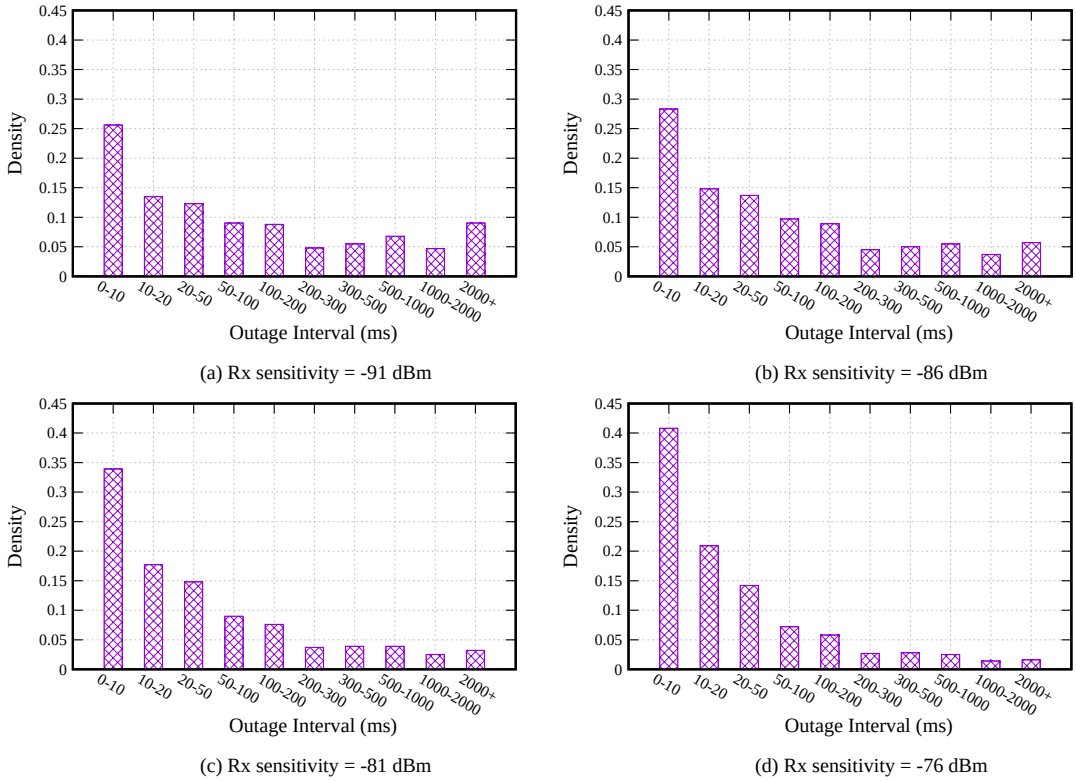

(a) Rx sensitivity = -91 dBm

(b) Rx sensitivity = -86 dBm

(c) Rx sensitivity = -81 dBm

(d) Rx sensitivity = -76 dBm

Figure 3.22: The outage interval distributions corresponding to different Rx sensitivity configurations.

• **Outage Magnitude**

Outage magnitude is the maximum fade depth during the period of outage. In other words, it is the maximal magnitude of $(Rx\ sensitivity - RSSI)$ for the whole duration of one outage, hence outage magnitude is always greater than 0 dB. The outage magnitude is an important indicator of the level of signal attenuation when the link encounters an outage, which is an important factor for the effectiveness of TPC (Transmission Power Control) methods. An outage with the outage magnitude small than 1 dB is called a light outage. The results in Figure 3.23 show that the light outage always possesses the greatest proportion, and the proportion of light outage tends to be higher with the increase of Rx sensitivity. Besides, the proportion of the outage with *Outage magnitude* greater than 30

dB apparently rises with the increase of Rx sensitivity.

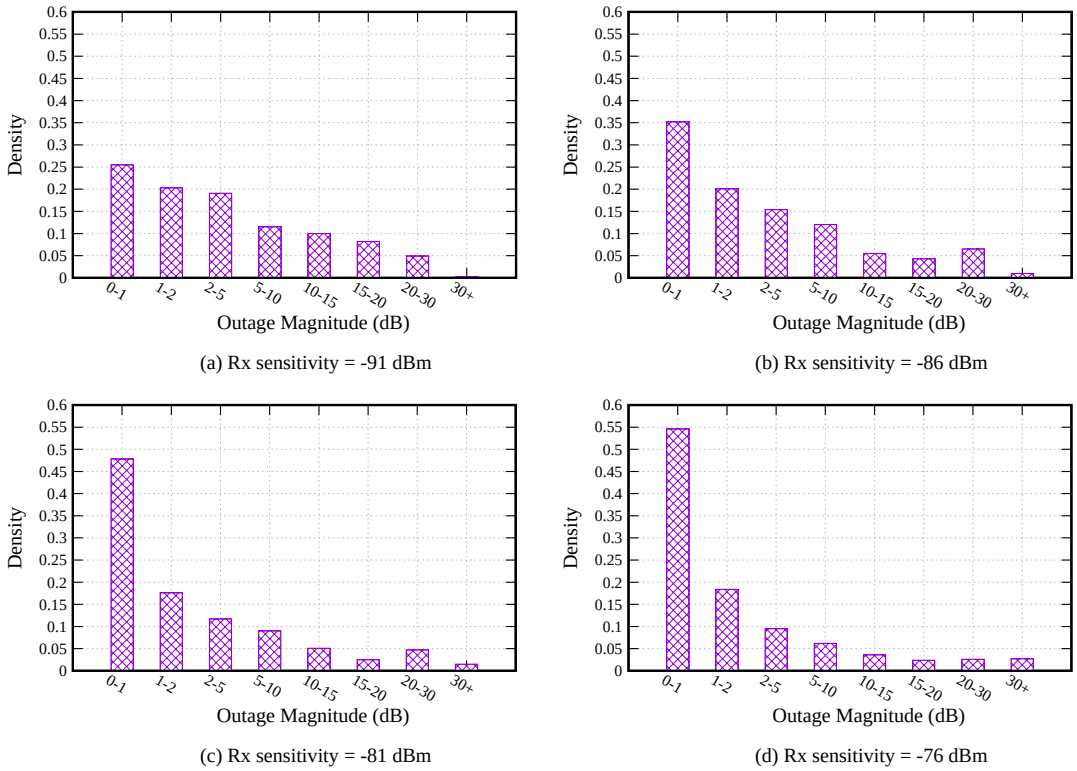

(a) Rx sensitivity = -91 dBm

(b) Rx sensitivity = -86 dBm

(c) Rx sensitivity = -81 dBm

(d) Rx sensitivity = -76 dBm

Figure 3.23: The outage magnitude distributions corresponding to different Rx sensitivity configurations.

3.5 Chapter Summary

In this chapter, we first detail the customized portable wireless transceiver for collecting realistic WBAN channel data. These wireless transceivers are used to measure the channel gain in two typical dynamic WBAN scenarios, i.e., walking scenarios and daily life scenarios. The measurement results confirm that body shadowing is a predominant factor for signal attenuation in the 2.4GHz ISM band. In the walking scenarios, a detailed illustration of the variation of the RSSI values and some second-order characteristics (autocorrelation, cross-correlation and path loss discrepancy) are derived. Strong periodicity is observed due to the swing of upper limbs. Interestingly, although the cross-correlation between on-body channels is not significant, the PLD (Path Loss Discrepancy) tends to remain big for a large proportion of time. These novel channel characteristics may facilitate more efficient system design and system evaluation schemes, including but not being limited to efficient network resource management and efficient cross-layer cooperative communication protocols. For example, motivated by the significant PLD in walking scenarios, we propose a novel cross-layer transmission scheme to achieve a better balance between energy consumption and throughput in Chapter 4.

As for the second dynamic scenarios: daily scenarios with mixed activities. We first focus on the autocorrelation of on-body channels. Statistical results show that the autocorrelation of on-body channels varies with changes of the test subject and the location of receivers. Besides, for a specific on-body channel, the channel autocorrelation also fluctuates in the timeline, due to the dynamic variation of body shadowing effects and the reflection from surrounding objects. However, in overall, the on-body channels in daily scenarios still exhibit a significant autocorrelation within a time lag of 500 ms. In addition, the outage analysis for on-body channels are provided from the perspective of *outage duration*, *outage magnitude*, and *outage interval*. These channel characteristics may provide important information to facilitate the design of more practical transmission schemes.

Chapter 4

Cooperation-Based Network Coding Scheme for Walking Scenarios in WBANs

4.1 Introduction

WBAN systems have strict energy constraints as frequent change of batteries is inconvenient or even infeasible. Besides, sensor nodes are usually placed either in or on the human body, thus the maximum radiated transmission power is restricted to comply with the limitation of Specific Absorption Rate (SAR) of local regulatory bodies (the limitation of Federal Communications Commission is 1.6 W/Kg). On the other hand, up to 10 Mbps throughput should be offered to satisfy the required set of entertainment and healthcare services [4]. It is a challenging task to maintain a high throughput while fulfilling the specific energy efficiency requirement of WBANs.

As demonstrated in the literature and our experiment works in Chapter 3, propagation paths in WBANs can experience severe fading due to different reasons, such as energy absorption, reflection, diffraction, and shadowing by the body. All these unique features lead to high packet losses. Relay nodes deployed outside of the human body might possess better channels and less stringent energy limitations. Therefore, cooperative communication (CC) [133] has received considerable interest in recent years [134]–[137]. Initial solutions apply the existing methods, which were proposed for general Wireless Sensor Networks (WSNs), to WBANs. These schemes may not be optimized for the unique challenges and specific characteristics of WBANs, such as spatial cross-correlation, stringent trade-off between energy requirement and throughput gains, and QoS requirements.

Due to the broadcast nature of wireless networks, Network Coding (NC) [2], which enables nodes to code or mix packets (or symbols) before forwarding, is a potential method to produce a significant improvement in the throughput, reliability, manageability, and

QoS of wireless networks [88], [90]. As introduced in Chapter 2, the applications of NC in WBANs are still an emerging area. Most existing works explore the expansions of conventional NC schemes, without considering the particular characteristics of WBAN channels.

One particular feature of WBANs is that the signal attenuation is significantly affected by the shadowing of body tissues in addition to the distance between two devices. In other words, the movement and posture of the human body have a dramatic effect on the strength of the received signal. Based on the measurement results presented in Chapter 3, the PLD (Path Loss Discrepancy) is significant in walking scenarios. Motivated by this characteristics, we propose a novel NC transmission scheme to achieve a better balance between throughput and energy consumption. In our scheme, two correlated sensors are allocated to the same uplink interval, i.e., they transmit data concurrently. This method is referred to as Aggregative Allocation (AA) in our scheme. The received signal by the relay nodes is, therefore, a combination of the two signals, mixed at the physical layer. The relay nodes forward the combination to the hub, and the hub performs the ANC (Analog Network Coding) decoding processes [92], [125], [126]. Since AA method is combined with ANC, our scheme is referred to as A3NC (AA+ANC). We detail the design and implementation of A3NC on the basis of IEEE 802.15.6 [4]. Moreover, in this chapter, we develop a mathematical model and a simulation model to carry out the performance evaluations.

The contributions of this chapter are as follows:

• Development of a new NC transmission based on the special characteristics of on-body channels in walking scenarios.

• The channel gain data collected from our measurement campaign are imported into the IEEE 802.15.6-compatible simulation model to evaluate the performance of A3NC. Simulations show that the proposed A3NC achieves a better performance with respect to upload throughput, energy efficiency, and throughput balance perspectives.

• To deepen the understanding of all key parameters that affect the system performance, we provide the mathematical model to explore the performance from all three perspectives, namely upload throughput, energy efficiency, and throughput balance.

The content of this chapter has been published in our papers [125], [126].

The rest of the chapter is organized as follows. In Section 4.2, the system model is presented. Then, the proposed A3NC scheme is detailed in Section 4.3. In Section 4.4, the mathematical model is provided. Performance evaluation results are presented in Section 4.5. Finally, Section 4.6 concludes the chapter.

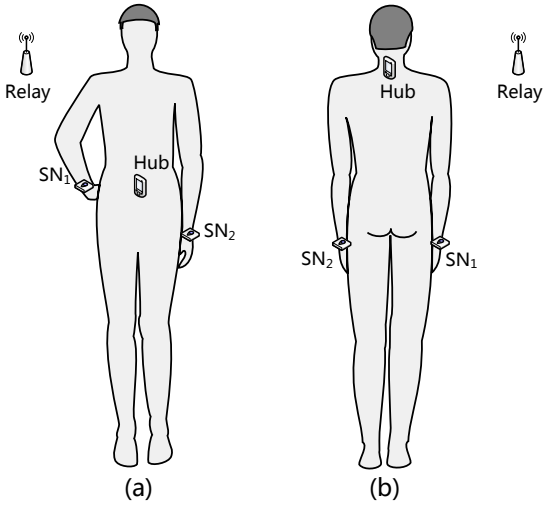

Figure 4.1: Deployment of the sensors, relay and hub.

4.2 System Model

In this section, we first present the network model for typical walking scenarios. Then channel models, including the on-body channel and relay channel, are introduced. Finally, the notations utilized throughout this chapter are presented.

4.2.1 Network Model

We consider the walking scenarios where two sensors (SN_1 and SN_2) mounted on the wrists communicate with a hub, and a relay node deployed outside the human body is optional. As the hub is expected to be larger than a sensor node, the torso is considered to be a preferable part to mount the hub. In this chapter, we consider two typical device deployments as depicted in Figure 4.1, where the hub is placed on the abdomen (attached to the belt buckle) or on the back collar. The main task for the sensors is to continually upload monitoring data to the hub with or without the help of the relay node. All wireless devices operate in the half-duplex mode, and Time Division Multiple Access (TDMA) is used to schedule the channel resource.

4.2.2 Channel Model

Some current works, including our paper [125], simply utilize the distance-based formulas, e.g., Friis transmission formula [138], to quantify the strength of received signal power. However, the path loss of on-body channels in WBANs is affected by many factors, such as the shadowing effect of human tissues and the mobility of the human body. In this chapter, the wireless channels in the walking scenarios are classified into two categories: on-body channel and relay channel (as shown in Figure 4.2). Since only the sensors and the hub are deployed on the body, the channels between the sensors and the hub are named

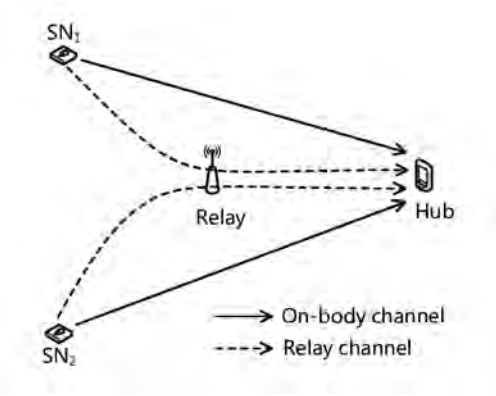

Figure 4.2: The on-body channels and relay channels.

the on-body channels. On the other hand, the channels to or from the relay node are called relay channels.

• **On-body Channel Model**

Due to the high variability of on-body channels, neither distance-based nor other formula-based methods seems to be sufficient to describe the on-body channel condition, especially in the activity scenarios. Therefore, adopting channel gain datasets collected from the real walking scenarios to model the on-body channels is a better choice. The portable wireless transceivers introduced in Chapter 3 are used to collect the realistic on-body channel gain data. As demonstrated in [117] and [128], in narrowband communication environments, the on-body channels show prominent reciprocity, which means the channel profiles of a downlink and an uplink are approximately the same. Therefore, these datasets collected from the experiment are utilized to model the on-body channels, including downlinks and uplinks. More details about these experiments and the analysis of channel datasets can be found in Chapter 3.

• **Relay Channel Model**

In the context of WBANs, due to severe fading caused by body shadowing, the relay node may improve the transmission reliability. In this work, we assume the relay node is deployed outside but near human body with light obstacle and shadowing from adjacent objects, the off-body channel is considered to be more stable than the on-body channel. In this work, the channel $SN_i - relay$ and channel $relay - hub$ are collectively called as "relay channel". Besides, since the swing motions of two arms are symmetrical when the human is walking, the average packet delivery ratios (PDRs) tend to be the same for the two relay channels, i.e., $SN_1 - relay - hub$ and $SN_2 - relay - hub$. Accordingly, we assume the average PDRs of the two relay channels are the same.

4.2.3 Notations

R (Kbps) refers to the transmission rate of the upload data from the sensor to the hub, which is assumed to be the same for the two sensors. L_p (Kbits) denotes the length of one packet. T_s refers to the length of one superframe, and T_c is the total time assigned to the two sensors and the relay node (if exist). Both T_s and T_c are in unit of second. β_i represents the average PDR of the channel $SN_i - hub$ when neither AA and CC are adopted. β_r is the average PDR of the relay channel $SN - relay - hub$. As mentioned before, the two relay channels are assumed to have the same β_r. In the proposed A3NC scheme, two sensors share a common time period to upload monitoring data. Therefore, some packets may be lost due to the signal collisions, and we denote the average Packet Loss Ratio (PLR) caused by collisions as e. Note that β_i is measured when the channel is only occupied by SN_i, without taking the packet losses caused by signal collisions into account. U_i denotes the actual upload throughput from SN_i to the hub with the influence of fading and collision. $\mathcal{P}_w$ is the working power of the sensor node, and we assume the two sensors have the same working power.

4.3 Joint Analog Network Coding and Channel Allocation

In A3NC, the Aggregative Allocation (AA) mechanism and the ANC [92] technique are incorporated to improve the system throughput and energy efficiency in walking scenarios. AA is the implementation method of simultaneous transmissions in IEEE 802.15.6. The ANC technique mainly focuses on the problem of energy efficiency, which is a crucial performance metric for WBANs. These two components of the proposed A3NC scheme are described below.

4.3.1 Aggregative Allocation

As mentioned in Section 3.4, a significant PLD (Packet Loss Discrepancy) between the two on-body channels is observed in a majority of cases of walking scenario. Therefore, by simultaneous transmission from the two sensors, there is a still a good chance of decoding the packets over the good channel. The significant PLD in the walking scenarios motivates us to design a transmission mechanism which supports simultaneous transmissions from different source nodes. The proposed AA mechanism aims to make the simultaneous transmission compatible with the IEEE 802.15.6 standard. As depicted in Figure 2.3 (Chapter 2), a superframe is divided into Exclusive Access Phases (i.e., EAP1 and EAP2), Random Access Phases (i.e., RAP1 and RAP2), Managed Access Phases (MAP) and a Contention Access Phase (CAP). In A3NC, only the RAP1 and one MAP are adopted to

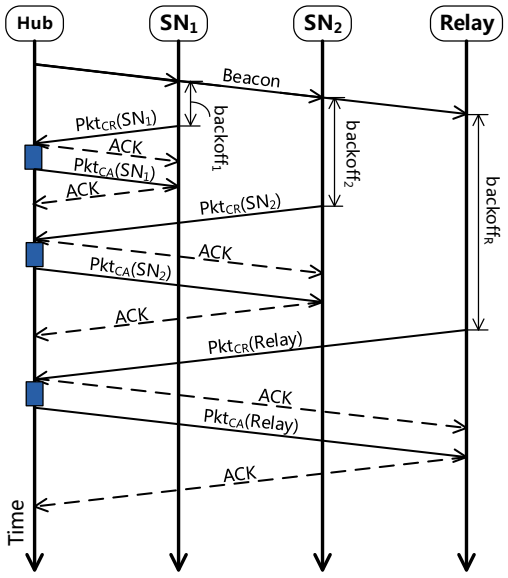

Figure 4.3: Transaction procedure of A3NC in RAP1.

compose the superframe in the beacon mode with superframes. Compared to the contention-based methods, TDMA channel access method provides better energy efficiency. Therefore, TDMA method is utilized to upload the data from the sensors and the relay to the hub. As suggested by the IEEE 802.15.6 standard, the TDMA time slots should be assigned to the MAP duration. This is the reason that the MAP is utilized to upload the data from the sensors or the relay to the hub. As for the RAP1 period, it precedes MAP to carry the transactions of the connection request and assignment on the basis of CSMA/CA method, which is the suggested approach for RAP in IEEE 802.15.6. These transactions in the RAP1 period are essential for the AA mechanism, as they assign a shared transmission period to a pair of sensors with a significant PLD and facilitate the cooperation of relay (the necessity of relay node will be discussed in Section 4.3.2). Besides, we adopt the one-periodic allocation, i.e., the assigned intervals are reoccurring in every beacon period (superframe). The details of the assignment transactions are illustrated in Figure 4.3.

The transactions depicted in Figure 4.3 occur in the RAP1 phase. Initially, the hub broadcasts the beacon frame to the sensors (SN_1 and SN_2) and relay, and all receivers contend for the channel access by a CSMA/CA mechanism. Suppose that SN_1 randomly chooses the smallest backoff value. SN_1 transmits the connection request packet (Pkt_{CR}) to the hub to request an uplink interval in the MAP. Then, the hub sends a connection allocation packet (Pkt_{CA}) to SN_1 to allocate a Scheduled Uplink Interval (SUI). The processes of allocating an SUI to SN_2 and the relay are similar. In addition, the relay's Scheduled Downlink Interval (SDI) is allocated to the same period with the sensors' SUI in order to receive the packets from the sensors, which will be detailed in the next subsection. Note that handling the received Pkt_{CR} in the hub is the key process for the AA mechanism, which is also marked as three blue rectangles in Figure 4.3.

The detail of processing Pkt_{CR} in the hub is depicted in Algorithm 1. We add a new

field, named PID (Pair Identifier), in the header of Pkt_{CR} to assist the relay cooperation. More specifically, the two sensors and their relay have the same PID value, and the SDI of the relay is assigned to overlap with the SUI of the two sensors to receive the packets from the two sensors. $NID_{assigned}$ denotes the NID (Node Identifier) assigned to the node. The hub maintains two independent maps, Map_{NID} and Map_{PID}. The Map_{NID} contains the mapping between MAC address and NID, and the Map_{PID} contains the mapping between PID and SUI or SDI. As illustrated in Algorithm 1 (Lines 2-5), a dedicated NID is assigned to each node (sensor or relay) with the help of Map_{NID}. Consequently, correlated sensors with the same PID share the same SUI by searching Map_{PID} (Lines 7-13). If Pkt_{CR} is sent by a relay, the relay node will be allocated with the SDI overlapped with the SUI of the two sensors with the same PID. Meanwhile, an SUI is allocated to the relay to forward data to the hub (as detailed in Lines 15-21). Note that SDI is not essential for sensors since their primary task is uploading the monitoring data to the hub.

After channel allocation, two sensors are allocated to share the same SUI, and the SDI of the relay is overlapped with the SUI of the two sensors. From the perspective of the hub, the two correlated sensors can be looked as one virtual sensor node. Meanwhile, as the beacon period is fixed, a longer SUI can be allocated to the sensors, allowing the AA technology to improve the system throughput in walking scenarios. The mathematical analyses will be presented in the Section 4.4.

4.3.2 Cooperative Communication with Analog Network Coding

In this subsection, we first explain the reasons for introducing the relay node. Firstly, by adopting pure AA without employing relay nodes, one of the sensors experiences more severe fading compared to the other one, which is a waste of energy. In other words, AA may achieve the throughput improvement at the cost of additional energy consumption, which is strictly limited in WBANs. Secondly, in the case that two correlated sensors experience different Packets Delivery Ratios (PDR), AA may cause the sensor with the lower PDR to experience even a worse throughput performance than the conventional TDMA scheme. These two issues can be addressed effectively by deploying a relay node.

Since two sensors broadcast their signals concurrently, the traditional decode-and-forward relay strategy is impractical [92]. Similarly, the digital network coding (DNC) technology [88], [89], which requires the relay node to decode and re-encode the packets in the MAC layer, is also unrealistic. Given that concurrently transmitted packets from two sensors are mixed naturally at PHY layer and the hub can receive at least one sensor's packet with a high probability, PHY layer network coding technology may be a better choice. In our proposed A3NC, the Analog Network Coding (ANC) technology originally proposed in [92] is adopted. The relay node simply amplifies and forwards the mixed signal to the hub without any decoding, and the hub undertakes the decoding using the

Algorithm 1: Uplink and downlink allocation

Input: Receive a Pkt_{CR} from radio layer

Get PID, MAC address, required time slots from Pkt_{CR};
if *Find a record in* Map_{NID} *by MAC Address* **then**
    Set $NID_{assigned}$ by Map_{NID};
else
    $NID_{assigned}$ = current free connected NID;
end
if Pkt_{CR} *comes from a sensor node* **then**
    if *Find a record in* Map_{PID} *by* PID **then**
        Set $SUI.startSlot$ and $SUI.endSlot$ by the record;
    else
        Set $SUI.startSlot$ and $SUI.endSlot$ from the end of Map_{PID};
        Update Map_{PID};
    end
else
    if *Find a record in* Map_{PID} *by* PID **then**
        Set $SDI.startSlot$ and $SDI.endSlot$ by the record;
        Set $SUI.startSlot$ and $SUI.endSlot$ from the end of Map_{PID};
        Update Map_{PID};
    else
        Discard Pkt_{CR};
    end
end
Construct a Pkt_{CA} based on $NID_{assigned}$, $SDI.startSlot$, $SDI.endSlot$, $SUI.startSlot$ and $SUI.endSlot$;
Add Pkt_{CA} to sending buffer;

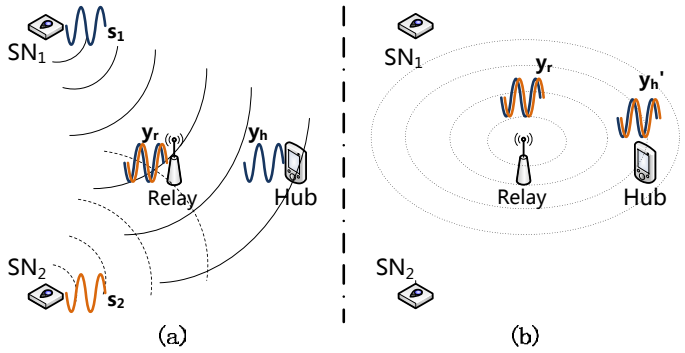

Figure 4.4: Cooperative communication with ANC. (a) Phase 1: sensors' SUI. (b) Phase 2: relay's SUI.

mixed signal and one original signal. Perfect synchronization is not required in the ANC technology. Besides, since decoding of packets is not required, the complexity of the relay node is reduced.

Similar to [92], the MSK (Minimum Shift Keying) is adopted as an example modulation scheme to explain the main principle of ANC, because it has a simple demodulation algorithm as well as good bit-error properties. Figure 4.4 illustrates how to incorporate ANC with cooperative communication. The cooperation procedure can be divided into two phases, which correspond to the SUI of the two sensors (also identical to the SDI of the relay) and the SUI of the relay. As depicted in Figure 4.4 (a), the signals transmitted from SN_1 and SN_2, respectively, can be represented as

$$s_1[n] = A_s[n]e^{i\theta_s[n]} \tag{4.1}$$

$$s_2[n] = B_s[n]e^{i\phi_s[n]} \tag{4.2}$$

where $A_s[n]$ and $B_s[n]$ are the amplitudes of the n-th sample, and $\theta_s[n]$, $\phi_s[n]$ are their phases.

If the signal from SN_2 (i.e., s_2) experiences a severe fading and the hub receives successfully the signal from SN_1, the received signal at the hub, $y_h[n]$, can be represented as

$$y_h[n] = hA_s[n]e^{i(\theta_s[n]+\gamma)} + w(n) \tag{4.3}$$

where $he^{i\gamma}$ is the complex coefficient for the channel $SN_1 - hub$ and $w(n)$ is the additive Gaussian noise. For brevity, $noise$ term will be ignored in our subsequent formulas.

Meanwhile, the relay node receives and stores the mixed signal $y_r[n]$ from two sensors

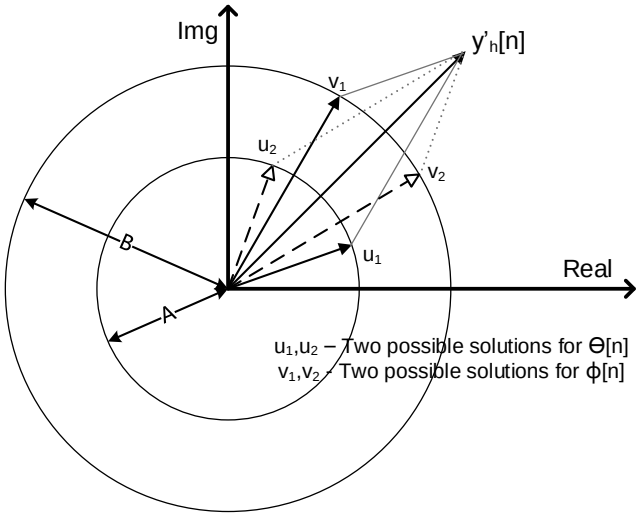

Figure 4.5: Two possible solutions for the phase computation.

as follows:

$$y_r[n] = h_1 A_s[n] e^{i(\theta_s[n]+\gamma_1)} + h_2 B_s[n] e^{i(\phi_s[n]+\gamma_2)} \tag{4.4}$$

where h_1 and γ_1 are the channel gain and phase shift respectively for the channel $SN_1 - Relay$, and h_2 and γ_2 are those for the channel $SN_2 - Relay$.

In the second phase (i.e., the SUI of the relay node), which is shown in Figure 4.4(b), the relay node amplifies the ANC mixed signal $y_r[n]$ and forwards it to the hub. Since the relay node only amplifies and forwards $y_r[n]$, for simplicity, we assume the received signal at the hub is the same as the mixed signal at the relay, which can be presented as

$$y'_h[n] = A[n] e^{i\theta[n]} + B[n] e^{i\phi[n]} \tag{4.5}$$

where $A = h_1 A_s$, $B = h_2 B_s$, $\theta[n] = \theta_s[n] + \gamma_1$, and $\phi[n] = \phi_s[n] + \gamma_2$. In the complex plane, $y'_h[n]$ is a sum of two vectors, which have lengths A and B respectively. As shown in Figure 4.5, the two vectors lie on two circles with radii A and B. As proved in [92], there exist two solutions for the pair ($\theta[n]$, $\phi[n]$)

$$\theta[n] = arg(y'_h[n](A + BD \pm iB\sqrt{1-D^2})) \tag{4.6}$$

$$\phi[n] = arg(y'_h[n](A + AD \mp iA\sqrt{1-D^2})) \tag{4.7}$$

where $D = \dfrac{|y'_h[n]|^2 - A^2 - B^2}{2AB}$, $|y'_h[n]|$ is the norm, and arg is the angle of the complex number. Note that for each solution $\theta[n]$, there is a unique solution for $\phi[n]$. Specifically, if $\theta[n] = arg(y'_h[n](A + BD + iB\sqrt{1-D^2}))$, the corresponding solution of $\phi[n]$ is $arg(y'_h[n](A + AD - iA\sqrt{1-D^2}))$. In addition, the amplitude of the two singnals (i.e., A and B) can be estimated by the received signals [92].

The next step is to estimate the phase difference between the signals from two sensors, i.e., $\theta[n+1]-\theta[n]$ and $\phi[n+1]-\phi[n]$. Corresponding to two potential phase pairs at each sample time, there are four possible pairs of phase differences

$$(\Delta\theta_{xy}[n], \Delta\phi_{xy}[n]) = (\theta_x[n+1]-\theta_y[n], \phi_x[n+1]-\phi_y[n]) \;\; \forall x, y \in \{1,2\} \tag{4.8}$$

Since the channel of $SN_1 - hub$ is in a "good" condition, the hub knows the signal transmitted from SN_1, $y_h[n]$ (cf. Equation (4.3)). Thus, the hub knows the phase difference $\Delta\theta[n]$. Next, the hub picks the $\Delta\theta_{xy}[n]$ that produces the smallest deviation to the $\Delta\theta[n]$ as the optimal one, and the matching $\Delta\phi_{xy}[n]$ is the optimal phase difference for the signal from SN_2. In the last step, the hub obtains SN_2's bits based on these estimated phase differences.

Since the focus of this chapter is the characteristics of on-body channels and the combination of AA and ANC, many other decoding details of ANC, such as the estimation of amplitudes A and B and the alignment of pilot sequences, are omitted in the above example. More details of the ANC technology can be found in [92]. In addition, the complexity of the A3NC is relatively low with a time complexity $O(n)$, where n the number of sensors.

4.4 Performance Analyses

In this section, the performance of the proposed scheme is analyzed and compared to the existing schemes from three perspectives: total throughput, energy efficiency, and throughput balance. The AA mechanism and ANC cooperation are two key components of the proposed A3NC scheme. Three alternative schemes that do not employ both AA and ANC are considered for comparison, and their time slot schedules are depicted in Figure 4.6.

As shown in Figure 4.6, suppose a certain period T_c is allocated to the two sensors and the corresponding relay node. A3NC and the other three schemes adopt different scheduling in the period of T_c.

1. **Con-TDMA:** In the conventional TDMA scheme, denoted as Con-TDMA (Figure 4.6 (a)), T_c is split into two for the SUIs of the two sensors.

2. **Only-AA:** When the AA mechanism is employed but without the cooperative communication part of A3NC, we denote the transmission scheme as Only-AA (Figure 4.6 (b)). In Only-AA, the two sensors share the whole T_c concurrently.

3. **TDMA+DNC:** On the other hand, if each of the two sensors possesses an exclusive SUI, i.e., the AA mechanism is not adopted, and the relay node forwards the Digital Network Coding (DNC) packets to the hub, we call this approach as TDMA+DNC.

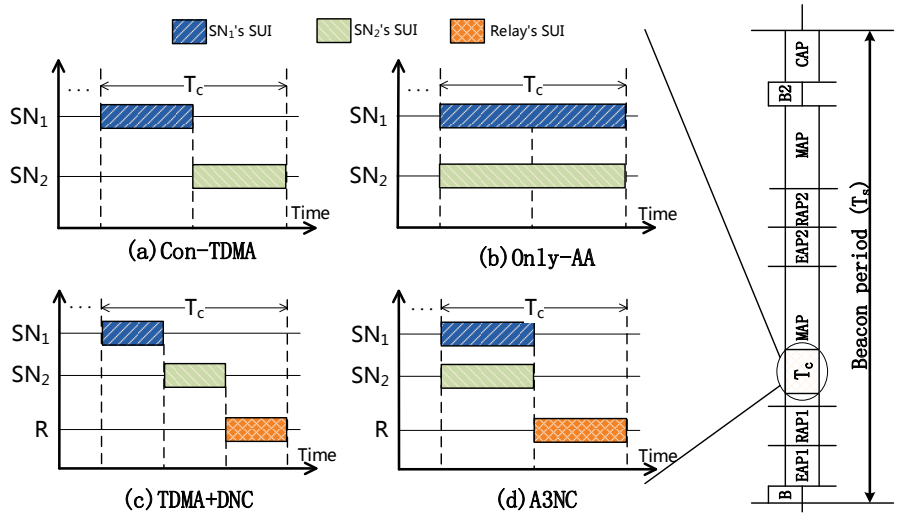

Figure 4.6: Slot schedules of four schemes.

In the TDMA+DNC scheme, the T_c is divided into three identical parts, the first two parts are allocated to the two sensors as the exclusive SUIs, and the third time interval is assigned to the relay node to forward the DNC packets (Figure 4.6 (c)).

4. **A3NC:** In the newly proposed scheme A3NC (Figure 4.6(d)), the two sensors are assigned to a shared SUI, and the ANC is adopted as the relay technology to improve the performance.

4.4.1 Throughput Analysis

Before analyzing the upload throughput of the four schemes, it is necessary to examine the packet loss ratio e in more detail. As introduced in Section 4.2.3, e is caused by signal collisions, which only occur when two sensors perform simultaneous transmissions in the MAP duration. Thus e only exists in Only-AA and A3NC. As presented in the next section, e in the typical walking scenario would be small enough (about 0.022) to be ignored. However, in order to explore the performance of A3NC in other situations, rather than being limited to walking scenarios, we consider e as a variable parameter in both mathematical and simulation analyses. Besides, we assume e for the two sensors to be identical due to their symmetry.

• Conventional TDMA

We first consider the Con-TDMA scheme without the cooperation of the relay node. In this scheme, every sensor is scheduled with a dedicated uplink interval. With the notations mentioned in Section 4.2.3, the expectation of upload throughput of SN_1, denoted as $E(U_1)$

(Kbps), can be calculated as

$$E(U_1)_{Con-TDMA} = (R \times \frac{1}{2}T_c \times \frac{1}{L_p} \times \beta_1 \times L_p) \times \frac{1}{T_s} = \frac{1}{2}\frac{RT_c\beta_1}{T_s} \tag{4.9}$$

Equation (4.9) is explained as follows. Since only two sensors share the time interval, every sensor occupies $\frac{1}{2}T_c$ upload interval; $R \times \frac{1}{2}T_c \times \frac{1}{L_p}$ is the number of packets transmitted in one beacon period by SN_1. $(R \times \frac{1}{2}T_c \times \frac{1}{L_p} \times \beta_1 \times L_p)$ is the amount of bits received by the hub. The calculation for the upload throughput of SN_2, i.e., $E(U_2)$, is similar. Thus, the expectation of the sum of upload throughput of the two sensors can be expressed as

$$E(U_1 + U_2)_{Con-TDMA} = \frac{1}{2}\frac{RT_c}{T_s}(\beta_1 + \beta_2) \tag{4.10}$$

• **Only-AA**

In the Only-AA scheme, since two sensors transmit simultaneously, the packet errors caused by signal collisions should be considered. The actual PDRs for SN_1 and SN_2 in this scheme are $(\beta_1 - e)$ and $(\beta_2 - e)$ respectively. Accordingly, the throughput of the two sensors can be expressed as

$$E(U_1 + U_2)_{Only-AA} = \frac{RT_c(\beta_1 - e)}{T_s} + \frac{RT_c(\beta_1 - e)}{T_s} = \frac{RT_c}{T_s}(\beta_1 + \beta_2 - 2e) \tag{4.11}$$

• **TDMA+DNC**

The TDMA+DNC scheme adopts DNC as the cooperative technology. As Figure 4.6 (c) shows, the relay node occupies the third time interval to transmit the network coding packets to the hub. Since the packet loss in the first two time slots may be recovered in the third time slot, the probability of effective cooperative communication should be taken into account to calculate the actual PDR (denoted as $\mathcal{B}_1$ and $\mathcal{B}_2$) of the TDMA+DNC scheme. If the result of whether the hub receives the packets from SN_1 is represented by a discrete random variable (D.R.V) X, then let $X = S$ denote the situation that the hub receives the packets from SN_1 successfully, and $X = F$ represents the failure of the hub to receive the packets from SN_1. Similarly, D.R.V Y and R denote the situations for SN_2 and the relay node respectively. Hence, $\mathcal{B}_1$ and $\mathcal{B}_2$ can be calculated as

$$\mathcal{B}_1 = P_{X,Y}(S,F) + P_{X,Y}(S,S) + P_{X,Y}(F,S)P_R(S) \tag{4.12}$$

$$\mathcal{B}_2 = P_{X,Y}(F,S) + P_{X,Y}(S,S) + P_{X,Y}(S,F)P_R(S) \tag{4.13}$$

where $P_{X,Y}$ is the joint probability that considers both D.R.V X and Y, and P_R denotes the probability of whether the hub receives the packets from the relay node. It is worth noting that $\beta_1 = P_{X,Y}(S,F) + P_{X,Y}(S,S)$, $\beta_2 = P_{X,Y}(F,S) + P_{X,Y}(S,S)$ and $\beta_r = P_R(S)$. Accordingly, $\mathcal{B}_1$ and $\mathcal{B}_2$ can be expressed as

$$\mathcal{B}_1 = \beta_1 + (\beta_2 - P_{X,Y}(S,S))\beta_r \tag{4.14}$$

$$\mathcal{B}_2 = \beta_2 + (\beta_1 - P_{X,Y}(S,S))\beta_r \tag{4.15}$$

For a general WBAN network, the probability that the packets from two sensors are received by the hub, i.e., $P_{X,Y}(S,S)$, can be calculated in a similar way as [136]. However, since we mainly consider the walking scenarios, $P_{X,Y}(S,S)$ can be approximated as

$$P_{X,Y}(S,S) \approx \begin{cases} 0; & \beta_1 + \beta_2 \leq 1 \\ (\beta_1 + \beta_2) - 1; & \beta_1 + \beta_2 > 1 \end{cases} \tag{4.16}$$

We derive the above approximation based on the following observations. Compared to the walking cycle (about 1000 ms - see Section 3.3), the superframe (about 100 ms) is relatively short. Moreover, the two upload intervals assigned to the two sensors are typically adjacent. So, based on the statistical results in Section 3.3.4, it is reasonable to assume the PLD between the two channels remains significant and stable in one superframe. To make the approximation in Equation (4.16) clear, suppose that each sensor only sends one packet in one superframe. Accordingly, in the case of $\beta_1 + \beta_2 \leq 1$, the hub tends to receive only one packet either from SN_1 or SN_2 with a high probability in one superframe, instead of receiving packets from both sensors simultaneously. On the other hand, in the case of $\beta_1 + \beta_2 > 1$, the received signal strength from the "bad" channel is still strong enough to decode, regardless of the big PLDs between the two channels. Note that the latter case is normally caused by the increase of Tx power of sensors. Therefore, based on Equations (4.14)-(4.16), the expected overall throughput can be obtained as

$$\begin{aligned} E(U_1 + U_2)_{TDMA+DNC} &= \frac{1}{3}\frac{RT_c\mathcal{B}_1}{T_s} + \frac{1}{3}\frac{RT_c\mathcal{B}_2}{T_s} \\ &\approx \begin{cases} \frac{1}{3}\frac{RT_c}{T_s}(\beta_1 + \beta_2)(1 + \beta_r); & \beta_1 + \beta_2 \leq 1 \\ \frac{1}{3}\frac{RT_c}{T_s}((\beta_1 + \beta_2)(1 - \beta_r) + 2\beta_r); & \beta_1 + \beta_2 > 1 \end{cases} \end{aligned} \tag{4.17}$$

• **A3NC**

As for the A3NC scheme, two sensors broadcast the data packets simultaneously in the first half period, and the ANC packet is relayed in the second half. This situation can be

considered as a combination of Only-AA and TDMA+DNC schemes. When calculating the actual PDRs, denoted as $\widetilde{\mathcal{B}}_1$ and $\widetilde{\mathcal{B}}_2$, both the cooperative communication and the packet loss caused by signal collision should be taken into account. The actual PDRs for SN_1 and SN_2 are expressed as

$$\widetilde{\mathcal{B}}_1 = (\beta_1 - e) + (\beta_2 - e)\beta_r \tag{4.18}$$

$$\widetilde{\mathcal{B}}_2 = (\beta_2 - e) + (\beta_1 - e)\beta_r \tag{4.19}$$

The first parts of Equations (4.18) and (4.19) refer to the PDRs for the SUI of the two sensors, and the second parts are the PDRs with the help of the relay node. Consequently, the upload throughput of the whole network can be written as

$$E(U_1 + U_2)_{A3NC} = \frac{1}{2}\frac{RT_c\widetilde{\mathcal{B}}_1}{T_s} + \frac{1}{2}\frac{RT_c\widetilde{\mathcal{B}}_2}{T_s} = \frac{1}{2}\frac{RT_c}{T_s}(\beta_1 + \beta_2 - 2e)(1 + \beta_r) \tag{4.20}$$

By comparing the analytical results of the four schemes, we have the following important observations.

Observation 1

If the packet loss ratio caused by signal collisions is below the quarter of $\beta_1 + \beta_2$, the throughput performance of Only-AA is better than that of Con-TDMA. That is

$$E(U_1 + U_2)_{Only-AA} \begin{cases} > E(U_1 + U_2)_{Con-TDMA}; & e < \frac{1}{4}(\beta_1 + \beta_2) \\ \leq E(U_1 + U_2)_{Con-TDMA}; & o.w. \end{cases}$$

Observation 2

The upload throughput of A3NC is always smaller than that of Only-AA because the PDR of the relay channel cannot exceed one, i.e., $\beta_r \leq 1$.

$$E(U_1 + U_2)_{A3NC} \leq E(U_1 + U_2)_{Only-AA}$$

.

Observation 3

The comparison between Con-TDMA and TDMA+DNC is complicated.

If $\beta_1 + \beta_2 \leq 1$, we have

$$E(U_1 + U_2)_{TDMA+DNC} \begin{cases} > E(U_1 + U_2)_{Con-TDMA}; & \beta_r > \frac{1}{2} \\ \leq E(U_1 + U_2)_{Con-TDMA}; & \beta_r \leq \frac{1}{2} \end{cases}$$

If $1 \leq \beta_1 + \beta_2 \leq \frac{4}{3}$, and we denote $Q = \frac{\beta_1 + \beta_2}{4 - 2(\beta_1 + \beta_2)}$, the relationship between these two

schemes can be expressed as

$$E(U_1+U_2)_{TDMA+DNC}\begin{cases} > E(U_1+U_2)_{Con-TDMA}; & \beta_r > Q \\ \leq E(U_1+U_2)_{Con-TDMA}; & \beta_r \leq Q \end{cases}$$

If $\beta_1+\beta_2 > \frac{4}{3}$, the throughput of TDMA+DNC cannot exceed that of Con-TDMA. That is

$$E(U_1+U_2)_{TDMA+DNC} < E(U_1+U_2)_{Con-TDMA}$$

Observation 4

When the PLR caused by signal collisions, i.e., e, is smaller than $\frac{1}{6}(\beta_1+\beta_2)$. The performance of A3NC scheme surpasses that of TDMA+DNC

$$E(U_1+U_2)_{A3NC} > E(U_1+U_2)_{TDMA+DNC}$$

It can be seen that both A3NC and Only-AA outperform the conventional schemes when the values of specific parameters (i.e. e, β_r and $\beta_1+\beta_2$) satisfy certain conditions. Detail performance evaluation based on walking datasets will be provided in the next section.

In addition, if the packet losses due to signal collisions and failed cooperations are small, i.e., $e \approx 0$ and $\beta_r \approx 1$, we can derive the upper bounds for the four schemes in the walking scenarios. For brevity, denote $M = \frac{RT_c}{T_s}(\beta_1+\beta_2)$. The upper bounds of upload throughput for four schemes are presented in Table 4.1. We notice that the upper bounds for Only-AA and A3NC are the same, i.e., $\frac{RT_c}{T_s L_p}(\beta_1+\beta_2)$, which achieve 2 and 1.5 throughput gains in comparison with Con-TDMA and TDMA+DNC respectively.

Table 4.1: The upper bounds of throughput.

	Con-TDMA	Only-AA	TDMA+DNC	A3NC
Expectation of throughput	$\frac{1}{2}M$	M	$\frac{2}{3}M$	M

4.4.2 Energy Efficiency Analysis

An effective MAC layer method for energy saving is prolonging sleep time of the sensors, which also means completing data transmission in a shorter active time. Generally, recharging and changing the battery in a hub are easier than in the sensors. The relay node is deployed out of human body. Hence, in this chapter, the energy efficiencies of hub and relay are not considered. Moreover, because the behaviors of hub, relay, and sensor nodes are repeated in each beacon period, we take the active time in one beacon period as an

Table 4.2: Energy efficiency comparison.

	Con-TDMA	Only-AA	TDMA+DNC	A3NC
T_{active}	T_c	$2T_c$	$\frac{2}{3}T_c$	T_c
EE	$\frac{1}{2}F$	$\frac{1}{2}F$	F	F

example. Note that the active state of the radio includes both Tx (transmitting) and Rx (receiving) states. Assuming the working power of sensors remains the same for both Rx and Tx states, the energy efficiency (EE) in Kbits/Joule can be defined as the ratio of the amount of uploading data and the power consumed in one beacon period

$$EE = \frac{E(U_1 + U_2)T_s}{T_{active}\mathcal{P}_w} \tag{4.21}$$

where T_{active} is the active time of the two sensors in one beacon period, and $\mathcal{P}_w$ is the working power of the sensor. $E(U_1 + U_2)$ is the expected sum of the upload throughput of the two sensors, and it has been analyzed before. We now focus on the T_{active}, which can be calculated from Figure 4.6. Similar to the analysis of throughput, if e=0, β_r=1 and denote $F = \frac{R(\beta_1+\beta_2)}{\mathcal{P}_w}$, from Equations (4.21), the upper bounds of EE are summarized in Table 4.2. From Table 4.2, the two cooperative schemes (TDMA+DNC and A3NC) achieve a twofold EE gain, compared to Con-TDMA and Only-AA.

Combining the results in Tables 4.1 and 4.2, we find that the A3NC scheme not only achieves the highest throughput upper bound but also retains the best energy efficiency. In other words, the A3NC scheme provides a better trade-off between network throughput and energy consumption.

4.4.3 Throughput Balance Analysis

The above analyses consider the total upload throughput of the two sensors. In this subsection, the throughput disparity between the two sensors (i.e., $E(U_1)$ and $E(U_2)$) is taken into account, instead of only considering their sum. The aim is to assess whether the proposed A3NC scheme may result in a severe throughput imbalance between the two sensors, for example, one sensor being completely starved. We define a new parameter called the balance factor (BF) to evaluate whether the transmission scheme can achieve a reasonable throughput balance between the two sensors. The balance factor BF is defined by the following equation

$$BF = \left| \log_2 \frac{E(U_1)}{E(U_2)} \right|$$

where $E(U_1)$ and $E(U_2)$ are the expected throughput of SN_1 and SN_2, respectively. If $BF = 0$, the two sensors achieve the same throughput, no matter whether β_1 is equal to β_2

or not. On the other hand, the larger the BF is, the bigger throughput disparity between the two sensors is. Table 4.3 summarizes the BF when the relay node achieves a perfect cooperation, i.e., $\beta_r = 1$.

Table 4.3: Balance factor comparison.

	Con-TDMA	Only-AA	TDMA+DNC	A3NC
BF	$\left\lvert \log_2 \frac{\beta_1}{\beta_2} \right\rvert$	$\left\lvert \log_2 \frac{\beta_1 - e}{\beta_2 - e} \right\rvert$	0	0

As shown in Table 4.3, the BFs of the two cooperative schemes TDMA+DNC and A3NC are zero, but the BFs of other two non-cooperative schemes vary with the ratio of two actual PDRs. That is because, with the help of the relay, the hub can decode the packet sent through the "bad" channel by receiving a network-coded packet from the "good" channel, which balances the throughput of the two sensors. Therefore, TDMA+DNC and A3NC achieve a better throughput balance, compared to the schemes without relay nodes.

In summary, the proposed A3NC scheme achieves a better throughput in comparison with the schemes without AA method. Meanwhile, due to the contribution of the relay node, the A3NC also achieves a better energy efficiency and throughput balance compared to the schemes without the relay.

4.5 Performance Evaluation

In this section, simulation results will be provided to show the performance of the A3NC scheme in terms of total throughput, energy efficiency, and throughput balance.

4.5.1 Simulation Model and Configurations

The protocol stack from the PHY layer to the application layer is developed based on the Castalia framework [139] in OMNeT++. All the important default parameters of protocol stacks and hardware are listed in Table 4.4. The parameters of the routing layer are not listed in the table because the routing layer in the model only forwards packets between the application layer and MAC layer. Besides, the initial energy of the sensor is set to 2430 Joules, which is the average energy of one CR2032 lithium button battery at 3 Ohms and 225 mAh capacity. For the fairness of comparison, the SUI of the sensors and the SUI of the relay are set up to different values in different schemes to make sure that the overall time (T_c) remains 120 ms (as depicted in Figure 4.6).

In this chapter, both the channel gain datasets and a simulated network model are utilized to construct channel-related parameters. First, the datasets collected from our experiments are imported to simulate the variation of the path loss in time. However, these datasets only cover a limited number of walking scenarios, and the critical parameters,

Table 4.4: Simulation parameters for A3NC.

Parameter	Value
Radio Layer	
dataRate	512 kbps
modulationType	DIFFBPSK
bandwidth	20 MHz
carrierFreq	2400.0 MHz
noiseFloor	-101 dBm
sensitivity	-91 dBm
CCAthreshold	-95 dBm
symbolsForRSSI	8 bits
Tx Power	-38 dBm
Tx state energy consumption	2.9 mW
Rx state energy consumption	3.1 mW
Idle state energy consumption	0.05 mW
MAC Layer	
SuperframeLength	160 ms
RAP1Length	40 ms
SlotLength	5 ms
pTIFS	0.03 ms
Data's AckType	N-Ack
Control's AckType	I-Ack
others	
sensor's initialEnergy	2430 J
simulationTime	50 s

i.e., β_i, β_r and e, in each scenario are fixed. In order to verify the theoretical analyses mentioned in Section 4.4, a simulated network model should also be used to adjust β_i, β_r and e. The combination of the experimental datasets and simulated network model create a more flexible simulation platform.

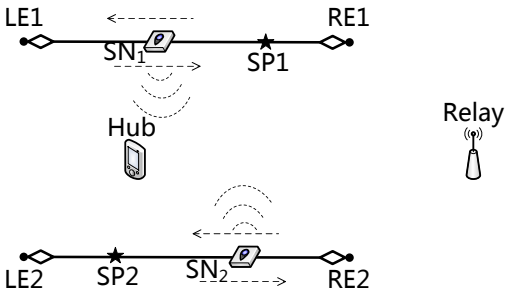

Figure 4.7: Simulated network model in OMNeT++.

Figure 4.7 presents the simulated network model. SP1, SP2 are the starting points for the two sensors. The reciprocating motion of the two sensors is simulated by importing the trace file, which records the path loss sequence during the walking activities. We now explain how to tune β_i, β_r and e. The "Outdoor+Belt" scenario with the transceivers bound in 0 degrees is chosen as an example, and the corresponding path loss dataset is imported into the network model. First of all, the average PDR for the channel $SN_i - hub$ (i.e., β_i) can be changed by modifying the Tx power. As shown in Figure 4.8, when the Tx power of the two sensors decreases, the sum of β_1 and β_2 also diminishes. Moreover, due to the two sensors having the same Tx power, β_1 and β_2 are also approximately identical.

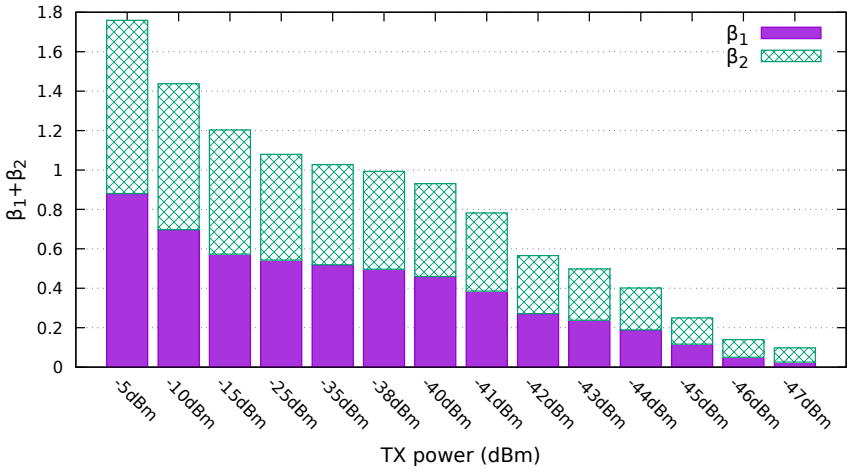

Figure 4.8: $\beta_1 + \beta_2$ vs. Tx power.

The average PDR of the channel $relay - hub$ (i.e., β_r) can be tuned by setting up a parameter (named PDR_Relay) in OMNeT++ to modify the behavior of the relay node. At last, the average PLR due to collisions (i.e., e) is controlled by changing the relative position between the two sensors' start points (SP1 and SP2). From Figure 4.7, intuitively, the interference between the two sensors is maximized (i.e., maximum e), if both SP1 and

SP2 are in the left endpoint of their motion trajectories (i.e. LE1 and LE2). But, if SP1 is on LE1 and SP2 is on RE2, which is a common situation in walking scenarios, e reaches its minimum value. Accordingly, we can change the value of e by changing the two start points of the sensors. Specifically, e can be changed by introducing a shift in the path loss sequence of the channel $SN_2 - hub$ while remaining the path loss sequence of the channel $SN_1 - hub$. As the sampling rate is fixed, the shift in the path loss sequence can also be denoted as a time shift compared to the normal arm swing in the walking scenarios.

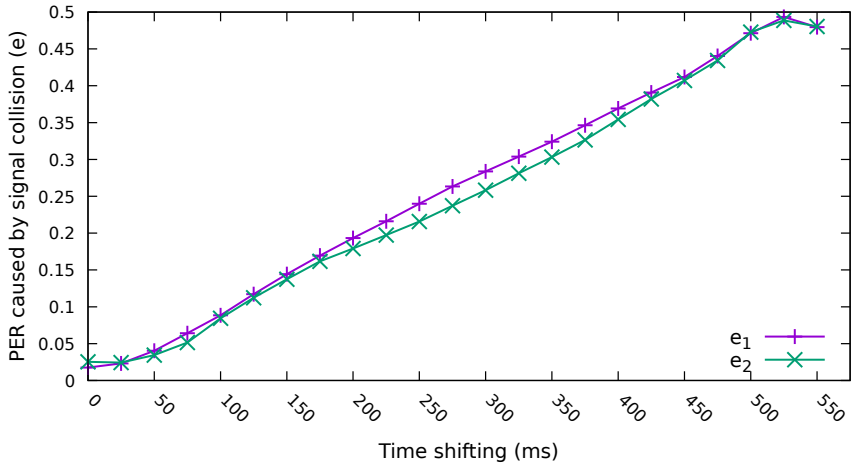

Figure 4.9: e vs. Time shift.

Figure 4.9 presents the curve of e versus time shift, when the Tx power of the two sensors is set to -38 dBm and $\beta_1 + \beta_2$ is approximately one. The case of "time shift = 0" corresponds to the normal swing motion of arm in walking scenarios. As shown in Figure 4.9, the average PLR due to collisions for normal walking scenarios is about 0.022. On the contrary, when the time shift reaches 525 ms, both e_1 and e_2 reach the maximum (about 0.5). In addition, it also implies that the cycle for chosen walking scenarios is around 1,050 ms. It is worth noting that the change of Tx power may also lead to the variation of e.

4.5.2 Simulation Results

• Throughput

Figure 4.10 shows the average total throughput of the proposed A3NC scheme in comparison with the Con-TDMA, Only-AA, and TDMA+DNC schemes in four typical walking scenarios, with consideration of four different deployment directions on the wrists. The Tx power and β_r are set at -38 dBm and 0.9 respectively. The "Total Throughput" here means the sum of the average upload throughput of the two sensors.

As shown in Figure 4.10, the performances of Only-AA and A3NC are slightly below that of Con-TDMA and TDMA+DNC in the "Indoor+Collar" scenario. The reason is that, compared to the cases where the hub is deployed in the belt, the PLD is relatively small when the hub is located on the back collar. Furthermore, the significant reflection

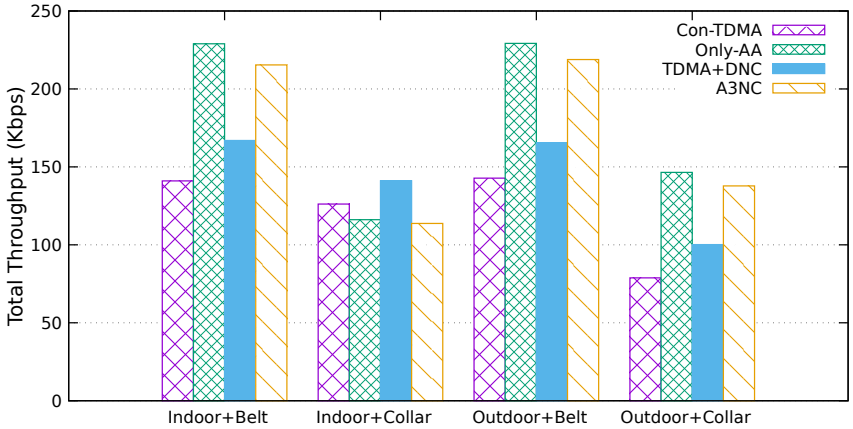

Figure 4.10: Throughputs of typical walking scenarios.

effect in the indoor environment reduces the PLD between the two channels. Nevertheless, Only-AA and A3NC achieve a significant improvement in terms of upload throughput in the other three scenarios, which confirms the feasibility of the AA method in the real walking scenarios. Besides, due to the β_r is set at 0.9 and e is not equal to zero in the real walking scenarios, based on Equations (4.11) and (4.20), the Only-AA scheme achieve a slightly better throughput performance.

Next, we explore relationship between the upload throughput and three key parameters, i.e., $\beta_1+\beta_2$, β_r, and e. Firstly, Figure 4.11 shows the results of total throughput vs. $\beta_1+\beta_2$, when $\beta_r = 0.9$ and the time shift is 0 ms. The Tx power of two sensors is amplified to increase the sum of β_1 and β_2, hence the value of e is also increased. The dash lines correspond to theoretical results derived from mathematical analyses in Section 4.4. The solid lines indicate the simulation results. Figure 4.11 clearly shows the good agreement between the mathematical analyses in Section 4.4 and the simulation results. The small deviation between the analytical and simulation curves is mainly due to two reasons. Firstly, the theoretical formulas analyze the throughput at the bit level, but the simulation model works at the packet level. The overhead of the packet header is not taken into account in the theoretical analyses. Meanwhile, because of the packetization of data, the tail end of the SUI would be a wastage of time resource when the tail period is too short to complete the transmission of one packet. Secondly, the idle interval between the transmission of two packets is not considered in the theoretical analysis.

Both theoretical and simulation results prove that Only-AA and A3NC achieve a remarkable improvement in comparison with Con-TDMA and TDMA+DNC, especially when $\beta_1+\beta_2 = 1$. Also, it can be seen that the performances of Only-AA, TDMA+DNC and A3NC reach their plateaus when the $\beta_1+\beta_2 > 1$. For the two schemes with the AA mechanism, based on Equations (4.11) and (4.20), the key part determining the throughput of Only-AA and A3NC is $\beta_1+\beta_2-2e$, i.e., $(\beta_1-e)+(\beta_1-e)$. However, since the signal collisions increase with the increase of Tx power, β_1-e and β_1-e cannot exceed 0.5. Therefore, after $\beta_1+\beta_2$ reaching one, further increase of β_1 or β_2 cannot improve the

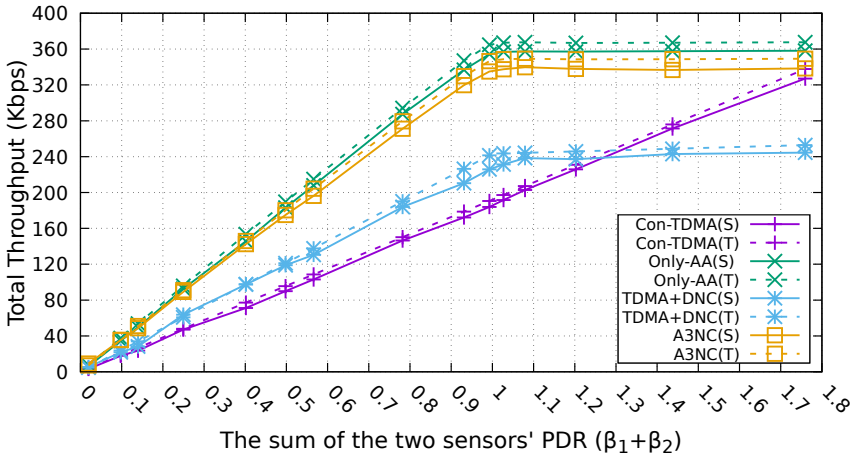

Figure 4.11: Throughput vs. $\beta_1 + \beta_2$.

total throughput. For the TDMA+DNC scheme, based on Equation (4.17), if $\beta_r = 0.9$ and $\beta_1 + \beta_2 > 1$, the increment of β_1 or β_2 affects the throughput slightly. The reason is that, if the probability of successful relay cooperation is close to one, the reception of either one packet from the two sensors can lead to the successful decoding of the other packet. In other words, when $\beta_1 + \beta_2 \geq 1$, the hub can receive both two sensors' packets which is the best situation in one transmission process. Therefore, the upload throughput of the TDMA+DNC is saturated if $\beta_1 + \beta_2 > 1$. As for the Con-TDMA, the SUI of the two sensors are separated in the time domain and the relay node is not adopted, so the total performance of Con-TDMA scheme raises linearly with the increase of $\beta_1 + \beta_2$.

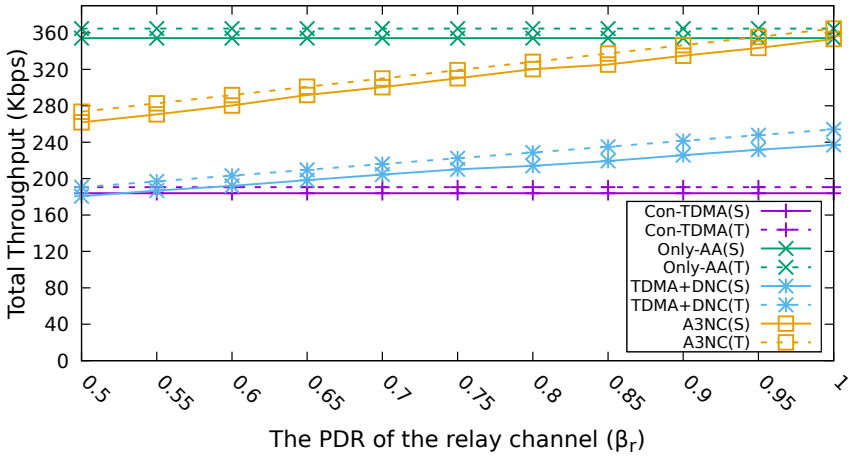

Figure 4.12: Throughput vs. β_r.

Figure 4.12 shows the throughput performance as a function of β_r, with the Tx power of -38 dBm and the time shift of 0 ms. As expected, the performances of both TDMA+DNC and A3NC improve with the increase of β_r, while those of Only-AA and Con-TDMA remain constant. Besides, when the time shift is 0 and Tx power is -38 dBm (i.e., $\beta_1 + \beta_2 < 1$), e is small enough to be ignored (around 0.022). Therefore, based on Equation (4.17) and (4.20), the slope of TDMA+DNC is $1/3(1 + \beta_r)$, while that slope of

A3NC is $1/2(1+\beta_r)$. That is the reason that the curve of A3NC is steeper than that of TDMA+DNC. In other words, A3NC is more sensitive to the relay channel condition, which is acceptable when the relay node is deployed outside the human body.

In Figures 4.11 and 4.12, the time shift is set to 0 ms, which matches the normal swing motion of arms in walking scenarios. However, if we increase the time shift, the resulting change of e will affect the system performance. Figure 4.13 shows the throughput performance as a function of e, when the other parameters are set to the default values (including $\beta_1+\beta_2=0.99$, and $\beta_r=0.9$). As expected, the performance of Con-TDMA is not affected by e, and the performances of the two schemes with the AA mechanism decrease with the increase of e. Moreover, since $\beta_r=0.9$, the slope of two AA schemes are almost the same. An exception is that, although the AA mechanism is not adopted in TDMA+DNC, its performance still declines with the rise of e, which does not match the analysis result in Equation (4.17). The reason for this exception is that because the two $SUIs$ of the two sensors are adjacent and are relatively short compared to the walking cycle, when e increases by changing the swing behavior of two arms, the hub tends to receive or discard both packets from the two sensors. Accordingly, the effectiveness of the relay cooperation is reduced.

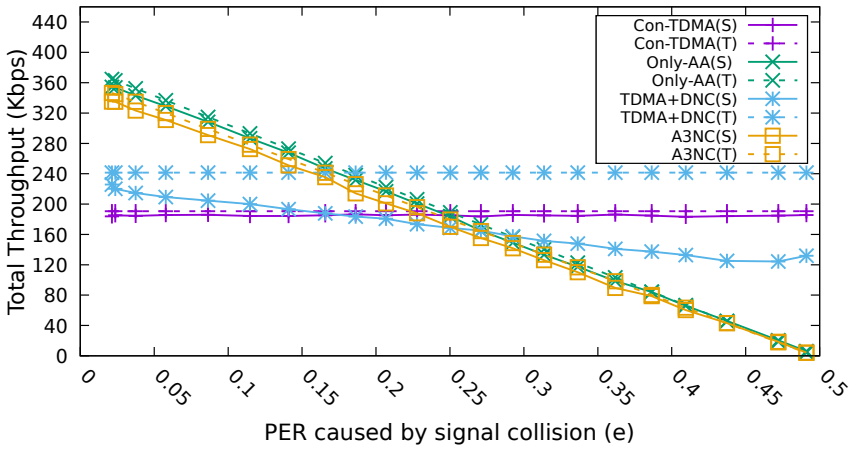

Figure 4.13: Throughput vs. e.

• Energy Efficiency

Figure 4.14 compares the energy efficiency of the four schemes when β_r and time shift are set to 0.9 and 0 ms, respectively. Since both the PDR sum of the two sensors (i.e., $\beta_1+\beta_2$) and the energy consumption are affected by the Tx power of the sensors, we evaluate the energy efficiency in different Tx power levels. The "Energy Efficiency" (EE) in Figure 4.14 represents how many megabytes (MB) of data are transmitted by consuming one joule energy of the two sensors (cf. Equation (4.21)). As mentioned before, the energy of the relays and hub are not considered in this chapter.

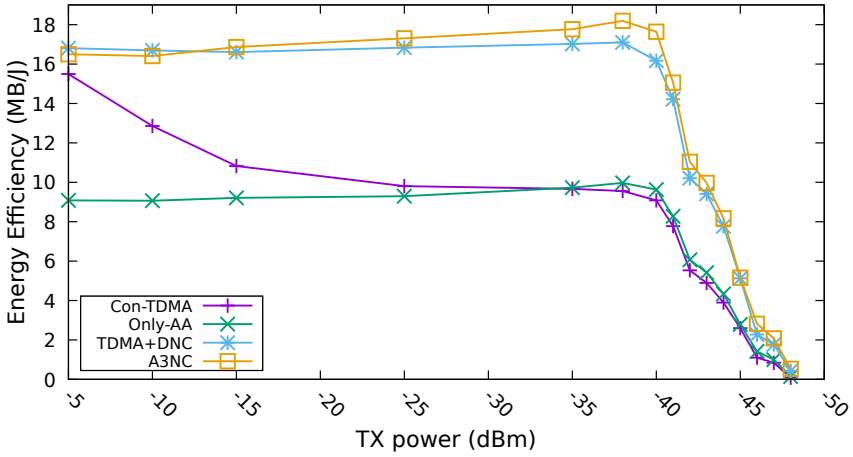

Figure 4.14: Measured energy efficiency (MB/Joule) vs. Tx power.

From Figure 4.14, the energy efficiency of Only-AA, A3NC and TDMA+DNC schemes increase slightly when the Tx power decreases from -5 dBm to -38 dBm, and reduces rapidly when Tx power is below -38 dBm. The curve trend can be explained by two reasons. First, combining the simulation results in Figure 4.11 and Figure 4.8, when the Tx power is below -38 dBm (i.e., $\beta_1 + \beta_1 < 1$), the upload throughputs rise up with the increase of the Tx power, and the throughputs reach a plateau after Tx power $\geqslant$ -38 dBm. On the other hand, the working power of the sensor is slightly reduced with the decline of Tx power. Accordingly, based on the definition of EE in Equation (4.21), the energy efficiency reaches the maximum at the point of -38 dBm. As for the Con-TDMA scheme, since its throughput declines continuously with the decrease of Tx power (see Figure 4.11), its energy efficiency experiences a similar trend. At last, combining Figure 4.11 and Figure 4.14, when the Tx power is -38 dBm, both the throughput and the energy efficiency reach the maximum. The Tx power -38 dBm is considered as the optimal value for Only-AA, TDMA+DNC, and A3NC for this simulation configuration.

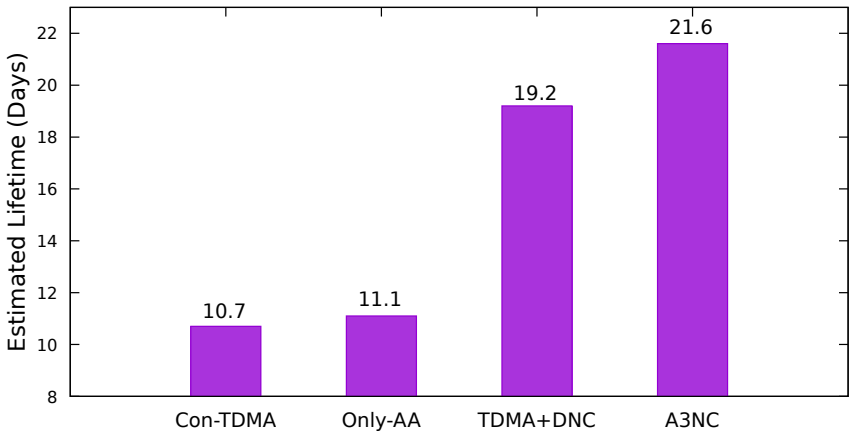

Figure 4.15: The comparison of the estimated lifetime.

We also estimate the lifetime for a typical WBAN application, in which an upload traffic of 200 kbps is required for each sensor equipped with one CR2032 button battery. In

this case, the Tx powers of the two sensors are set to the optimal value: -38 dBm. Figure 4.15 shows that the estimated lifetime of Con-TDMA or Only-AA is less than 12 days, while A3NC lasts over 21 days, which is a significant improvement.

• **Throughput Balance**

All the above results are derived when the PDRs of two sensors are approximately equal, i.e., $\beta_1 \approx \beta_2$. Here we consider the case where β_1 and β_2 are different.

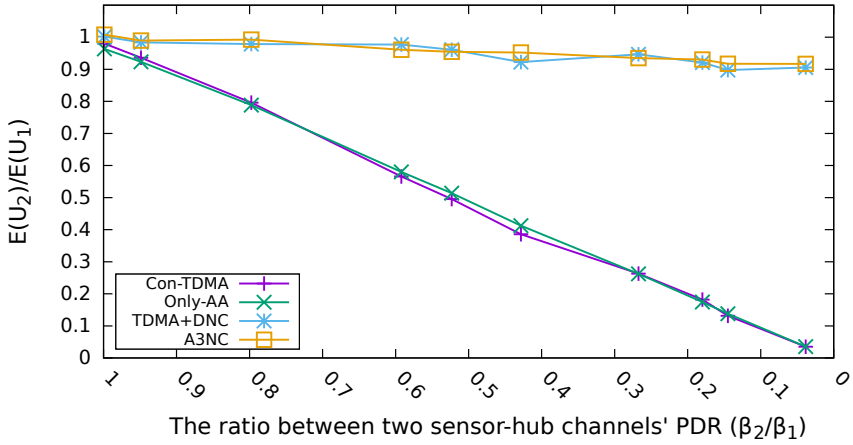

Figure 4.16: The comparison of throughput between the two sensors.

Figure 4.16 shows the average ratio between the upload throughput of the two sensors, $E(U_2)/E(U_1)$, as a function of β_2/β_1. The curves of both TDMA+DNC and A3NC are almost constant and are approximately equal to one, i.e., $E(U1) \approx E(U2)$. That means the two schemes with relay cooperation can achieve a better throughput balance between the two sensors. In contrast, when the relay node is not utilized (Con-TDMA and Only-AA schemes), the difference between $E(U1)$ and $E(U2)$ increases significantly with the decrease of β_2/β_1. The simulation results in Figure 4.16 also confirm our analysis in Table 4.3.

In summary, the simulation results confirm the theoretical analyses in Section 4.4. In contrast to conventional methods, the newly proposed A3NC scheme achieves a significant throughput improvement (about 10%-40% in normal walking scenarios), while attaining substantial power saving. Besides, with the help of cooperative communication, A3NC maintains a good throughput balance between two correlated sensor nodes.

4.6 Chapter Summary

Motivated by the significant PLD (Path Loss Discrepancy) between two on-body channels in walking scenarios, in this chapter, we propose a novel cross-layer network coding scheme, called A3NC, to achieve a better trade-off between energy consumption and

throughput. The A3NC scheme integrates the ANC technology in the PHY layer and a time slot allocation algorithm in the MAC layer to improve transmission performance in the walking scenarios. In A3NC, two sensors with a significant path loss discrepancy simultaneously transmit packets to the relay and hub. Then, the relay forwards network coding packets to the hub and the hub performs the decoding process after the first two phases. We derived the mathematical analyses for the proposed A3NC from three perspectives, namely sum throughput, energy efficiency, and throughput balance, in comparison with three other existing schemes. Moreover, by importing the channel gain data collected from walking scenarios, we build a Castalia-based simulation model to validate the performance of A3NC. Simulation results show that the A3NC scheme achieves the best trade-off between the energy efficiency and the throughput, compared to the other three existing schemes. Meanwhile, A3NC provides a better sum throughput than the Con-TDMA and TDMA+DNC and roughly the same sum throughput as the Only-AA one. To the best of our knowledge, this is the first work attempting to bridge network coding to a spatially correlated WBAN system.

Chapter 5

Dynamic Slot Scheduling for Daily Life Scenarios in WBANs

5.1 Introduction

In recent years, many dynamic schemes which adjust key transmission parameters in accordance with the real-time channel state or application requirement have been proposed to meet the transmission challenges in WBANs. Among these works, Adaptive Duty Cycle (ADC) [14], [52]–[54] and Transmission Power Control (TPC) [20], [22], [23], [25], [28], [38], [41] are the two key research topics. However, both ADC and TPC methods require additional hardware or software costs on the sensor side. In this chapter, we focus on the Dynamic Slot Scheduling (DSS) method, which dynamically optimizes the permutation of time slots in each superframe. Because of the advantages in collision-free and energy efficiency, the TDMA-based approach is put forth as one of the most appropriate MAC solutions. However, due to the high volatility of on-body channels, a simple static TDMA allocation may lead to a significant waste. Specifically, if a time slot is assigned to a particular sensor node with a bad channel to the hub (coordinator or sink), the data packets from this sensor are prone to be lost. This slot cannot be used by any other node that may have a good link. This not only wastes the energy but also decreases the throughput. Ideally, we would like to allocate a transmission slot to a sensor node only when the state of its link to the hub allows a successful data transfer. The core idea of DSS methods is scheduling the time slots according to the variation of link conditions, rather than a fixed scheduling. It is worth noting that all the additional controls are added to the hub and there is no increase in sensors' complexity.

The core idea of DSS has been somewhat mentioned in the literature, which is usually referred to as "opportunistic scheduling" in the context of cellular networks [57]. However, traditional opportunistic scheduling approaches are not compatible with WBAN systems as they require that the slave nodes are continuously available for communication [11]. This

requirement is unacceptable for the energy-constrained sensors, which are in a sleep mode most of the time. Besides, most opportunistic scheduling methods for cellular networks do not consider the peculiarities of WBAN channels, e.g., high variation and predominant shadowing from the body. As introduced in Chapter 2, there are also some DSS works proposed for WBANs. However, most existing works use a two-state Markov model to describe the on-body channel, which is insufficient for the complex WBAN application scenarios, especially the daily scenarios with mixed activities. In this chapter, motivated by the significant temporal autocorrelation of the on-body channels in the human daily activity scenarios, a Temporal Autocorrelation-based DSS method (DSS-TA) is proposed. DSS-TA utilizes a temporal autocorrelation model to estimate the on-body channel condition for future time slots and then optimizes the permutation of scheduled time slots for all connected sensor nodes based on the estimation results. The new method is designed to be compatible with the IEEE 802.15.6 standard.

The major contributions of this chapter are as follows:

• We first propose to utilize a temporal autocorrelation model to optimize the slot scheduling and detail its implementation in IEEE 802.15.6. The new method jointly takes the latest and historical channel states into consideration, thus achieving a more accurate prediction of channel conditions.

• We evaluate the performance of our DSS-TA method through importing the real channel datasets into the simulation model. Simulation results show that, compared to conventional DSS methods, the new method achieves a much better performance in terms of Packet Loss Ratio (PLR).

Our publication [127] is based on the content of this chapter.

The rest of the chapter is organized as follows. The system model and problem formulation are presented in Section 5.2. Section 5.3 details the newly proposed DSS-TA method. Performance evaluation results based on the real channel datasets are presented in Section 5.4. Finally, Section 5.5 summarizes this chapter.

5.2 System Model and Problem Formulation

5.2.1 System Model

In this chapter, we consider a one-hop star topology composed of one hub and a number of sensors. As the health monitoring is considered as the application of interest, all sensors periodically upload data packets to the hub. In the MAC layer, the MAC model of the IEEE 802.15.6 standard [4] is adopted. In the IEEE 802.15.6 standard, a hub shall operate in three types of access modes: beacon mode with superframes, non-beacon mode with superframes, and non-beacon mode without superframes. As stated before, the beacon mode with superframes provides the most flexible option in terms of access phases, we

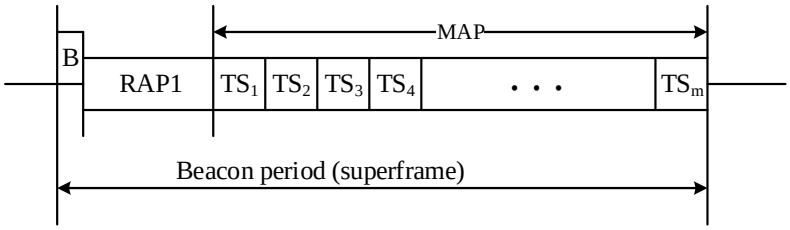

Figure 5.1: Superframe structure for DSS-TA.

consider this mode in this chapter. As shown in Figure 5.1, one active superframe (beacon period) consists of two access phases: Random Access Phase (RAP1) and Managed Access Phase (MAP). Both RAP1 and MAP consist of several time slots with same length, i.e., T_s. In the RAP1, the CSMA/CA (Carrier Sense Multiple Access/Collision Avoidance) access method is performed to exchange management and control packets, including the connection request and assignment packets. In the MAP, the TDMA access method is utilized to schedule the upload interval for sensor nodes. After the scheduling of the hub, the exclusive upload intervals for the sensor nodes are located in the MAP. For brevity, we call the exclusive intervals as SUIs (Scheduled Upload Intervals). In this study, we assume that the hub assigns the same length of SUI to each sensor in one superframe, and we call this constraint as "fairness constraint". It is worth noting that for comparison, we also consider the method which the hub allocates the time slots only based on the channel condition, without the restriction of the equal SUI length. However, as presented in Section 5.4, there exists a significant imbalance in the data rate of different sensors in the latter case. For the radio layer, all wireless devices operate in a half-duplex mode and no relay nodes are used in the network. All sensors are configured with the same transmission power level. As the hub device is usually less energy-constrained, the transmission power level of the hub is higher than that of sensors. Therefore, the downlink channels (from the hub to the sensors) are assumed to be much more reliable than the uplink channels (from the sensors to the hub).

5.2.2 Problem Formulation

In the classical TDMA method, upon accomplishing the scheduling in the first TDMA round, the order of SUI for all sensor nodes will remain the same for several TDMA rounds. However, some time slots may be occupied by a sensor with a bad channel condition to the hub. These time slots cannot be assigned to another sensor that may have a better link. Moreover, as the sensor is assigned to an interval with a bad channel condition, it also loses the opportunity to have a better channel condition in another interval. Unlike the static TDMA method, DSS methods focus on the problem of how to dynamically schedule the time slots in each superframe. Ideally, DSS methods aim to allocate transmission slots to a sensor only when the state of its link to the hub is likely to result in a successful data

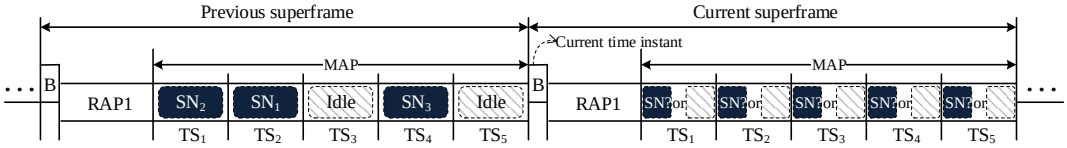

Figure 5.2: Time slot scheduling problem.

transfer.

Assuming there are n sensors ($SN_1 - SN_n$) in the network, and each MAP is split into m slots with the same duration (cf. Figure 5.1), denoted as $TS_1, TS_2, \ldots, TS_m$. Each sensor node is assigned with q slots to upload data packets in MAP, so there are $\lfloor m/q \rfloor$ available intervals. We denote $K(i)$ as the SUI assigned to SN_i, $1 \leqslant K(i) \leqslant \lfloor m/q \rfloor$, and vector $\mathbf{K} = (K(1), K(2), ..., K(n))$ represents the SUI permutation in one MAP. Theoretically, the total number of possible values of $\mathbf{K}$ is the n-permutation of $\lfloor m/q \rfloor$, i.e., $\prod_{i=0}^{n-1}(\lfloor m/q \rfloor - i)$, for each superframe. In DSS methods, $\mathbf{K}$ does not remain the same across different superframes, which is the key difference compared to a static TDMA assignment. Let us consider the example in Figure 5.2. Assuming there are three sensors in the network and five time slots in one MAP, each sensor is assigned one time slot, i.e., $m = 5$, $n = 3$, and $q = 1$. In the previous beacon period, TS_2, TS_1, and TS_4 are assigned to SN_1, SN_2 and SN_3, respectively, i.e., $\mathbf{K} = (2, 1, 4)$. In the static TDMA method, $\mathbf{K}$ remains the same for several superframes. Our aim is to choose the optimal value of $\mathbf{K}$ for the current superframe based on the historical channel information.

The main target of all DSS methods is to minimize the packet loss from the sensors to the hub. More specifically, at the start of each superframe, the permutation of SUI for the current superframe should be optimized based on the following criteria:

$$\begin{gathered} \min_{\mathbf{K}} \sum_{i=1}^{n} p_i(K(i)) \\ for \;\; i \neq j, \; K(i) \leqslant \lfloor m/q \rfloor \; and \; K(i) \neq K(j) \end{gathered} \tag{5.1}$$

where $p_i(K(i))$ represents the average PLR (Packet Loss Ratio) of the link "SN_i-Hub" in the $K(i)^{th}$ time interval. Therefore, the more accurate estimation of $p_i(K(i))$, the better performance of the DSS method. However, estimating the full channel state information at the start of each round is not trivial, especially in the dynamic WBAN scenarios. The key challenge of DSS schemes is how to predict the channel conditions using the channel information from the previous superframes and then optimize the time slot scheduling in the current superframe based on the prediction results.

5.3 Proposed DSS-TA Method

In the proposed DSS-TA method, the hub predicts the channel condition based on a temporal autocorrelation model at the beginning of each superframe. Specifically, DSS-TA consists of three parts: channel information collection, PLR prediction, and slot permutation optimization. Except for the first part that needs the assistance of sensor nodes, DSS-TA is mainly implemented on the hub side, which is considered to be less constrained by energy, storage, and computation resources.

5.3.1 Channel Information Collection

As presented in Equation (3.1), historical channel gains are needed at the granularity of time slots to calculate the latest autocorrelation coefficient. Intuitively, the hub could collect the channel conditions by receiving the upload packets from the sensor nodes. However, every sensor node only uploads the data packets during their SUI, which misses the channel information during the other time slots. Meanwhile, if multiple sensor nodes simultaneously upload packets to the hub, it may result in severe signal collisions. Therefore, broadcast from the hub to all sensors, i.e., downlink transmission, is used to track the channel condition. As demonstrated in [117] and [128] , the on-body channels show prominent reciprocity in narrowband communication environments, which means the channel profiles of downlink and uplink are about the same. Therefore, the channel gain of uplink channels can be estimated by the measurement of the downlink channel. Specifically, the hub keeps broadcasting control or sample packets to all sensors, then the sensor nodes will feedback the RSSI values to the hub during their SUIs.

Consider an example in Figure 5.3. There are five time slots ($TS_1 - TS_5$) in the MAP, and three sensor nodes ($SN_1 - SN_3$) are assigned one time slot each. In order to record the channel gain for each time slot, we introduce an extra subslot in the tail of each time slot. On the hub side, depending on whether the current time slot is free or not, the hub shall broadcast one control or sample data packet, respectively, to all sensor nodes in the extra subslot. If the current time slot is assigned to a sensor (i.e., $TS_1 - TS_3$ in Figure 5.3), the hub shall broadcast a B-Ack packet during the extra subslot. The B-Ack packet means block acknowledgment packet, which is combined with the block acknowledgment later (L-Ack) packet to support the L-Ack & B-Ack acknowledgment policy of IEEE 802.15.6. In DSS-TA, L-Ack & B-Ack policy is adopted in the uplink data transmission. That means the Ack policy field of all data packets would be set to L-Ack, except the last data packet in each time slot which is set to B-Ack. On the other hand, if the current time slot is set as free (TS_4 and TS_5 in Figure 5.3), instead of broadcasting the acknowledgment packet, the hub shall broadcast a sample packet to all sensor nodes during the extra subslot. At the sensor side, if the current time slot is assigned to a certain sensor, this sensor will stay in a normal active state. Otherwise, the sensor will be in the sleep state. During

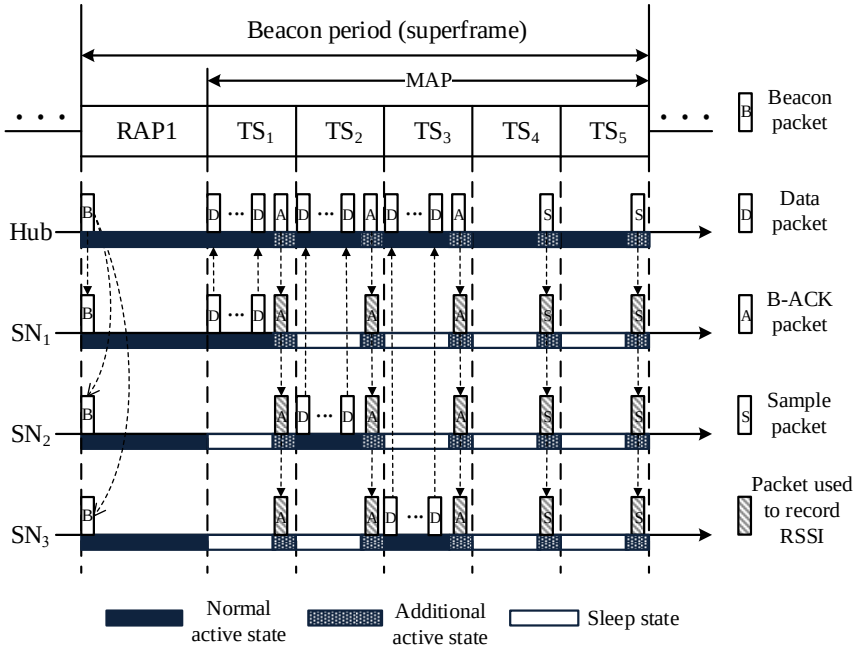

Figure 5.3: Channel information collection.

the extra subslots, three sensor nodes will stay in Rx (reception) state to receive B-Ack or sample packets from the hub. Upon receiving the B-Ack or sample packet from the hub, the sensor nodes record the RSSI values and assemble them into the headers of data packets, which would be uploaded during the next superframe. Note that the hub knows the Tx power level of the B-Ack or sample packets, thus, it is easy to calculate the channel gain (or path loss) after receiving the historical RSSI values. By this approach, the hub keeps track of the channel conditions of each channel in every time slot, while the sensor nodes only stay active during the extra subslots and its allocated interval. Although an extra subslot is only a small portion of a time slot, the extra subslots still consume extra energy compared. In Chapter 6, by introducing TPC (Transmission Power Control), the extra energy consumption will be removed.

In DSS-TA, the hub stores the channel gain data of the latest 2 seconds, which contain 400 channel gain values for each sensor. Note that, choosing an appropriate sample size to estimate the autocorrelation is not a trivial task. On one hand, with the increase of sample size, more data points are utilized to calculate the channel autocorrelations, which may appear to result in a more accurate estimation of autocorrelation. On the other hand, since the sampling frequency is fixed, a bigger sample size means these data points are collected from a wider time span. However, as demonstrated in [116], on-body channels show a low probability of WSS assumption outside the time span of 500 ms. In other words, the timeliness of autocorrelation calculation is weakened with the increase of sample size. In fact, there exists a trade-off between accuracy and timeliness when choosing the sample size. We will explore the effect of the sample size in Section 5.4.

5.3.2 Packet Loss Ratio Prediction

We first introduce the temporal autocorrelation model used to predict the PLR. Suppose the sensor node SN_i transmits a data packet to the hub with the transmission power P_{Tx}, and the hub receives the packet with the power P_{Rx}. Then the channel gain for the channel "SN_i-Hub" is defined as

$$G_i|_{dB} = P_{Rx}|_{dBm} - P_{Tx}|_{dBm} \tag{5.2}$$

Meanwhile, as proved in [119], [120], [128], [140], the lognormal distribution provides a good fit for the long-term average on-body channel gain. Therefore, the channel gain in the channel "SN_i-Hub" can be described by a Gaussian random variable (r.v.)

$$G_i|_{dB} \sim \mathcal{N}(\mu_i, \sigma_i^2) \tag{5.3}$$

where μ_i and σ_i are the mean and standard deviation of the channel gain, respectively. Note that both μ_i and σ_i depend directly on the type of human activity, the position of transmitting and receiving nodes, and propagation environment. In this study, we assume the variation of the channel gain is a WSS process within 500 ms, thus μ_i and σ_i remain the same within 500 ms. Accordingly, the channel gains within this period follow the same distribution

$$G_i(T_0) \sim \mathcal{N}(\mu_i, \sigma_i^2) \tag{5.4}$$

$$G_i(T_0+\tau) \sim \mathcal{N}(\mu_i, \sigma_i^2) \;\; \tau \leqslant 500ms \tag{5.5}$$

where $G_i(T_0)$ and $G_i(T_0+\tau)$ are the channel gains at the time instants T_0 and $T_0+\tau$, respectively. Therefore, the joint distribution of the two channel gains recorded at different time instants can be expressed as [141]

$$(G_i(T_0), G_i(T_0+\tau)) \sim \mathcal{N}(\mu_i, \mu_i, \sigma_i^2, \sigma_i^2, \rho_i(\tau)) \tag{5.6}$$

where $\rho_i(\tau)$ denotes the autocorrelation coefficient for a time lag of τ. Furthermore, the conditional distribution of $G_i(T_0+\tau)$ can be deduced to [141]:

$$G_i(T_0+\tau) \sim \mathcal{N}((1-\rho_i(\tau))\mu_i + \rho_i(\tau)G_i(T_0), (1-\rho_i^2(\tau))\sigma_i^2) \tag{5.7}$$

The PLR is the probability of the received signal power below the pre-defined receiving power threshold. Thus, the PLR for the time instant $T_0+\tau$ is given by

$$\begin{aligned} p_i(T_0+\tau) &= Prob(P_{Rx}(T_0+\tau) \leqslant {P_{Rx}}^*) \\ &= Prob(G_i(T_0+\tau) + P_{Tx}(T_0+\tau) \leqslant {P_{Rx}}^*) \\ &= Prob(G_i(T_0+\tau) \leqslant G^*) \end{aligned} \tag{5.8}$$

where $p_i(T_0+\tau)$ is the PLR, $P_{Tx}(T_0+\tau)$ and $P_{Rx}(T_0+\tau)$ are the signal transmitting and receiving power respectively, ${P_{Rx}}^*$ is the pre-defined receiving power threshold, and $G^* = {P_{Rx}}^* - P_{Tx}(T_0+\tau)$ is defined as the channel gain threshold. Consequently, combining Equations (5.7) and (5.8), $p_i(T_0+\tau)$ can be predicted by

$$\begin{aligned} p_i(T_0+\tau) &= \int_{-\infty}^{G^*} f_{G_i(T_0+\tau)}(G_i)dG_i \\ &= \Phi\left(\frac{G^* - (1-\rho_i(\tau))\mu_i - \rho_i(\tau)G_i(T_0)}{\sigma_i\sqrt{(1-\rho_i^2(\tau))}}\right) \end{aligned} \tag{5.9}$$

where $f_{G_i(T_0+\tau)}(G_i)$ is the probability density function of $G_i(T_0+\tau)$, and $\Phi(\cdot)$ is the cumulative distribution function of the standard normal distribution.

Equations (5.7)-(5.9) are called the temporal autocorrelation model (TAM), which is first proposed in [141]. In [141], the TAM model is used to choose dynamically between the relay and direct transmissions. In DSS-TA, the collected historical channel gain data is combined with TAM at the hub side to predict the PLR for each channel.

Based on Equation (5.9), the following parameters: $G_i(T_0)$, μ_i, σ_i and $\rho_i(\tau)$ are required in the hub side. Firstly, the latest channel gain record in the previous superframe is chosen as $G_i(T_0)$. Then, the channel gain expectation μ_i and standard deviation σ_i can be estimated by the sample mean ($\hat{\mu}_i$) and sample standard deviation ($\hat{\sigma}_i$)

$$\hat{\mu}_i = \bar{G}_i = \frac{1}{n}\sum_{x=1}^{n} G_i(x) \tag{5.10}$$

$$\hat{\sigma}_i = \sqrt{\frac{1}{n}\sum_{x=1}^{n}(G_i(x)-\bar{G}_i)^2} \tag{5.11}$$

where $G_i(x)$ $(x = 1, 2, \ldots, n)$ are the historical channel gain records, and $n = 400$ is the sample size. Next, we will calculate the autocorrelation coefficient $\rho_i(\tau)$. We convert the time lag of τ to the number of time slots, i.e., $\lfloor \tau/T_s \rfloor$. Hence, $\rho_i(\tau)$ can be estimated as $\gamma_i(\lfloor \tau/T_s \rfloor)$, based on Equation (3.1). In addition, in order to predict the channel condition for multiple future time slots, the hub should calculate an autocorrelation coefficient vector for each channel. In DSS-TA, the autocorrelation coefficients within the time lag of 500 ms are calculated. For instance, if the length of one time slot is 5 ms, each autocorrelation vector has $500/5 = 100$ elements, which are denoted for the channel "SN_i-Hub" as $\vec{\gamma_i} = (\gamma_i(1), \gamma_i(2), \gamma_i(3), \ldots, \gamma_i(100))$. Besides, when the time lag exceeds 500 ms, the autocorrelation coefficient is considered as $\gamma_i(100)$.

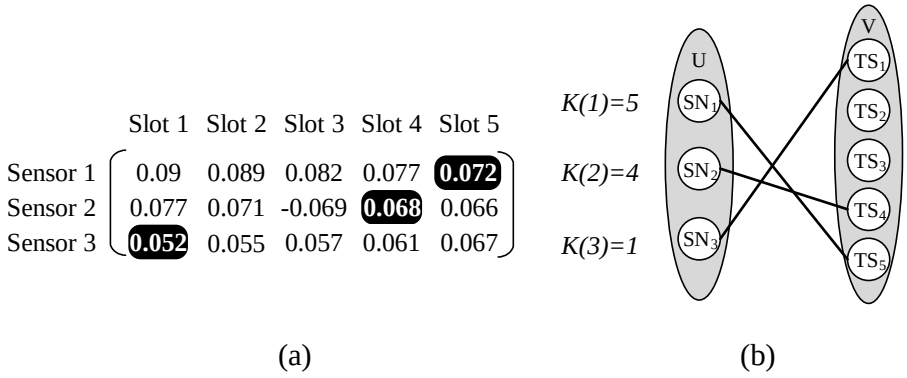

Figure 5.4: An example of finding the minimum-cost matching.

5.3.3 Slot Permutation Optimization

As presented in Equation (5.1), the aim of DSS approaches is to find a permutation of SUI, i.e., **K**, to minimize the sum of PLR of all links. In fact, the process of finding an optimal **K** for the current superframe can be converted into a minimum-cost matching problem in a bipartite graph. The bipartite graph can be denoted as $G = (U, V, E)$, where U and V denote the sensor node set and time interval set, respectively, E denotes the edges between the two subsets. In the DSS-TA, the cost of the edge from the sensor SN_i to the time interval x, namely TI_x, is weighted by the average PLR of the link "SN_i-Hub" during TI_x. If each sensor is assigned with q time slots, the length of one time interval equals $q \times T_s$, and the predicted PLR for one time interval is estimated as the mean value of q predicted PLR values within that time interval. Accordingly, using the PLR prediction algorithm mentioned before, a $|U| \times |V|$ adjacency matrix can be built to represent the bipartite graph, and the entries of the matrix are all estimated PLR values. $|U|$ and $|V|$ denote the size of the sets U and V, respectively. The assignment problem in the bipartite graph can be solved by the Hungarian algorithm [142], which is also called as Kuhn-Munkres algorithm. In addition, the time complexity in worst cases of this algorithm depends is $O(J^3)$, $J = max\{n, \lfloor m/q \rfloor\}$, where n the number of sensors and $\lfloor m/q \rfloor$ is the number of time intervals. Considering both n and m are below 256 [4], this complexity is acceptable.

Figure 5.4 illustrates the process of finding the minimum-cost matching. There are three sensor nodes in the network and five time slots in one MAP, and suppose each sensor is assigned with one time slot, i.e., $n = |U| = 3$, $m = |V| = 5$ and $q = 1$. Figure 5.4 (a) presents the predicted PLR matrix for the current superframe. The entry at the coordinate (a, b) denotes the predicted average PLR for the channel "SN_a-Hub" during TS_b. By performing the Hungarian algorithm on this matrix, the selected edges are depicted in Figure 5.4 (b). The optimal slot scheduling is that TS_5, TS_4, and TS_1 are assigned to SN_1, SN_2, SN_3 respectively, i.e., $\mathbf{K} = (5, 4, 1)$. The cases when $q > 1$ are similar, except that the cost of each edge is the mean value of q predicted PLR values within the considered time interval.

In short, at the start of each beacon period, the hub performs the PLR prediction algorithm to predict the PLRs for each time interval in the MAP and then performs the Hungarian algorithm to calculate the optimal permutation vector **K**. Then the optimal **K** is inserted into the beacon packet, which would be broadcasted to all sensor nodes. Upon receiving the beacon packet, sensor nodes obtain their exclusive upload intervals, set radio state timer, and control their data uploading process in the scheduled time slots.

5.4 Performance Evaluation

In this section, we evaluate the performance of the proposed DSS-TA. To do that, we build a simulation model as follows. The channel datasets collected from our measurement campaigns are imported into the simulation model to represent the variation of actual on-body channels in the daily scenarios. To demonstrate the effectiveness of DSS-TA, we compare the performance of the DSS-TA method with the following methods.

1. **Static TDMA:** The uplink time slots of all sensors are fixed after being assigned in the first superframe. The order of sensors' SUIs is chosen randomly in the first superframe.

2. **Random:** Unlike the static approach, the random scheme re-schedules the time slots at the start of each superframe, and the permutation of SUI is selected randomly.

3. **Flipping:** The flipping method schedules all "bad" links of the previous superframe last, preserving the order in time in which they were observed. Meanwhile, it schedules all "good" links first but reversing the order in which they were observed in the previous superframe. The original *Flipping* [58], [59] method assumes the number of sensors is identical to the number of available upload intervals. In this section, we consider a more general version where the number of available upload intervals may be larger than the number of sensors. Accordingly, some slots located in the middle of the MAP may remain idle.

4. **Perfect prediction:** This scheme is designed to explore the upper bound of DSS approaches. The hub is assumed to know exactly the channel gain of any time slot in the next beacon period. Therefore, the perfect prediction method can optimize the assignment based on the accurate value of channel gain. This method is infeasible for real WBAN systems because it assumes perfect prediction of future states.

5. **Fairness unconstrained:** Unlike all the aforementioned methods, this method does not restrict the SUI length for the sensors. A sensor may obtain the whole time slots if the channel condition from the sensor to the hub is predicted as the best during the MAP. On the other hand, another sensor may not be allocated any time slot to

upload packets due to its bad channel conditions. For the purpose of comparison, the fairness unconstrained method adopts the PLR prediction mechanism which we propose in the DSS-TA method. The hub adopts a greedy strategy to schedule the time slots, each time slot is assigned to the sensor with the lowest predicted PLR.

5.4.1 Simulation Model and Configurations

We build the simulation model from wireless channels to the application layer based on the Castalia framework [139]. Compared to other simulators, Castalia provides more realistic network features, such as accurate realistic radio model, clock drift, and energy consumption model. All the important default parameters of the protocol stack and hardware are listed in Table 5.1. In the wireless channel layer, the "TraceChannel" model is selected, in which the on-body channels are simulated by the channel datasets collected from our measurement campaign, i.e., CD_1, CD_2, ..., CD_{16}. Corresponding to the 16 channel datasets, we carry 16 simulations for each simulation configuration by importing different channel datasets to the simulation model. Because each channel realization lasts 3,600 seconds (1 hour), the simulation time is also set to 3,600 seconds. The functions of application and routing layer are relatively simple. The application layer generates sample data packets with the rate of "PacketRate", and the routing layer forwards packets between the application layer and MAC layer. In the MAC layer, one time slot is set to 5 ms. The 4 ms period in the front is used for uploading data packets and the 1 ms period at the end is the extra subplot used for receiving B-Ack or sample packets from the hub. As for the radio layer, all the parameters are set based on a low power RF transceiver module: CC2420 [143]. Besides, taking the overheads of different layers into account, the size of one data frame is 110 bytes (87+10+7+6), hence the transmission delay for one frame is $(110 \times 8)/250 = 3.52$ ms (the transmission rate is 250 Kbits/sec). Taking the guard time and $pSIFS$ (short interframe separation time) into account, the sensor nodes only transmit one data packet in one time slot.

5.4.2 Simulation Results

As mentioned before, there exists a trade-off between accuracy and timeliness when choosing the sample size in DSS-TA. By presenting the relationship between the PLR and the sample size, we explore the best sample size for daily scenarios. Four channel datasets collected from four test subjects, i.e., CD_1, CD_5, CD_9, and CD_{13}, are selected as the examples to show the PLR as a function of the sample size. As shown in Figure 5.5, the PLR reaches the minimum when the sample size is about 400. Since the sampling frequency of our measurements is 200 Hz, 400 data points corresponding to the time duration of 2 seconds. The accuracy of autocorrelation estimation is weakened by a sample size smaller than 400. On the other hand, when the sample size is bigger than 400, the

Table 5.1: Simulation parameters for DSS-TA.

Parameter	Value
Application Layer	
PacketSize	87 bytes
PacketRate	30 Pkts/s
Routing Layer	
PacketOverhead	10 bytes
MAC Layer	
SuperframeLength	70 ms
RAP1Length	10 ms
SlotLength	5 ms
SubslotLength	1 ms
SUI	10 ms
pTIFS	0.03 ms
Data's AckType	L-Ack & B-Ack
Control's AckType	I-Ack
PacketOverheader	7 bytes
Radio Layer	
dataRate	250 kbps
modulationType	PSK
bandwidth	20 MHz
carrierFreq	2400.0 MHz
noiseFloor	-101 dBm
sensitivity	-95 dBm
CCAthreshold	-95 dBm
symbolsForRSSI	8 bits
Tx Power	-15 dBm
FrameOverheader	6 bytes
pTimeSleepToTx	0.05 ms
pTimeSleepToRx	0.05 ms
others	
Wireless Channel	TraceChannel
simulationTime	3600 s

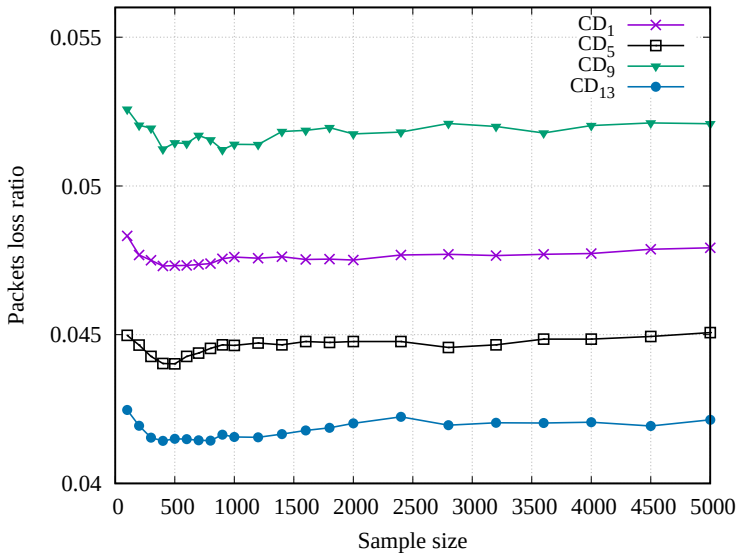

Figure 5.5: Packet loss ratio vs. sample size in DSS-TA, superframe length 70 ms, P_{Tx} = -15 dBm.

PLR increases slightly. The reason is that, when the time duration is longer than 2 seconds (corresponding to 400 data points), the non-stationary property of on-body channels starts to offset the accuracy despite having more data points, leading to an increase of the PLR. Accordingly, the latest 400 channel gain values are chosen as the sample data points to perform the PLR prediction algorithm in both the proposed DSS-TA and the fairness unconstrained method.

Next, the comparison between the DSS-TA method and the fairness unconstrained method is presented. The comparison will explain the reason for introducing the "fairness constraint", where all sensors shall have the same length of SUI in each MAP. Taking four typical channel datasets (CD_1, CD_5, CD_9, and CD_{13}) as the examples, the upload data rate for each sensor and average data rate are depicted in Figure 5.6. As expected, the fairness unconstrained method exhibits a better performance in terms of the average data rate. However, in most cases, the fairness unconstrained method shows a significant discrepancy of data rates between different sensor nodes. We consider the significant discrepancy as "unfairness" between sensors. Specifically, SN_{RW}, SN_{RA}, SN_{LA} are severely starved in CD_1, CD_9, and CD_{13}, respectively. In other words, the discrepancy of data rates between different sensor nodes could be significant and unpredictable in the fairness unconstrained method. If the WBAN application aims at the maximum average data rate and does not require a minimum data rate for the sensor nodes, the fairness unconstrained method may be the best choice. However, the unpredictable and significant discrepancy is not suitable for the majority WBAN applications. This is the rationale for introducing the "fairness constraint" in this chapter.

The following simulations will focus on the comparison among four DSS methods, namely the static, random, flipping, perfect prediction, and newly proposed DSS-TA

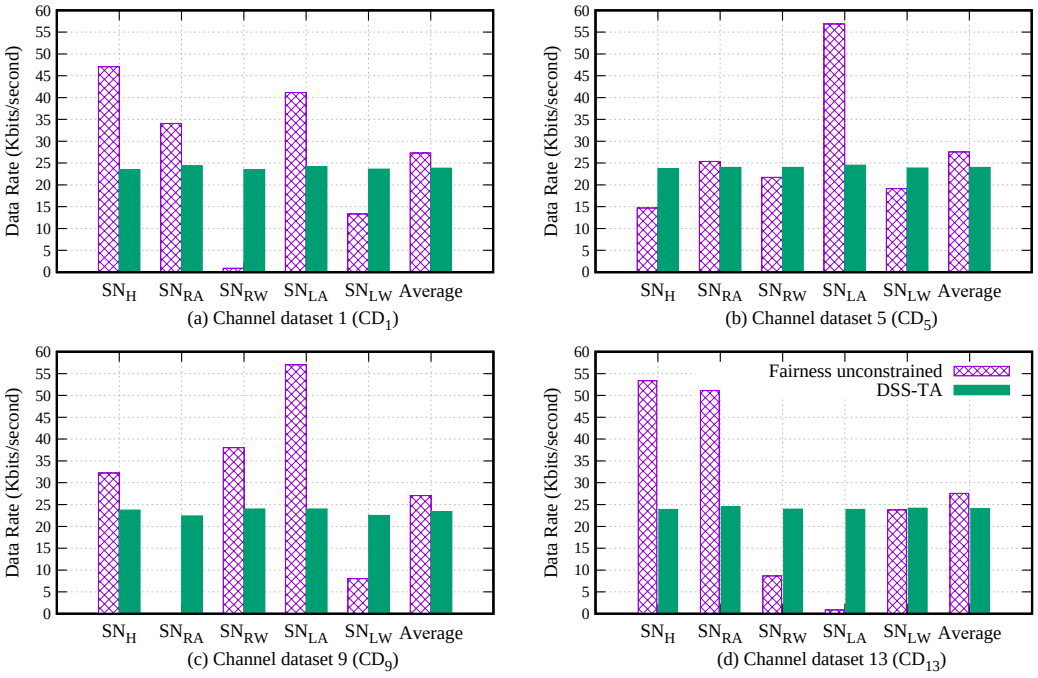

Figure 5.6: The comparison of upload data rates between DSS-TA and the fairness unconstrained method, superframe length 70 ms, P_{Tx} = -15 dBm.

methods under the "fairness constraint". Since these schemes comply with the "fairness constraint", the data rates of all sensors would be roughly same. Hence the average upload packet loss ratio (PLR) is considered to be the main performance metric. We first explore the PLR performance when adopting different levels of Tx power. Clearly, boosting the Tx power can decrease the PLR, but also increases the power consumption, which is strictly limited in WBAN systems. On the other hand, a low Tx power may cause the PLR to exceed the guideline of PLR in WBAN system. As summarized in [144], a PLR less than 10% is considered as a guideline in this study. Accordingly, we set the range of Tx power from -18 dBm to -8 dBm. Figure 5.7 shows the PLR performance of different scheduling methods by importing the first channel dataset CD_1 into the simulation model. As expected, the PLR decreases with the increase of Tx power. The proposed DSS-TA is significantly better than the static, flipping and random methods.

Figure 5.8 shows the mean and standard deviation of PLR reduction over the static method for the four DSS methods, namely the random, flipping, perfect prediction and DSS-TA. Note that the PLR reduction over the static method represents the percentage of the improvement in terms of PLR, compared to the static method, defined as $(PLR_{static} - PLR_{DSS})/PLR_{static}$. Clearly, DSS-TA achieves a much better PLR reduction (6.43%-10.28%) in comparison with the conventional flipping method (0%-2.89%). Figure 5.8 also shows that the PLR reduction of DSS-TA is more significant when the Tx power is higher.

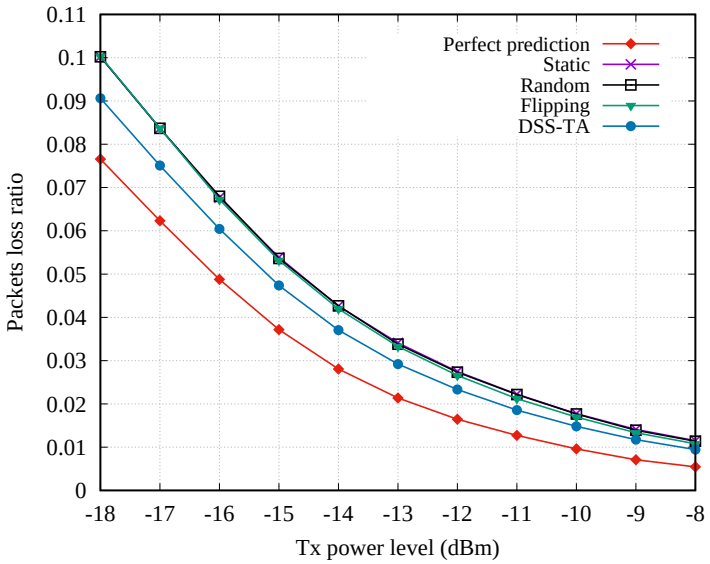

Figure 5.7: PLR vs. Tx power lever, superframe length 70 ms, CD_1.

The superframe length (the duration of one beacon period) is another key parameter. We now focus on exploring the PLR as a function of the superframe length. To avoid a significant decrease in throughput when extending the superframe length, we prolong the SUI for sensors with the extension of the superframe length. Specifically, we allocated one more time slot (5 ms) to each sensor when the superframe length is augmented by 35 ms. Figure 5.9 presents the simulation results by importing the first channel dataset CD_1, while Figure 5.10 illustrates the mean and standard deviation of the PLR reduction over the static method.

From Figure 5.9 and Figure 5.10, we have the following observations. Firstly, as expected, the PLR performances of both static and random methods do not change with the extension of the superframe length. Secondly, the performance of the perfect prediction method continuously improves with the extension of the superframe length. The reason may be the "bad" channel has a longer time to recover when a longer superframe length is adopted. Besides, since the perfect prediction scheme represents the upper bound performance of DSS methods, this observation also indicates that DSS methods have more potential when a longer superframe is adopted. Thirdly, the performance of DSS-TA slightly improves when the superframe length increases from 35 ms to 105 ms, then it degrades with the prolongation of superframes. On one hand, when the superframe is too short, there is not enough time to "revive" the "bad" channels, even the TAM model could provide an accurate PLR prediction. On the other hand, the channel autocorrelation decreases with the extension of the superframe length. Thus, the accuracy of PLR prediction results also decreases when a longer superframe is adopted, which decreases the performance of DSS-TA. At last, we found that when the superframe length is larger than 490 ms, the flipping and DSS-TA methods achieve the roughly same performance.

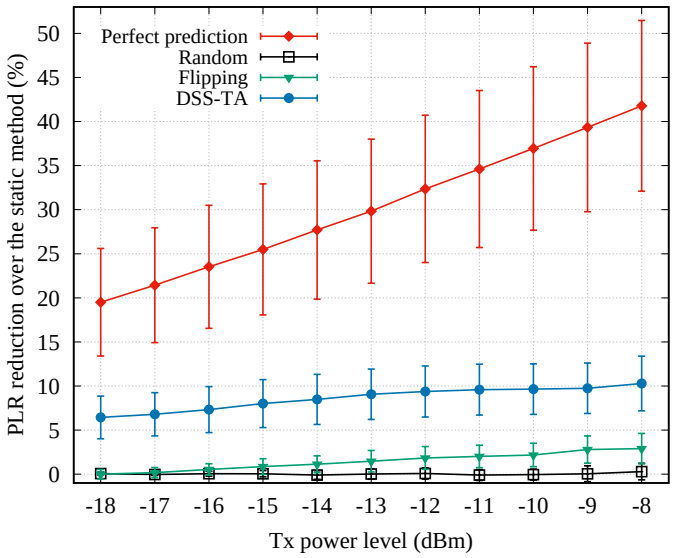

Figure 5.8: PLR reduction over the static method vs. Tx power level, superframe length 70 ms.

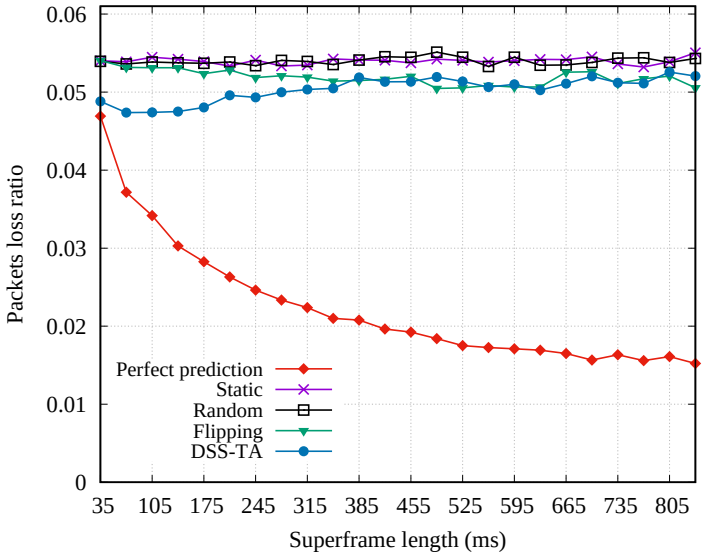

Figure 5.9: PLR vs. superframe length, P_{Tx} = -15 dBm, CD_1.

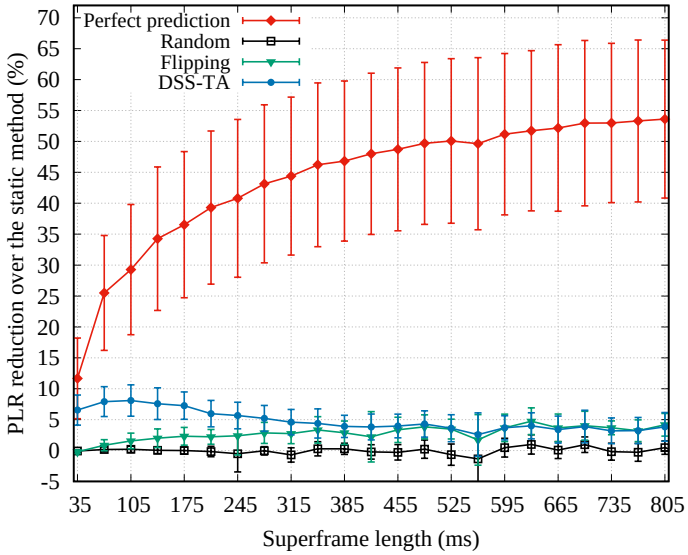

Figure 5.10: PLR reduction over the static method vs. superframe length, P_{Tx} = -15 dBm.

Compared to the flipping method, the TAM used in the DSS-TA considers not only the latest channel gains but also the channel gains in the past two seconds. Therefore, this observation indicates that TAM may not provide further accuracy in terms of channel condition prediction when the target future time slot is far away. However, a superframe length longer than 490 ms is normally impractical for most WBAN applications, because even for non-medical applications, the packet latency should be less than 250 ms [144], which limits the superframe to at most 250 ms. Accordingly, except for the applications that are not constrained with respect to packet latency, the DSS-TA provides a more accurate estimation of future channel conditions and hence achieves a better transmission performance in terms of PLR.

5.5 Chapter Summary

In this chapter, we focus on exploring DSS (Dynamic Slot Scheduling) methods in daily activity scenarios for WBAN systems. Based on the analyses in Chapter 3, the autocorrelation of on-body channels is significant within a time lag of 500 ms, regardless of the location of transceiver or test subject. Motivated by the significant autocorrelation, we propose a new slot scheduling method, namely DSS-TA. In DSS-TA, the hub uses a temporal autocorrelation model to predict PLR for future time slots. Then, the slot scheduling problem is transformed into a minimum-cost bipartite matching problem, and the edges in the bipartite are weighted by the predicted average PLRs. DSS-TA is designed to be compatible with the IEEE 802.15.6 standard. We add an extra subslot at the tail of each time slot to keep track the variation of channel gains. At the beginning of every

beacon period, the hub broadcasts the slot scheduling decision to the sensor nodes.

To evaluate its performance, the real channel realizations are imported into our simulation model to mimic the channel condition variation in the daily life scenarios. Simulation results show that the DSS approach exhibits a great potential in decreasing the PLR for daily scenarios. Moreover, we find that the superframe length is a key parameter which affects not only the upper bound of DSS methods but also the performance of the flipping and DSS-TA methods. There exists a superframe threshold for the flipping and DSS-TA method when the superframe length is shorter than the threshold, DSS-TA is more effective than the flipping method. When the superframe length is longer than the threshold, DSS-TA almost remains the same performance with the flipping method. In the daily activity scenarios, the threshold is around 490 ms. Considering the packet latency requirement for the majority WBAN applications is below 250 ms, DSS-TA is a more feasible choice.

In addition, we also explore the effect of transmission power on the sensor side. The transmission power level is a key parameter affecting both PLR and energy consumption. DSS method may provide a new insight to balance the trade-off between transmission reliability and energy consumption.

In this chapter, all sensor nodes are assumed to have the same Tx power level and the Tx power do not change over time. We will explore the combination of transmission power control and DSS methods in the next chapter.

Chapter 6

Joint Transmission Power Control and Relay Cooperation for WBAN Systems

6.1 Introduction

With the developments and technological advancements in Micro-Electro-Mechanical Systems (MEMS) technology and integrated circuits, especially industry's migration to smaller process technologies, the power consumption of microprocessors (MPUs) or microcontrollers (MCUs) has reduced significantly. On the other hand, the energy consumption from wireless communication, especially RF front ends, becomes a significant component for the sensor node. Accordingly, designing an effective Transmission Power Control (TPC) scheme is of great importance for WBAN systems. As introduced in Chapter 2, TPC refers to the adaptive method which optimizes the transmission power based on the channel conditions or QoS requirements. In fact, as a classical research topic, TPC has been extensively explored in the context of cellular networks and WSNs (Wireless Sensor Networks). However, due to the presence of the human body, the extremely low power requirement and high flexibility requirement of transmission protocol designs, simple adoption of the TPC methods designed for other networks is not appropriate. For example, the TPC method not only should consider the energy consumption but also the temperature rise of the human tissue resulting from the radiation absorption. A prolonged temperature rise within the body tissue may result in tissue damage, blood flow reduction in certain organs and enzymatic reactions [145].

Although applying TPC approach at the sensor side is capable of reducing the energy consumption, only considering TPC may not be sufficient to meet the stringent transmission reliability requirement of some WBAN applications, e.g., m-medical or e-health WBAN systems. In recent years, there are some works exploring relay-aided TPC methods in WBANs to achieve a better balance between energy consumption and transmission reliability. In [29], the authors propose a dynamic cooperative transmission scheme based

on the last round channel condition. When the direct channel is too bad to complete the packet transmission, the relay-aided two-hop transmission is introduced to improve the transmission reliability. In the scheme proposed in [26], the diversity gain from the two-hop relay link is utilized to decrease the outage probability, and radio transmission power control is integrated into sensor and relay nodes to extend the system lifetime and mitigate the signal interference from other WBAN systems. To achieve a better balance between transmission reliability and energy efficiency, the work of [30] proposes to jointly consider TPC, relay selection, and transmission time, and then convert the problem of controlling these parameters to a non-convex mixed-integer optimization problem.

Integrating Network Coding (NC) and cooperative communication in the context of WBANs is another research topic, which has been discussed in Chapter 2. However, most of the existing works either consider multi-hop or cluster-based network topology. Given that the transmission range of WBAN is usually limited to 2-5 meters, the feasibility of these two topologies in the context of WBANs is questionable. Moreover, most of the existing NC schemes for WBANs neglect the direct (or one-hop) transmission, which is considered as the most important component for WBAN systems.

In this chapter, we focus on the adaptive transmission protocol in the real daily life WBAN scenarios. Inspired by the autocorrelation analyses presented in Chapter 3, we propose an Autocorrelation-based Adaptive Transmission (AAT) scheme which jointly considers TPC, DSS (Dynamic Slot Scheduling) and two-hop cooperation. Firstly, the slot scheduling results are taken into account to optimize the transmission power level on the sensor side. Then, in order to further improve the transmission reliability, AAT provides an advanced cooperation option in which the two-hop transmission mechanism is designed to utilize the spatial diversity. The newly proposed scheme is designed on the basis of IEEE 802.15.6. The channel datasets collected from real WBAN daily scenarios are imported into our simulation model to carry out the performance evaluation. The simulation results demonstrate that the AAT significantly improves the transmission reliability and enhances the energy efficiency. Besides, considering extensive research works explore the application of NC technology in WBAN systems, we also provide a primary performance evaluation of the effectiveness and feasibility of NC technology in practical WBAN systems where both one-hop and two-hop transmissions are taken into account.

The main contributions of this chapter are summarized as follows.

• Motivated by the significant autocorrelation feature of on-body channels, we propose an adaptive TPC algorithm. The new TPC method optimizes the transmission power level based on the autocorrelation characteristic between two consecutive superframes.

• Since DSS operations are carried out at the hub, a DSS mechanism is incorporated into the newly proposed TPC method to further optimize the transmission power.

• The combination of TPC and two-hop relay cooperation is explored. We detail the protocol implementation on the basis of IEEE 802.15.6, including relay node selection,

relayed node selection and adaptive allocation of relay slots.

• The performances of the proposed protocol are evaluated using the measured channel data collected from the real daily scenarios. The evaluation results show that the newly proposed protocol achieves a remarkable high PDR (Packet Delivery Ratio) while the energy consumption remains at a low level.

The contents of this chapter were partly published in [146].

The rest of the chapter is organized as follows. In Section 6.2, the system model is presented. Section 6.3 details the newly proposed AAT method. The performance evaluation results are presented in Section 6.4. Finally, Section 6.5 summarizes this chapter.

6.2 System Model

In this section, the network architecture, channel model, and the energy consumption model are described.

6.2.1 Network Model

In this chapter, we consider the WBAN composed of n on-body sensor nodes (denoted as $SN_1, SN_2, \ldots, SN_n$) and one hub node. All sensor nodes periodically upload monitoring data to the hub. Then, these monitoring data are transmitted to a data server or remote sink node by the hub, but the off-body link is out of the scope of this chapter. As shown in Figure 6.1, both one-hop (direct) transmission and two-hop (relay) transmission are considered in the star topology. In the case of Figure 6.1, the two sensors on the wrists act as the relay nodes. Specifically, the right wrist node is scheduled to relay the packets from the sensor located on the head and the sensor bound on right knee, while the left wrist node is assigned to relay the data packets from the left ankle. Note that a sensor node is called a relayed node only when its packets are scheduled to be relayed by a relay node. In this chapter, the relay nodes are not dedicated, they are selected from sensor nodes.

The uplink transmissions for all sensor nodes are regulated in a TDMA fashion, where each sensor node has its own SUI (Scheduled Upload Interval) to transmit monitoring data to the hub, and the selected relay node has its SRI (Scheduled Relay Interval) to transmit the packets. As for the exchange of management and control packets, the CSMA/CA access method is performed before the SUIs of sensor nodes. Specifically, we adopt the beacon mode with superframes in the IEEE 802.15.6 standard [4], as this mode provides the most flexible options in terms of access phases. As shown in Figure 6.2, one active beacon period (superframe) consists of two access phase: Random Access Phase (RAP1) and Managed Access Phase (MAP). The CSMA/CA access method is adopted in the RAP1 phase, which occupies a fixed length after the transmission of beacon packet. The time

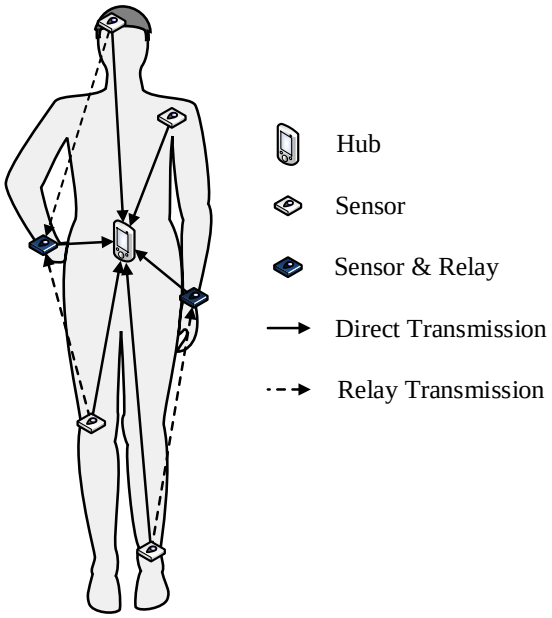

Figure 6.1: Network architecture.

period in the MAP phase is divided into two sub-phases: Direct Transmission Phase (DTP) and Relay Transmission Phase (RTP) to support both one-hop and two-hop transmissions. The SUIs assigned to sensor nodes are located in DTP. As demonstrated in Chapter 5, if we do not constrain the SUIs of all sensors at the same length, there exists an unpredictable and significant data rate discrepancy between different sensors. Therefore, in this chapter, we still consider the "fairness constraint", in which all sensor nodes are allocated with SUIs of the same length. As for the RTP, the SRI assigned to the relay node is located in this phase to forward the packets from relayed nodes. Both DTP and RTP consist of multiple time slots with the same length. In Figure 6.2, the last four time slots in the MAP are set as the RTP. If each sensor node is assigned with the SUI with two time slots, the relay node is capable to forward the data packets from at most 2 relayed nodes during the RTP. In order to focus on evaluating the performance of TPC and relay cooperation, the No acknowledgment (N-Ack) policy is adopted in the uplink. This means the packets from sensor nodes do not require an acknowledgment from the recipient, either immediately or later. Moreover, all hub, relay and sensor nodes are considered to operate in the half-duplex mode.

The hub performs the slot scheduling, relay/relayed nodes selection, and transmission power control, and then embeds these decisions into the beacon packet at the beginning of a superframe. If a sensor node also acts as a relay node, it would stay at the Rx state during the SUI(s) of the relayed node(s) to listen and receive the packets from the relayed node(s), and it would try to send the received packets to the hub in RTP. On the other hand, if a sensor node does not act as a relay node, except for the corresponding SUI period, the sensor would stay in the sleep mode in other time slots of the MAP.

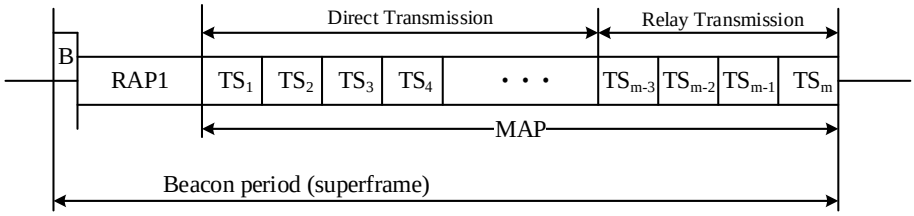

Figure 6.2: Superframe structure for AAT.

6.2.2 Channel Model

According to the experiments illustrated in [20], the Packet Loss Ratio (PLR) is a function of RSSI. The PLR could remain around zero when RSSI is larger than a certain threshold. In this chapter, this threshold is referred to as Rx sensitivity. and we recognize that a packet is correctly received when its RSSI value is greater than the Rx sensitivity. The RSSI of a packet can be expressed as follows:

$$RSSI = P_{Tx} - Pathloss \tag{6.1}$$

where P_{Tx} represents the transmission power of this packet at the transmitter and $Pathloss$ is the path loss that the packet undergoes. Since the P_{Tx} of a sensor node can be adjusted based on a TPC algorithm, the key part of modeling the on-body channel is describing the variation of path loss. As discussed before, the path loss of on-body channels is affected by many factors, such as the shadowing effect of human tissues and the mobility of the human body. In this work, the on-body channels in the daily scenarios are classified into two categories: direct channel and relay channel (cf. Figure 6.1). Specifically, the channel between the sensor and the hub is called the direct channel, while the channel from the sensor node to the relay node is denoted as the relay channel. Since the relay node is a sensor node, the channel between the relay node and the hub is also a direct channel.

• Direct Channel Model

Due to the high variability of on-body channels, neither distance-based nor other formula-based methods seem to be sufficient to describe the on-body channel condition, especially in the dynamic scenarios. Therefore, adopting channel datasets collected from the real daily scenarios to model the on-body channel is a better choice. The portable wireless transceivers introduced in Chapter 3 are used to collect the on-body channel gain data. As the on-body channels show a prominent reciprocity in narrowband communication environments [117], [128], the channel profiles of downlink and uplink are approximately the same. Therefore, these channel datasets collected from the experiment are utilized to model the on-body channels, including downlink and uplink. More details about these

experiments and the analyses of channel gain datasets can be found in Chapter 3.

• **Relay Channel Model**

Our portable wireless transceivers work in a half-duplex mode, and the path losses of all direct channels are recorded by broadcasting sample packets from the hub to the sensors. Therefore, the path loss information between different sensors is missing in the channel datasets, which means the relay channel is not represented in these datasets. In this study, we adopt a relatively straightforward relay model in which the channel condition from the relayed node to the relay node is described by one parameter PLR_r, i.e., the packet loss ratio for the channel from relayed node to the relay node. Moreover, as we focus on the channel condition from source or relay nodes to the hub, these parameters for all relay channels are assumed to be the same. Accordingly, the success of one two-hop transmission is decided by not only the channel gain recorded in the channel datasets but also the parameter PLR_r.

6.2.3 Energy Consumption Model

There are considerable energy consumption models designed for WBANs in the literature, e.g. the model used in [30], [147], [148]. However, most of these works do not take the energy consumption of the radio state transition and the energy consumption in sleep mode into account, and the transmission time is simply equal to the time interval allocated to the transmitter. To achieve a more accurate calculation of energy consumption, we adopt the energy consumption model in the network simulator Castalia [139], which we believe is quite accurate for WBANs. Besides, as the hub node is usually considered to be less constrained by energy, we focus on the energy consumption of sensor nodes.

Because the MAC layer works in the beacon mode with superframes and the superframe length is defined as a fixed parameter in IEEE 802.15.6, taking the energy consumption in one superframe is enough to explain the energy consumption model. In each superframe, the energy consumption for one sensor node consists of four parts: the energy consumption in the Tx state, the energy consumption in the Rx state, the energy consumption in the sleep state, and the energy consumption used to complete the state transition. Hence, the energy consumption in one superframe for one sensor can be expressed as follows

$$E_{sum} = E_{Tx} + E_{Rx} + E_{sleep} + E_{transition} \tag{6.2}$$

where E_{Tx}, E_{Rx}, E_{sleep} and $E_{transition}$ represent the four components of the whole energy consumption, respectively. Figure 6.3 illustrates the variation of radio states during one SUI or SRI. T_{x2y} in the figure refers to the transition delay from state x to state y, $pSIFS$

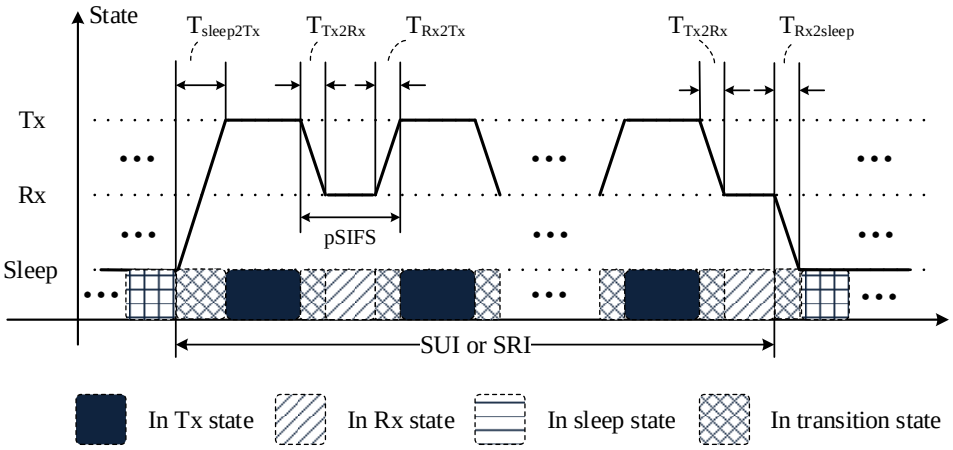

Figure 6.3: Energy consumption in one SUI or SRI.

is the time interval between two consecutive transmissions. As the default active state is Rx state, the radio returns to the Rx state after completing each transmission.

We first detail the calculation of E_{Tx} in one superframe as follows

$$E_{Tx} = P_{Tx} \times T_{Tx} \tag{6.3}$$

where P_{Tx} stands for the transmission power that the sensor node adopts in the superframe, and T_{Tx} represent the time in the Tx state. Note that the value of P_{Tx} may vary in different superframes since TPC is considered in this study. The length of T_{Tx} varies with the role of the sensor in that beacon period. If the node does not act as a relay node, T_{Tx} can be expressed as

$$T_{Tx} = \frac{L_p}{R} \times \left\lfloor 1 + \frac{SUI - (T_{sleep2Tx} + L_p/R)}{L_p/R + pSIFS} \right\rfloor \tag{6.4}$$

where R (Kbps) refers to the transmission rate, which is assumed to be the same for all sensors. L_p (Kbits) denotes the length of one data packet or frame. $\frac{L_p}{R}$ is the time of transmitting one data packets. As the sensor only transmit packets during its SUI, the number of transmitting packets is $\left\lfloor 1 + \frac{SUI - (T_{sleep2Tx} + L_p/R)}{L_p/R + pSIFS} \right\rfloor$ which is denoted as PN_1. Hence, the time duration in Tx state is $\frac{L_p}{R} \times PN_1$. On the other hand, if the sensor is selected as a relay node, it not only transmits its own data packets during its SUI but also forwards the relaying packets. In this case, the T_{Tx} can be calculated as

$$T_{Tx} = \frac{L_p}{R} \times \left(PN_1 + \left\lfloor 1 + \frac{SRI - (T_{sleep2Tx} + L_p/R)}{L_p/R + pSIFS} \right\rfloor \right) \tag{6.5}$$

If we denote the number of relaying packets as $PN_2 = \left\lfloor 1 + \frac{SRI - (T_{sleep2Tx} + L_p/R)}{L_p/R + pSIFS} \right\rfloor$, the

T_{Tx} for a relay node can be expressed as $\frac{L_p}{R} \times (PN_1 + PN_2)$.

Next, we detail the calculation of E_{Rx}, which can be expressed by

$$E_{Rx} = P_{Rx} \times T_{Rx} \tag{6.6}$$

where P_{Rx} denotes the power when sensor node is in the Rx state, and T_{Rx} represents the time duration in this state. Similar to the calculation of T_{Tx}, whether a node acts as a relay node affects the length of T_{Rx}. If the node does not act as a relay node, the T_{Rx} is given by

$$\begin{aligned} T_{Rx} &= (PN_1 - 1)(pSIFS - T_{Tx2Rx} - T_{Rx2Tx}) \\ &+ \left(SUI - T_{sleep2Tx} - \frac{L_p}{R} - T_{Tx2Rx} - (PN_1 - 1) \times (pSIFS + \frac{L_p}{R}) \right) \end{aligned} \tag{6.7}$$

Partitioned by the plus sign, the T_{Rx} in Equation (6.7) has two parts. The first part is the Rx time between two consecutive packet transmissions, and the second part is the Rx time at the end of SUI, which is not long enough to transmit one data packet. The calculation of T_{Rx} for a relay node is more complicated than a sensor node. It not only includes the Rx time during SUI and SRI but also includes the time spent on receiving the data packets from relayed nodes

$$\begin{aligned} T_{Rx} &= (PN_1 - 1)(pSIFS - T_{Tx2Rx} - T_{Rx2Tx}) \\ &+ \left(SUI - T_{sleep2Tx} - \frac{L_p}{R} - T_{Tx2Rx} - (PN_1 - 1) \times (pSIFS + \frac{L_p}{R}) \right) \\ &+ (PN_2 - 1)(pSIFS - T_{Tx2Rx} - T_{Rx2Tx}) \\ &+ \left(SRI - T_{sleep2Tx} - \frac{L_p}{R} - T_{Tx2Rx} - (PN_2 - 1) \times (pSIFS + \frac{L_p}{R}) \right) \\ &+ (SRI - T_{sleep2Rx} \times \alpha) \end{aligned} \tag{6.8}$$

Partitioned by the plus signs, the first two parts are similar to the Equation (6.7), which represent the Rx time during its SUI. The middle two parts are the Rx time during its SRI to forward the relaying packets to the hub. The last parts is the duration when the relay node stays in the Rx state to receive the data packets from relayed node(s). Note that we introduce a parameter α, which varies with the number of relayed nodes and whether their SUIs are adjacent. For example, if two sensor nodes are selected as the relayed nodes and their SUIs are not adjacent, α is two. On the other hand, if their SUIs are adjacent, α is one.

Then, we calculate the energy consumption of the state transition. We first detail this

kind of energy consumption for a sensor node, which can be expressed as follows

$$\begin{aligned} E_{transition} = & P_{sleep2Tx} \times T_{sleep2Tx} \\ & + (PN_1 - 1)(P_{Tx2Rx} \times T_{Tx2Rx} + P_{Rx2Tx} \times T_{Rx2Tx}) \\ & + P_{Tx2Rx} \times T_{Tx2Rx} \\ & + P_{Rx2sleep} \times T_{Rx2sleep} \end{aligned} \tag{6.9}$$

Partitioned by the plus signs, the first and the last two parts in Equation (6.9) represent the energy consumption of state transition before and after the data packet transmissions, respectively. The second part is the energy consumption of the state transition during the transmissions of consecutive data packets. Next, if the node is selected as the relay node, the energy consumption used to complete the radio state transitions is calculated by:

$$\begin{aligned} E_{transition} = & P_{sleep2Tx} \times T_{sleep2Tx} \\ & + (PN_1 - 1)(P_{Tx2Rx} \times T_{Tx2Rx} + P_{Rx2Tx} \times T_{Rx2Tx}) \\ & + P_{Tx2Rx} \times T_{Tx2Rx} \\ & + P_{Rx2sleep} \times T_{Rx2sleep} \\ & + P_{sleep2Tx} \times T_{sleep2Tx} \\ & + (PN_2 - 1)(P_{Tx2Rx} \times T_{Tx2Rx} + P_{Rx2Tx} \times T_{Rx2Tx}) \\ & + P_{Tx2Rx} \times T_{Tx2Rx} \\ & + P_{Rx2sleep} \times T_{Rx2sleep} \\ & + (P_{sleep2Rx} \times T_{sleep2Rx} + P_{Rx2sleep} \times T_{Rx2sleep2}) \times \alpha \end{aligned} \tag{6.10}$$

The first eight lines of Equation (6.10) represent the energy consumptions of the state transitions during its SUI and SRI. The last line calculates the energy consumption of the state transition during the SUI(s) of the relayed node(s). The value of α varies with the number of relayed nodes and whether their SUIs are adjacent, its meaning has been explained in Equation 6.8.

At last, the energy consumption in sleep state can be expressed as

$$E_{sleep} = P_{sleep} \times T_{sleep} \tag{6.11}$$

where P_{sleep} represents the power when a sensor node is in the sleep mode, and T_{sleep} is the time duration in the sleep mode. The T_{sleep} in one superframe is not provided in this section, as it can be easily calculated by subtracting the time in other three radio states from the superframe length.

In this study, we adopt the energy consumption parameters from the CC2420 radio chip [143]. The power consumptions in different states for CC2420 are listed in Table 6.1,

Table 6.1: The power consumptions in different states for CC2420.

State	Output (dBm)	Power (mW)
Rx	-	62
Sleep	-	1.4
Tx	0	57.42
	-1	55.18
	-3	50.69
	-5	46.2
	-7	42.24
	-10	36.3
	-15	32.67
	-25	29.04

Table 6.2: The transition delay and power consumption for CC2420.

From	To	Power (mW)	Delay (ms)
Sleep	Rx	62	0.194
Sleep	Tx	62	0.194
Rx	Sleep	1.4	0.05
Rx	Tx	62	0.01
Tx	Sleep	1.4	0.05
Tx	Rx	62	0.01

while the transition delay and power between different states are detailed in Table 6.2.

6.3 Proposed Transmission Scheme

Given that the hub is typically more powerful than the sensor nodes in terms of storage and computational resources, it is desirable to push more control and computational tasks to the hub. In the proposed AAT scheme, except for requiring the capacity of changing transmission power and optional relaying at the sensor side, the hub side implements all control and calculation operations, including channel condition prediction, transmission power level decision, and adaptive relaying scheduling, etc. Specifically, AAT scheme consists of three main steps, which are summarized as follows:

1. The hub keeps track of the channel conditions from all sensor nodes, and then predicts the channel condition in the next TDMA round based on a temporal autocorrelation model.

2. Based on these predicted channel conditions, the hub adjusts the transmission power and reschedules the SUI order for all sensors.

3. After configuring the transmission power and SUI order, some channels may still be predicted to be in an outage state. In this case, the hub selects the relay and relayed nodes based on the predicted channel conditions, and then schedules the relay slots adaptively.

6.3.1 Channel Condition Prediction

The temporal autocorrelation model used to predict the channel condition is firstly introduced. Suppose the sensor node SN_i transmits a data packet to the hub with the transmission power P_{Tx}, and the hub receives the packet with a signal power of P_{Rx}. Then the channel gain for the channel "SN_i-Hub" is defined as

$$G_i|_{dB} = P_{Rx}|_{dBm} - P_{Tx}|_{dBm} \tag{6.12}$$

Meanwhile, as proved in [119], [120], [128], [140], the lognormal distribution provides a good fit for a long-term average on-body channel gain. Therefore, the channel gain in the channel "SN_i-Hub" can be described by a Gaussian random variable (r.v.)

$$G_i|_{dB} \sim \mathcal{N}(\mu_i, \sigma_i^2) \tag{6.13}$$

where μ_i and σ_i are the mean and standard deviation of the channel gain, respectively. Note that both μ_i and σ_i depend directly on the type of human activity, the position of transmitting and receiving nodes, and propagation environment. As proved in [116], the variation of the channel gain can be considered as a WSS process within 500 ms. If the superframe length is less than 250 ms, the channel gain for this channel in the next superframe follows the same distribution

$$G_i(S) \sim \mathcal{N}(\mu_i, \sigma_i^2) \tag{6.14}$$

$$G_i(S+1) \sim \mathcal{N}(\mu_i, \sigma_i^2) \tag{6.15}$$

where $G_i(S)$ and $G_i(S+1)$ are the channel gains in the superframe S and $S+1$, respectively. Therefore, the joint distribution of the two channel gains recorded during two consecutive superframes can be expressed as

$$(G_i(S), G_i(S+1)) \sim \mathcal{N}(\mu_i, \mu_i, \sigma_i^2, \sigma_i^2, \rho_i) \tag{6.16}$$

where ρ_i denotes the autocorrelation coefficient between the two channel gains recorded in the two adjacent superframes. Furthermore, the conditional distribution of $G_i(S+1)$ can be deduced to

$$G_i(S+1) \sim \mathcal{N}\left((1-\rho_i)\mu_i + \rho_i G_i(S), (1-\rho_i^2)\sigma_i^2\right) \tag{6.17}$$

Now, the expectation of the channel gain in the next superframe $S+1$ can be estimated by $(1-\rho_i)\mu_i + \rho_i G_i(S)$. In fact, Equation (6.17) can be considered as a "lite version" of the temporal autocorrelation model (TAM) used in Chapter 5. Since the work in the previous chapter focuses on the DSS, the hub should keep track of the channel condition at the granularity of time slots to accurately calculate the autocorrelation coefficient between different time slots. To this end, an extra wake-up period was introduced at the price of additional energy consumption. In this chapter, the autocorrelation characteristic is used to optimize the TPC, in which the energy consumption is one of the primary metrics. For this reason, we propose the simplified TAM which only needs the channel information by receiving normal data packets from sensor or relay nodes.

6.3.2 Transmission Power Control

To estimate the channel condition in the next superframe using the Equation (6.17), the following parameters $G_i(S)$, μ_i, σ_i and ρ_i are required in the hub side. Firstly, the latest channel gain record in the previous superframe is chosen as $G_i(S)$. Then, channel gain expectation μ_i and standard deviation σ_i can be estimated by the sample mean ($\hat{\mu}_i$) and sample standard deviation ($\hat{\sigma}_i$).

$$\hat{\mu}_i = \bar{G}_i = \frac{1}{N}\sum_{x=1}^{N} G_i(x) \tag{6.18}$$

$$\hat{\sigma}_i = \sqrt{\frac{1}{N}\sum_{x=1}^{N}(G_i(x)-\bar{G}_i)^2} \tag{6.19}$$

where $G_i(x)$ $(x = 1, 2, \ldots, N)$ are the historical channel gain records, and N is the sample size. According to the discussion in Section 5.4, there exists a trade-off between accuracy and timeliness when choosing the sample size. In this chapter, we adopt the optimal sample size used in Chapter 5, i.e., recording the channel gain values of the past 2 seconds. For example, if the superframe length is 80 ms, the hub stores the latest $\lfloor 2000/80 \rfloor = 25$ channel gain values. Next, we calculate the autocorrelation coefficient ρ_i based on the following equation

$$\rho_i = \frac{\sum_{x=1}^{N-1}(G(x)-\hat{\mu}_i)(G(x+1)-\hat{\mu}_i)}{\sum_{x=1}^{N}(G(x)-\hat{\mu}_i)^2} \tag{6.20}$$

where $G_i(1)\ldots G_i(N))$ are sample channel gain values recorded in N consecutive superframes.

At the beginning of each superframe, the hub preforms the calculations of $G_i(S)$, $\hat{\mu}_i$, $\hat{\sigma}_i$ and ρ_i for each channel, i.e., $SN_i - hub,\ i = (1, 2, \ldots, n)$. Then the adaptive algorithm presented in Algorithm 2 is carried out to decide the transmission power level for each sensor in the current superframe.

Algorithm 2: Adaptive transmission power control method

Input: The known channel gains in the last superframe, i.e.,
$G_1(S), G_2(S), \ldots, G_n(S)$.

Input: Autocorrelation coefficients between two consecutive superframe, i.e.,
$\rho_1, \rho_2, \ldots, \rho_n$.

Input: Sample means, i.e., $\hat{\mu_1}, \hat{\mu_2}, \ldots, \hat{\mu_n}$.

Input: Sample standard deviations, i.e., $\hat{\sigma_1}, \hat{\sigma_2}, \ldots, \hat{\sigma_n}$.

Output: The transmission power levels of n sensor nodes for current superframe,
i.e., $P_{Tx1}(S+1), P_{Tx2}(S+1), \ldots, P_{Txn}(S+1)$.

Output: The scheduled SUI orders of n sensor nodes for current superframe, i.e.,
$O_1(S+1), O_2(S+1), \ldots, O_n(S+1)$.

Define $Txlevel = [-25,\ -15,\ -10,\ -7,\ -5,\ -3,\ -1,\ 0]$;

for $i \leftarrow 1$ ***to*** n **do**

  $\hat{G}_i(S+1) = (1-\rho_i)\hat{\mu}_i + \rho_i G_i(S)$;

end

Sorting array $\hat{G_1}(S+1), \hat{G_2}(S+1), \ldots, \hat{G_n}(S+1)$ in a descending order;

$O_i(S+1)$ = the order of $\hat{G_i}(S+1)$ in the sorted array;

for $i \leftarrow 1$ ***to*** n **do**

  $M_i(S+1) = \hat{\sigma_i} \times (BasicMargin + O_i(S+1) \times GradientMargin)$;

  $P_{Txi}(S+1) = \underset{x}{\operatorname{argmin}}\ TxLevel[x] \geqslant \left(Rx_{sensitivity} - \hat{G}_i(S+1) + M_i(S+1)\right)$;

end

Algorithm 2 requires the following four inputs: the last known channel gain, autocorrelation coefficients between two consecutive superframes, the sample means, and the sample standard deviations. These inputs are used to schedule the SUI order and adapt the transmission power. Correspondingly, there are two output arrays: transmission power array $(P_{Tx1}(S+1), P_{Tx2}(S+1), \ldots, P_{Txn}(S+1))$ and SUI order array $O_1(S+1), O_2(S+1), \ldots, O_n(S+1)$. Specifically, the radio output powers in different transmission levels are predefined in Line 1. Since the CC2420 chip is adopted, the $TxLevel$ array is configured based on the parameters listed in Table 6.1. Lines 2-4 computes the expectation of channel gains in the current superframe by adding the sample mean to the last known channel gain, and the weights of these two part are adjusted by the value of autocorrelation coefficient. Lines 5-6 re-adjust the order of sensors' SUIs in the way that the sensor with the best channel quality, i.e., the highest expectation of the channel gain, is scheduled in the first position of DTP (Direct Transmission Phase), and the sensor with the worst channel quality is scheduled at the end of DTP. The rationale behind such scheduling is that all "bad" links are given a longer time to recover (i.e., to get out of the outage), while the "good" links are assigned to front positions to ensure a high probability of successful delivery. Lines 7-10 are used to finalize the transmission power levels for the n sensor nodes. $M_i(S+1)$ refers to the transmission power margin for SN_i, which takes the channel variation into account to ensure that the RSSI is higher than the Rx sensitivity (RSSI threshold). $BasicMargin$ and $GradientMargin$ are two margin parameters used to adjust the sensitivity of TPC to the order of SUI. In this chapter, the adaptation of the two margin parameters is not considered, they are configured at fixed values. At last, the minimum predefined output power levels that is equal or higher than the target transmission powers, i.e., $\hat{G}_i(S+1) + M_i(S+1),\ i = 1, 2, \ldots, n$, are selected. In addition, as we adopt "Bubble Sorting" algorithm in Line 5, the time complexity in worst cases of this algorithm is $O(n^2)$, where n is the number of sensors.

After performing Algorithm 2 at the beginning of each beacon period, the hub obtains the two arrays: $[P_{Tx1}(S+1), P_{Tx2}(S+1), \ldots, P_{Txn}(S+1)]$ and $[O_1(S+1), O_2(S+1), \ldots, O_n(S+1)]$. These two arrays are embedded into the beacon packet which would be broadcasted to all sensor nodes. Upon receiving the beacon packet, sensor nodes set their radio state timer, control data packet uploading based on their SUI scheduling, and their transmission power level based on the configured values.

6.3.3 Two-hop Cooperative Option for AAT

The major advantage of TPC methods lies in significantly reducing the energy consumption of sensor nodes. However, WBAN applications also have a stringent requirement in terms of PLR, e.g., m-medical or e-health WBAN systems. As shown in Section 6.4 later, when the channel is in deep fading, the PLR might still be over 10% even with the maximal

transmission power. In this sense, only considering TPC may not be enough for WBAN applications with a high transmission reliability requirement. As one of the most classical mechanisms to decrease the PLR, retransmission schemes arrange the retransmission of lost packets after detecting the packet loss. However, retransmission schemes are only effective when the outage duration is significantly shorter than the packet delivery deadline, but this premise may not be valid in the daily WBAN scenarios. As shown in Chapter 3, over 50% of outage durations exceed 10 ms in the real WBAN scenarios. In this case, the immediate retransmission may have a high probability of failure, which results in energy waste. On the other hand, the delayed retransmission may cause severe transmission delay, which is also unacceptable for many WBAN applications. Accordingly, cooperative transmission approaches are presented as a promising solution to further improve the transmission reliability. As cooperative communication has the advantage of spatial diversity, the packets from nodes in an outage duration could be delivered by the relay node instead.

In AAT schemes, the two-hop cooperative communication is considered as an option when a lower PLR is required or a severe channel fading is detected. As a relay node not only sends its own packets but also assists the relayed nodes, the extra energy consumption resulting from acting as a relay node should be carefully considered. In particular, two aspects should be designed when cooperative communication is jointly considered with the TPC method. First, the relay node must remain awake to receive the packets from the relayed node, but when the direct channel from the relayed node to the hub is in a good condition this extra awake period is a waste of energy. Therefore, choosing the relayed node(s) effectively could reduce unnecessary energy consumption. Second, relay node selection is of great importance in terms of the system lifetime. If the relay node is selected simply based on the channel condition or the distance to the hub node, some sensor nodes may run out of energy much quicker than the other nodes due to their heavy traffic load. Hence, the whole system lifetime is shortened. Considering the aforementioned two aspects, the following two-hop cooperative mechanism is proposed.

1. **Relayed node selection.** When the estimated channel gain in the next superframe ($\hat{G}_i(S+1)$) is below the Rx sensitivity, the corresponding sensor node is selected as a relayed node. The rationale for the selection is when $\hat{G}_i(S+1)$ is smaller than the Rx sensitivity, even if the transmission power is set to the maximum (0 dBm), the $RSSI = 0 + \hat{G}_i(S+1)$) would still be below the Rx sensitivity. Note that, the maximal number of the relayed nodes is limited by the length of DTP. If DTP is q times longer than one SUI, then at most q sensor nodes can be set as relayed node. Therefore, if more than q sensors satisfy the above condition for relayed node selection, the q sensors with the worst channel gains are selected.

2. **Relay node selection.** In this chapter, only one relay node is considered. Besides, to avoid some sensor nodes selected as relay nodes frequently, all sensor nodes

whose predicted channel gains are greater than the Rx sensitivity are the candidate for becoming a relay node. Then, the actual relay node is randomly selected from these candidates.

3. **Time slot scheduling for the relay node.** There is no additional action for a sensor node when the node is selected as a relayed node. But, there are some extra radio state transitions and packet relaying tasks for the selected relay node. Similar to the TPC decision broadcast, the relayed and relay nodes selection results are also embedded into the beacon packet. Upon receiving the beacon packet, all sensor nodes check whether they are selected as the relay node. If yes, the relay node would turn to the Rx state during the SUI(s) of the relayed node(s), and then relay the received packet(s) to the hub during RTP.

In short, at the start of each beacon period, the hub estimates the channel gains for each link based on the temporal autocorrelation model and performs the Algorithm 2 to optimize the transmission power and SUI scheduling for the next superframe. Moreover, if the two-hop cooperative option is selected, the relay and relayed nodes are selected to further improve the transmission reliability. Then all these optimal configurations in terms of TPC, DSS and two-hop cooperation are inserted into the beacon packet, which is broadcasted to all sensor nodes. At last, the sensor nodes adapt the transmission parameters based on the configuration information in the beacon packet.

6.4 Performance Evaluation

In this section, the performance of AAT is evaluated through simulations and compared with other transmission methods. To improve the authenticity of performance evaluation, the channel datasets collected from our measurement campaigns are imported into the simulation model to represent the variation of actual on-body channels in the daily scenarios. We compare the performance of the following methods with or without two-hop cooperation:

1. **Static scheme:** The hub does not control the transmission power level of the sensor nodes. The transmission power is fixed at a predefined value, e.g., 0 dBm, -3dBm, etc. In this section, we choose 0 dBm as the default transmission power level. Besides, the static scheme does not change the slot scheduling for all sensors. In other words, the permutation of SUIs is fixed after assigned randomly in the first superframe.

2. **Xiao's scheme:** This the TPC method proposed in [20], which firstly investigates the potential benefits of the adaptive TPC in the context of WBANs. Xiao's scheme adapts the transmission power level based on the variation of channel conditions. Specifically, the hub node alters the transmission power level according to the

feedback RSSI value obtained from the sensor node. The latest feedback RSSI value and previous average RSSI are jointly considered to estimate the new average RSSI ($\bar{R}$), and the new transmission power level is configured based on the comparison between the new average RSSI and two configured thresholds T_H and T_L. If $\bar{R}$ drops below the lower threshold T_L, then the transmission power is doubled. If $\bar{R}$ is above the upper threshold T_H, the transmission power is reduced by a fixed constant. Based on different weighting configurations (i.e., α_u and α_d) between the latest RSSI and previous $\bar{R}$, three TPC schemes: *Conservative*, *Balance* and *Aggressive* are designed for different applications with different requirements in terms of PLR and energy consumption. Considering the significant autocorrelation of on-body channels, the *Balance* scheme with $\alpha_u = 0.8$ and $\alpha_d = 0.8$ is picked as the TPC method for comparison.

3. **AAT scheme:** This is the adaptive transmission scheme we propose in this chapter. Unlike the Xiao's scheme, a temporal autocorrelation model is adopted to adjust the weight between the latest channel gain and the sample mean of historical channel gains. Moreover, the permutation of SUIs is also taken into account to optimize the transmission power margin. In this section the two margin parameters, i.e., $BasicMargin$ and $GradientMargin$, are set to 0.6 and 0.2, respectively.

4. **Ideal scheme:** In the ideal scheme, the hub knows all the channel gain information for the next superframe. Accordingly, the transmission power could be controlled at the best level, which not only avoids unnecessary energy waste but also keeps the PLR at the lowest level. This scheme is considered here to explore the upper bound of TPC approaches. Note that this method is infeasible for real WBAN systems because it assumes a perfect prediction of future states.

6.4.1 Simulation Model and Configurations

To evaluate the performance of the newly proposed adaptive transmission scheme, a comprehensive simulation model from wireless channels to the application layer is built based on the Castalia framework [139]. All the important default parameters of the protocol stack and hardware are listed in Table 6.3. On the wireless channel layer, the "TraceChannel" model is selected, in which the on-body channels are simulated by the channel dataset collected from our measurement campaign. As one channel dataset contains the channel gain variation in a time period of 3,600 seconds (1 hour), the simulation time is also set to 3,600 seconds. The functions of application and routing layers are relatively simple. The application layer generates sample data packets with the rate of "PacketRate", and the routing layer forwards packets between application layer and MAC layer. In the MAC layer, the superframe length is set to 80 ms, and the length of one time slot is 5 ms.

Hence, one superframe consists of 16 time slots, in which the first two time slots are set as the RAP1 period, the middle 10 time slots belong to the DTP and the last 4 time slots are RTP. The 10 time slots in DTP are assigned to 5 sensor nodes, and the SUI for one sensor node is 2 time slots, i.e., 10 ms. Note that the length of the active time slot in RTP depends on how many sensor nodes are estimated to be in outage for the current superframe. If one sensor node is predicted to be in outage, only two slots in the RTP period is activated for the transmission from the relay node to the hub. If more than one sensor node is predicted to be in outage, then all 4 time slots would be activated. As for the radio layer, all the parameters are set based on a low power RF transceiver module: CC2420 [143]. Taking the overheads of different layers into account, the size of one data frame is 128 bytes (105+10+7+6), thus the transmission delay for one frame is $(128 \times 8)/250 = 4.096$ ms. Taking the guard time and $pSIFS$ into account, the sensor nodes only transmit one data frame in one time slot. Consequently, the sensor node transmits two data frames to the hub during its SUI.

6.4.2 Simulation Results

In this chapter three performance evaluation metrics are considered, namely PLR (Packet Loss Ratio), energy consumption and energy efficiency. Specifically, the PLR in this section presents the average PLR value of the five sensor nodes and the energy consumption refers to the sum energy consumed by the five sensors. The energy efficiency (in KB/J) is defined as the ratio of data received in the hub side and the total power consumed by the five sensors.

• Adaptive Transmission without Cooperation

We first compare the newly proposed AAT scheme with the static or other TPC schemes when the two-hop cooperative transmission is not used. By importing an example channel dataset, i.e., CD_1, into the simulation model. Figure 6.4 shows the performance of average PLR of the five sensor nodes when the Rx sensitivity of hub varies. It can be seen that the PLR rises quickly with the increase of the Rx sensitivity because more packets are dropped at low RSSI values. The ideal and static schemes achieve almost the same PLR performance, which is also the lowest among the four schemes. The lowest PLR value achieved by the ideal scheme is the upper bound for TPC approaches. The static method with the transmission power of 0 dBm achieves the best PLR performance, but at the price of a significant waste of energy, which will be illustrated later. The PLR performance of AAT is close to the ideal method and much lower than Xiao's scheme due to the fact that AAT makes use of channel autocorrelation to adaptively adjust the transmission power and the SUI scheduling as explained before. Another observation is that the PLR gap between AAT and Xiao's scheme becomes smaller with the increasing value of Rx sensitivity. In

Table 6.3: Simulation Parameters for AAT.

Parameter	Value
Application Layer	
PacketSize	105 bytes
PacketRate	25 Pkts/s
Routing Layer	
PacketOverhead	10 bytes
MAC Layer	
SuperframeLength	80 ms
SlotLength	5 ms
RAP1Length	10 ms
DTPLength	50 ms
RTPLength	20 ms
SUI	10 ms
pTIFS	0.03 ms
Data's AckType	N-Ack
Control's AckType	I-Ack
PacketOverheader	7 bytes
Radio Layer	
DataRate	250 kbps
ModulationType	PSK
Bandwidth	20 MHz
CarrierFreq	2400.0 MHz
NoiseFloor	-101 dBm
Rx_sensitivity	-89 dBm
CCAthreshold	-95 dBm
SymbolsForRSSI	8 bits
InitialTxPower	0 dBm
FrameOverheader	6 bytes
others	
SensorNumber	5
sensor's initialEnergy	2430 J
Wireless Channel	TraceChannel
PLRBetweeenSensors	0.02
SimulationTime	3600 s

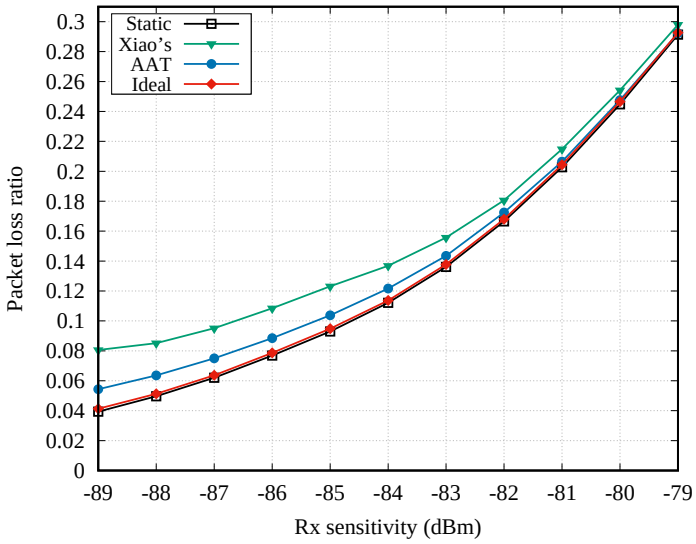

Figure 6.4: Packet loss ratio vs. Rx sensitivity.

other words, the performance advantage of the AAT scheme is more significant when Rx sensitivity is at a low level. For example, when the Rx sensitivity is -89 dBm, the PLR of AAT is 0.05434 while that of Xiao's scheme is 0.08058, which is a 32.56% improvement in terms of PLR.

In WBANs, reducing the energy consumption is another challenge for wireless transmission. Figure 6.5 shows the energy consumption of five sensors as a function of Rx sensitivity, when CD_1 is imported to the simulation model. It can be seen from the figure that the energy consumption of all TPC methods rise with the increase of Rx sensitivity, but always below that of the static method. Combining Figure 6.4 and Figure 6.5, the static method achieve the best PLR performance at a heavy price of energy consumption. The ideal method consumes the least energy as it always sets the Tx power at the optimal level. The energy consumptions of AAT and Xiao's scheme are between the static and the ideal method. Besides, the energy consumption of AAT is always below that of Xiao's scheme, and the gap becomes bigger with the increase of Rx sensitivity.

In Figure 6.6, we provide the simulation results in terms of energy efficiency, which jointly consider the throughput and the consumed energy. Clearly, the ideal and the static methods achieve the best and the worst energy efficiency, respectively. The performances of AAT and Xiao's method lie between those of the ideal and the static methods, and AAT exhibits a significant improvement in comparison with Xiao's method. Moreover, with the increase of Rx sensitivity, the energy efficiencies of the four scheme decrease, and the gaps between them become narrower. This is mainly because that a higher Rx sensitivity leads to more packets loss, even though the maximal transmission power level is adopted.

All aforementioned figures are provided for the case in which only one channel dataset, i.e., CD_1, is imported. Simulations for other datasets are similar. Figure 6.7 shows the average energy efficiency improvement over the static method for the AAT and Xiao's

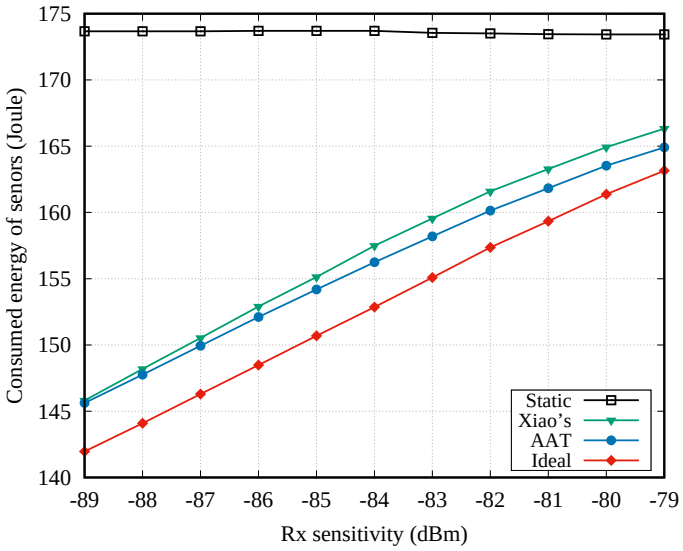

Figure 6.5: Energy consumption vs. Rx sensitivity.

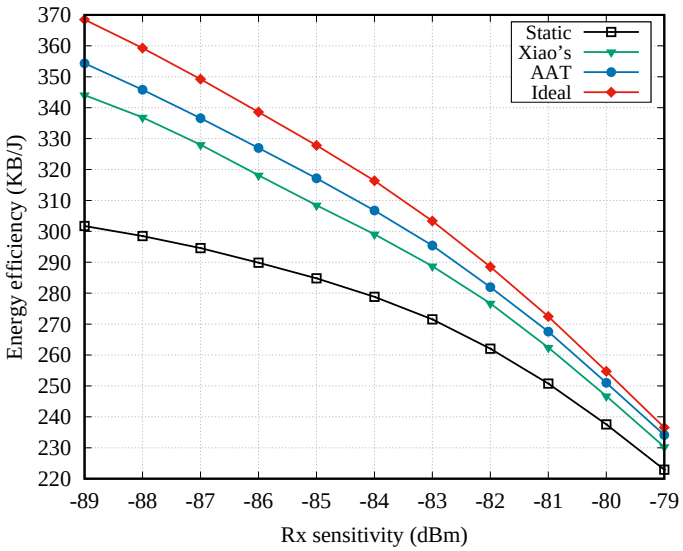

Figure 6.6: Energy efficiency vs. Rx sensitivity.

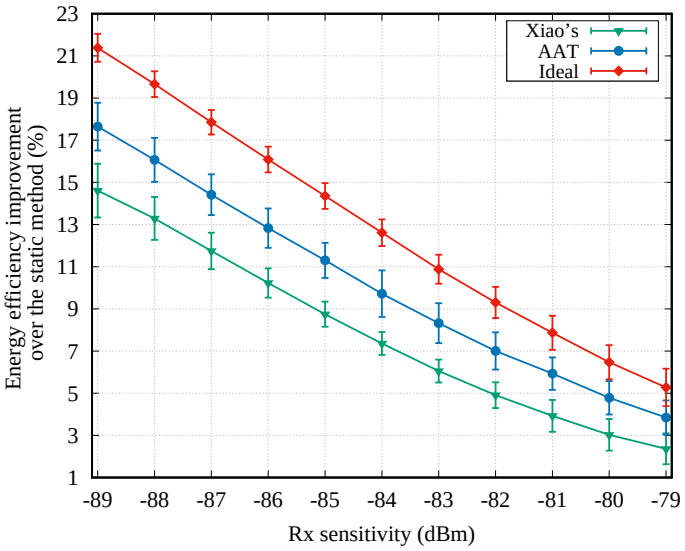

Figure 6.7: Energy efficiency improvement over the static scheme vs. Rx sensitivity.

scheme. This figure shows the overall simulation results over all 16 channel datasets. Note that the energy efficiency improvement refers to the percentage improvement, compared to the static method in terms of energy efficiency. Clearly, AAT achieves a much better energy efficiency improvement (6.43%-10.28%) in comparison with the conventional Xiao's method (0%-2.89%). Figure 6.7 also shows that the energy efficiency advantage of AAT is more significant when the Rx sensitivity is lower

• **Adaptive Transmission with Cooperation**

As cooperative transmission and NC technologies are considered as promising methods for increasing the transmission reliability, we evaluate the performances when two-hop cooperation is considered. Specifically, we provide the performance comparison when two types of cooperative mechanisms are adopted. The first cooperative mechanism does not take the NC into account, and this mechanism is called non-NC cooperative mechanism. The sensor node(s) predicted to be in outage in current beacon period is (are) selected as the relayed node(s), and one relay node is chosen randomly from the other sensor nodes. The second cooperative mechanism (denoted as NC cooperative mechanism) explores the RLNC (Random Linear Network Coding) technology in the relay node. Specifically, the hub selects one relay node, which stays in the Rx state during the whole DTP period to receive the data packets from all other sensor nodes. Then, the relay node performs the RLNC operation on all received packets to generate NC packets. These NC packets are sent to the hub in RTP. One of the biggest advantages of the NC cooperative mechanism is the hub does not specify the relayed node(s), and data packets from all sensor nodes have the chance to be recovered by the successful two-hop cooperative transmission. For instance, if the sensor node transmits two packets during its SUI and the RTP is configured

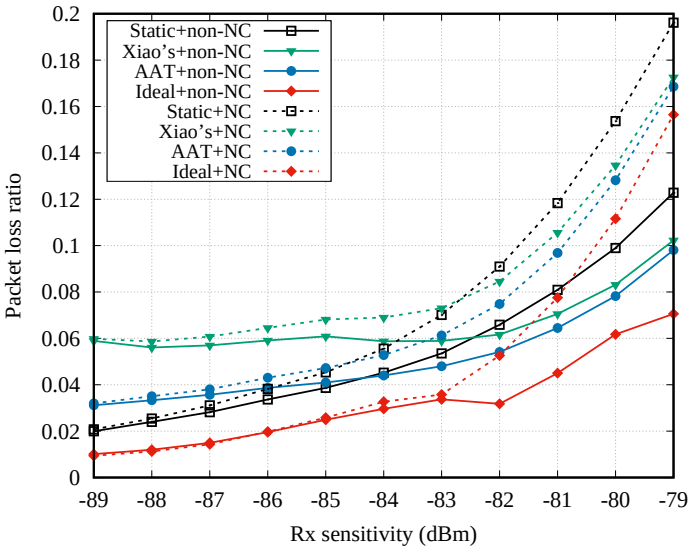

Figure 6.8: Packet loss ratio vs. Rx sensitivity.

as two times of the length of one SUI. Then all loss equal or less than four packets in the DTP can be recovered by the successful transmission of four NC packets. However, the NC cooperative mechanism requires the relay node to stay in the active state during the entire DTP period, which increases the energy consumption.

By importing the channel dataset CD_1, Figure 6.8 shows the average PLR of sensor nodes with varying Rx sensitivity in the hub side. As expected, both non-NC and NC cooperative mechanisms significantly reduce the PLR in comparison with the case without cooperation (cf. Figure 6.4). From Figure 6.8, non-NC cooperative mechanism always has a better performance than the NC cooperative mechanism in terms of PLR. Moreover, the PLR gap between the curves becomes bigger with the increasing Rx sensitivity. Based on the simulation configurations listed in Table 6.3, the length of RTP is two times of the length of one SUI, and one sensor node sends two packets in its SUI. Hence, the relay node transmits at most four native or NC packets to the hub during the RTP period. In the NC cooperative mechanisms, if more than four packets are lost in the DTP, all lost packets could not be recovered because the degree of freedom is not sufficient [149]. Instead, in the non-NC cooperative mechanisms, the relay node could always recover the lost packets from the relayed node if the two-hop transmission is successful, regardless of the number of lost packets in one DTP. This is the main reason why the gap between non-NC and NC cooperative mechanisms is widened when the Rx sensitivity is increased.

Next, the energy consumption results are illustrated in Figure 6.9. As shown in this figures, the NC cooperative mechanisms consume much more energy compared to the non-NC cooperative mechanisms. The main reason is that, in the NC cooperative mechanisms, when the sensor is selected as the relay node, the relay node stays in the Rx state during the entire DTP to receive the data packets from the remaining sensors. In contrast, the relay node in non-NC cooperative mechanisms only wakes up during the SUI(s) of the

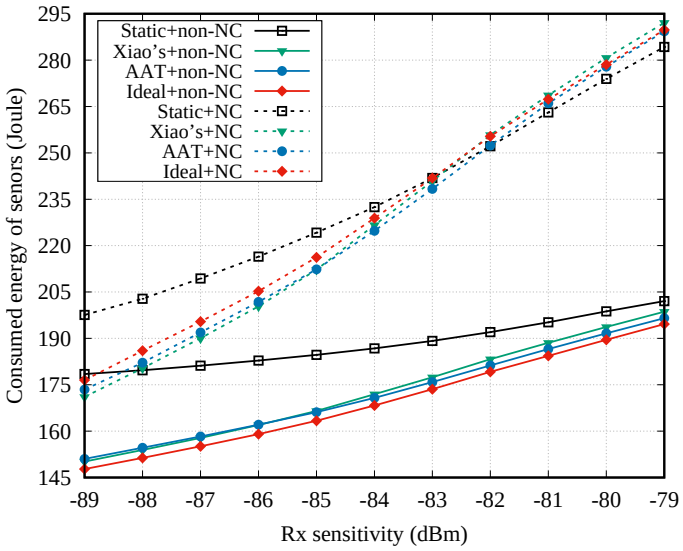

Figure 6.9: Energy consumption vs. Rx sensitivity.

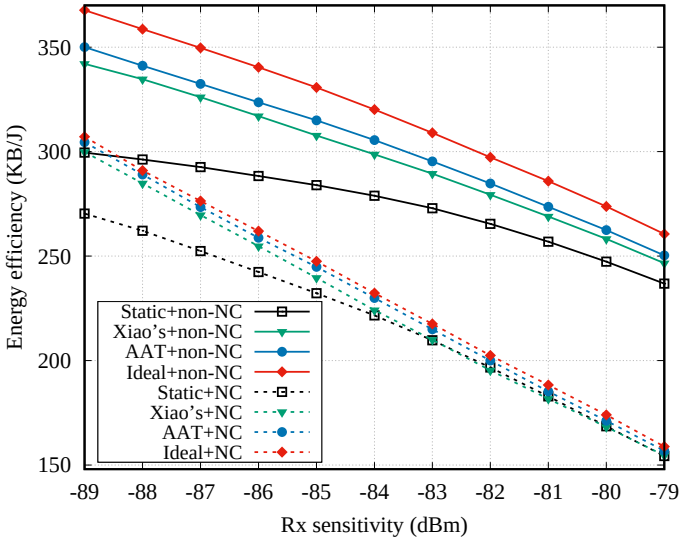

Figure 6.10: Energy efficiency vs. Rx sensitivity.

relayed node(s), which consumes less energy.

Figure 6.10 shows the energy efficiency when the two cooperative mechanisms are adopted. Clearly, compared to the NC cooperative mechanism, the non-NC method exhibits an advantage in terms of energy efficiency.

Similar to the cases without two-hop cooperation, we also provide the overall energy efficiency results over all 16 channel datasets. Figure 6.11 shows the average energy efficiency improvement of the "AAT+non-NC" scheme over the "AAT+NC" scheme. As shown in this figure, the non-NC cooperative mechanism achieves a much better energy efficiency in comparison with the NC cooperative mechanism for all collected channel datasets, and the improvement is enlarged (from 17.4% to 59.3%) with the increase of Rx sensitivity.

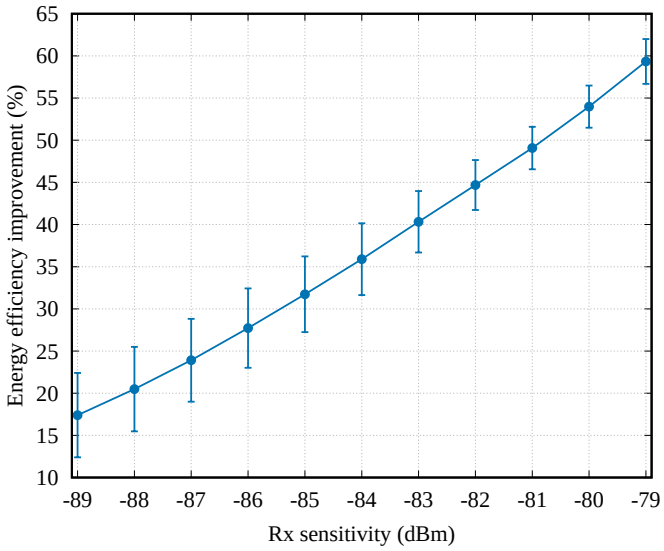

Figure 6.11: The energy efficiency improvement of the "AAT+non-NC" scheme over the "AAT+NC" scheme, when the Rx sensitivity varies.

Based on all above simulation results, we have the following observations. Firstly, our newly proposed AAT scheme is capable of improving the transmission reliability and at the same time reducing the energy consumption. Compared to the Xiao's TPC scheme, AAT improves the performance in terms of PLR, energy consumption, and energy efficiency. Secondly, we find that, in the star topology network, using NC technology to assist the uplink two-hop transmission may not be a good choice. The newly proposed non-NC cooperative mechanism achieves a better PLR performance while consuming less energy.

6.5 Chapter Summary

In this chapter, we jointly consider transmission power control, dynamic slot scheduling and two-hop cooperative mechanism to achieve a better trade-off between transmission reliability and energy consumption. Motivated by the significant autocorrelation characteristic of on-body channels in the daily WBAN scenarios, we propose an Autocorrelation-based Adaptive Transmission (AAT) scheme which uses a temporal autocorrelation model to predict channel conditions. Then, the estimated channel conditions are used to optimize the transmission power level and the transmission order of all sensor nodes for the next superframe. AAT scheme is designed to be compatible with IEEE 802.15.6. We also evaluate the performance of the newly proposed scheme by importing the channel datasets collected from real WBAN daily scenarios into our simulation model. Simulation results demonstrate that the proposed method can effectively improve the transmission reliability while reducing the energy consumption. Moreover, we provide the performance evaluation when two-hop cooperative transmission is used to further reduce the PLR. Two types of cooperative mechanisms are compared, i.e., the non-NC mechanism we proposed for AAT

and the NC cooperative mechanism. Based on the evaluation results, the NC cooperative mechanism does not exhibit the advantage in all performance metrics, i.e., PLR, energy consumption, and energy efficiency. Hence, using NC technology to assist the uplink two-hop transmission may not be practical in the context of WBANs.

Chapter 7

Conclusions and Future Works

In this chapter, we summarize the works presented in this thesis and put forward several directions for further research.

7.1 Conclusions

This thesis has investigated the reliable, energy-efficient transmission protocols for WBAN systems. We carefully collect a large amount of channel gain data from real WBAN scenarios, and then study the characteristics of on-body channels based on these channel datasets. Based on the analysis of this data, we jointly consider network coding, aggregative allocation, dynamic slot scheduling, transmission power control, and cooperative communication to optimize the transmission parameters and behaviors.

Chapter 2 provides the state of art literature reviews with in-depth insights on WBAN systems, IEEE 802.15.6, adaptive transmission schemes, and network coding in WBANs. These background knowledge and related works are essential to understanding the issues related to this thesis and the state of art. Many works focus on the simple migration of existing schemes from other network systems (including WSNs, Ad-hoc, cellular networks, etc.) to the WBAN environment, without carefully taking the peculiarities of WBAN channels into account. Besides, there are limited works that optimize the transmission reliability and energy efficiency from the perspectives of real WBANs scenarios and practical transmission protocol stacks.

In order to capture the real channel information in the dynamic WBAN scenarios, a customized portable wireless transceiver is built from easy-assembled hardware components. In Chapter 3, measurements are conducted by the test subjects wearing multiple wireless transceivers in two typical dynamic scenarios: walking and daily scenarios. Based on these channel datasets, on-body channel characteristics, including body shadowing effect, cross-correlation, autocorrelation, and transmission outage, are analyzed. The analysis results confirm that body shadowing is a predominant factor for the signal attenuation in

the 2.4GHz ISM band. In the walking scenarios, a strong periodicity is observed due to the upper limbs' swing. We also provide a detailed illustration of the RSSI variation and its corresponding walking phases. In daily scenarios with mixed activities, the outage analysis for on-body channels is provided from the perspective of outage duration, outage magnitude, and outage interval. The statistical results show that over 60% outage last longer than 10 ms, and the majority of outage magnitude (70.6%-82.5%) is smaller than 5 dB. The outage analyses provide the rationale for introducing cooperative communication and TPC technologies into WBAN systems. Moreover, the autocorrelation and cross-correlation of on-body channels are analyzed on both walking and daily scenarios. Interestingly, although the cross-correlation between on-body channels is not significant in the walking scenarios, the PLD (Path Loss Discrepancy) tends to remain big for a large proportion of time. This channel characteristic motivates us to propose a novel cross-layer transmission scheme to achieve a better balance between energy consumption and throughput in Chapter 4. As for the daily scenarios, we focus on the autocorrelation of on-body channels. Analysis results show that the autocorrelation of on-body channels is affected by many factors from the environment or the body tissue itself. However, overall, the on-body channel still exhibits a significant autocorrelation within a time lag of 500 ms. The works of Chapter 5 and Chapter 6 are motivated by the significant autocorrelation characteristic of on-body channels. Moreover, it is worthwhile to note that these channel datasets collected from real dynamic scenarios are imported into our simulation model to facilitate the performance evaluation.

In Chapter 4, we propose a novel cross-layer scheme, named A3NC, for WBAN walking scenarios. A3NC explores the combination of the aggregative allocation mechanism in the MAC layer and the analog network coding technique in the PHY layer. By comprehensive theoretical analyses of data rate, energy efficiency, and throughput balance, we demonstrate the upper bound and advantage of A3NC in the walking scenarios. Simulation results confirm that A3NC achieves a better trade-off between throughput and energy consumption, compared to the conventional approaches. To the best of our knowledge, this is the first work attempting to apply network coding to a spatially correlated WBAN system.

Starting from Chapter 5, we consider more completed dynamic WBAN scenarios, i.e., daily scenarios with mixed activities. We explore the dynamic slot scheduling method for daily WBAN scenarios. Dynamic slot scheduling does not require any extra hardware or software overhead on the sensor side. We propose a new DSS method, namely DSS-TA, which applies a temporal autocorrelation model to predict the channel condition for the future time slots. In DSS-TA, the slot scheduling problem is transformed into a minimum-cost bipartite matching problem, and the edges in the bipartite are weighted by the predicted average PLRs. DSS-TA is designed to be compatible with the IEEE 802.15.6 standard. Simulation results show that the DSS approach exhibits a great potential in decreasing the

PLR for daily scenarios. Moreover, we find that the superframe length is a key parameter which affects not only the upper bound of DSS methods but also the performance of the flipping and DSS-TA methods. There exist a superframe threshold for the flipping and DSS-TA methods. When the superframe length is shorter than the threshold, DSS-TA method is more effective than the flipping method. When the superframe length is longer than the threshold, DSS-TA almost remains the same performance with the flipping method. In the daily activity scenarios, the threshold is around 490 ms. Considering the packet latency requirement for the majority WBAN applications is below 250 ms, DSS-TA is a more feasible choice. As the transmission power level is a key parameter affecting both PLR and energy consumption. In Chapter 5, we also explore the effect of transmission power on the sensor side. In addition, we did not combine DSS-TA and A3NC in one WBAN architecture. Since A3NC is proposed for walking scenarios while the DSS-TA is designed for daily life scenarios, combining A3NC into DSS-TA requires more overhead to support the combination but is possible. For example, a human motion or posture recognition algorithm is needed to detect the nature of activity and trigger the A3NC, which may require extra acceleration sensors or designing new walking motion recognition algorithm based on RSSI variation feature. One advantage of DSS-TA is its simplicity, as it does not require extra relay nodes and most of the operation of DSS-TA is performed at the hub side. Addition of A3NC will increase the system complexity. Hence, by carefully designing motion recognition algorithm and considering the deployment of relay node, the combination of DSS-TA and A3NC might further improve the transmission performance not only in walking scenarios but also in daily life scenarios.

The work of DSS-TA assumes the transmission power level on the sensor side is fixed and remains the same for all sensor nodes. In Chapter 6, we jointly consider transmission power control, dynamic slot scheduling, and two-hop cooperative mechanism to achieve a better trade-off between transmission reliability and energy consumption for daily scenarios. Motivated by the significant autocorrelation characteristic of on-body channels, we propose an autocorrelation-based adaptive transmission (AAT) scheme which uses a temporal autocorrelation model to predict the channel condition in the next superframe. Then, the estimated channel conditions are used to optimize the transmission power level and the transmission order of all sensor nodes for the next superframe. The AAT scheme is designed to be compatible with IEEE 802.15.6. We also evaluate the performance of the newly proposed scheme by importing the real channel datasets into our simulation model. Simulation results demonstrate that the AAT method can effectively improve the transmission reliability while reducing the energy consumption. Moreover, we provide the performance evaluation when two-hop cooperative transmission is used to further reduce the PLR. Two types of cooperative mechanisms, i.e., the non-NC mechanism we proposed for AAT and the NC cooperative mechanism, are compared. Based on the evaluation results, the NC cooperative mechanism does not exhibit the advantage in all

performance metrics, i.e., PLR, energy consumption, and energy efficiency. Hence, using the NC technology to assist the uplink two-hop transmission may not be practical in the context of WBANs.

7.2 Future Works

Based on the works presented in this thesis, several issues remain open for possible future research.

1. With regard to the measurement campaigns, we only considered the on-body channels, and the number of sensors is limited to 5. Either enriching the types of WBAN channels, e.g., the channel from implant nodes to on-body nodes and the channels from on-body nodes to off-body nodes, or increasing the sensor number may provide new insights for the design of transmission system. Besides, each channel gain dataset used in the thesis is collected from a single WBAN deployed on one person. It is a challenging task to design and carry out the measurement campaigns when multiple WBANs coexist in a small area, and then collect effective channel information that could be used to analyze the interference and the potential of cooperative communication between different WBANs.

2. Interference mitigation is another research topic in the context of WBAN systems. As the PHY network coding technique (e.g., analogy network coding) mixes the received signals at PHY layer, it may provide a new insight to solve the severe interference problem when multiple WBANs overlap each other.

3. The priority of sensor nodes or traffic is not considered in this thesis. It is also an interesting research problem to take the traffic priority into account in designing adaptive transmission schemes.

4. In this thesis, adaptive transmission schemes consider the following transmission parameters: transmission power level, transmission order, adjustment between cooperation and non-cooperation. Other parameters, such as modulation type, channel hopping, and transmission data rate, are also promising to overcome the transmission challenges in WBAN systems. Besides, in this thesis, the contention-based MAC approach is only used for the transaction of control and management packets in a fixed time period, and schedule-based MAC approach is used to complete the transmission of data packets in the uplink. It would be an interesting research area if more transmission mechanisms and parameters are adaptively optimized to provide a more flexible transmission protocol for WBANs.

Bibliography

[1] B. Touijer, Y. B. Maissa, and S. Mouline, "MAC protocols for wireless body area networks: An overview," in *Proc. International Wireless Communications and Mobile Computing Conference (IWCMC)*, Jun. 2017, pp. 1227–1232.

[2] R. Ahlswede *et al.*, "Network information flow," *IEEE Trans. Inf. Theory*, vol. 46, no. 4, pp. 1204–1216, Jul. 2000.

[3] S. Movassaghi *et al.*, "Wireless body area networks: A survey," *IEEE Commun. Surveys Tuts.*, vol. 16, no. 3, pp. 1658–1686, Mar. 2014.

[4] IEEE Standards Association, "IEEE standard for local and metropolitan area networks - part 15.6: Wireless body area networks," *IEEE Standard 802.15.6-2012*, pp. 1–271, Feb. 2012.

[5] M. A. Razzaque, M. T. Hira, and M. Dira, "QoS in body area networks: A survey," *ACM Trans. Sens. Netw.*, vol. 13, no. 3, 25:1–25:46, Aug. 2017.

[6] S. Ullah *et al.*, "A comprehensive survey of wireless body area networks," *J. Med. Syst.*, vol. 36, no. 3, pp. 1065–1094, Jun. 2012.

[7] K. Y. Yazdandoost and K. Sayrafian-Pour, "Channel model for body area network (BAN)," *IEEE P802.15.6*, Apr. 2009.

[8] M. Sudjai, L. C. Tran, and F. Safaei, "Performance analysis of STFC MB-OFDM UWB in WBAN channels," in *Proc. IEEE International Symposium on Personal, Indoor and Mobile Radio Communications (PIMRC)*, Sep. 2012, pp. 1710–1715.

[9] L. W. Hanlen *et al.*, "Interference in body area networks: Distance does not dominate," in *Proc. IEEE International Symposium on Personal, Indoor and Mobile Radio Communications (PIMRC)*, Sep. 2009, pp. 281–285.

[10] J. Zhang *et al.*, "Stability of narrowband dynamic body area channel," *IEEE Antennas Wireless Propag. Lett.*, vol. 8, pp. 53–56, Dec. 2009.

[11] A. Boulis *et al.*, "Challenges in body area networks for healthcare: The MAC," *IEEE Commun. Mag.*, vol. 50, no. 5, pp. 100–106, May 2012.

[12] B. SIG. (2014). Bluetooth specification version 4.2, [Online]. Available: `https://www.bluetooth.org/en-us/specification/adopted-specifications`.

[13] IEEE Standards Association, "IEEE standard for information technology– local and metropolitan area networks– specific requirements– part 15.4: Wireless medium access control (MAC) and physical layer (PHY) specifications for low rate wireless personal area networks (WPANs)," *IEEE Standard 802.15.4-2006*, pp. 1–320, Sep. 2006.

[14] M. S. Akbar, H. Yu, and S. Cang, "TMP: Tele-medicine protocol for slotted 802.15.4 with duty-cycle optimization in wireless body area sensor networks," *IEEE Sensors J.*, vol. 17, no. 6, pp. 1925–1936, Mar. 2017.

[15] M. Singh and N. Jain, "Performance and evaluation of smartphone based wireless blood pressure monitoring system using bluetooth," *IEEE Sensors J.*, vol. 16, no. 23, pp. 8322–8328, Dec. 2016.

[16] B. Yu, L. Yang, and C. C. Chong, "ECG monitoring over bluetooth: Data compression and transmission," in *Proc. IEEE Wireless Communications and Networking Conference (WCNC)*, Apr. 2010, pp. 1–5.

[17] A. Fort *et al.*, "Ultra-wideband channel model for communication around the human body," *IEEE J. Sel. Areas Commun.*, vol. 24, no. 4, pp. 927–933, Apr. 2006.

[18] D. Smith *et al.*, "Power delay profiles for dynamic narrowband body area network channels id: 15-09-0187-01-0006," *IEEE submission*, 2009.

[19] M. Sudjai, L. C. Tran, and F. Safaei, "On the energy efficiency of adaptive WBAN systems for mhealth services," *EAI Endorsed Transactions on Pervasive Health and Technology*, vol. 17, no. 9, pp. 1–12, Mar. 2017.

[20] S. Xiao *et al.*, "Transmission power control in body area sensor networks for healthcare monitoring," *IEEE J. Sel. Areas Commun.*, vol. 27, no. 1, pp. 37–48, Jan. 2009.

[21] D. B. Smith *et al.*, "Simple prediction-based power control for the on-body area communications channel," in *Proc. IEEE International Conference on Communications (ICC)*, Jun. 2011, pp. 1–5.

[22] W. Gao *et al.*, "Transmission power control for IEEE 802.15.6 body area networks," *ETRI Journal*, vol. 36, no. 2, pp. 313–316, Apr. 2014.

[23] A. H. Sodhro, Y. Li, and M. A. Shah, "Energy-efficient adaptive transmission power control for wireless body area networks," *IET Commun.*, vol. 10, no. 1, pp. 81–90, Jan. 2016.

[24] W. Lee, B.-D. Lee, and N. Kim, "Hybrid transmission power control for wireless body sensor systems," *Int. J. Distrib. Sens. Netw.*, vol. 10, no. 10, Oct. 2014.

[25] D. B. Smith, L. W. Hanlen, and D. Miniutti, "Transmit power control for wireless body area networks using novel channel prediction," in *Proc. IEEE Wireless Communications and Networking Conference (WCNC)*, Apr. 2012, pp. 684–688.

[26] J. Dong and D. Smith, "Joint relay selection and transmit power control for wireless body area networks coexistence," in *Proc. IEEE International Conference on Communications (ICC)*, Jun. 2014, pp. 5676–5681.

[27] F. D. Franco, Y. Ge, and I. Tinnirello, "On-body and off-body transmit power control in IEEE 802.15.6 scheduled access networks," in *Proc. IEEE International Symposium on Personal, Indoor and Mobile Radio Communications (PIMRC)*, Sep. 2014, pp. 1254–1258.

[28] S. Archasantisuk *et al.*, "Transmission power control in WBAN using the context-specific temporal correlation model," in *Proc. IEEE International Symposium on Personal, Indoor and Mobile Radio Communications (PIMRC)*, Sep. 2016, pp. 1–6.

[29] Y. Zhang and B. Zhang, "A relay-aided transmission power control method in wireless body area networks," *IEEE Access*, vol. 5, pp. 8408–8418, Apr. 2017.

[30] Y. Zhou *et al.*, "Topology design and cross-layer optimization for wireless body sensor networks," *Ad Hoc Networks*, vol. 59, pp. 48–62, May 2017.

[31] M. Vallejo, J. R. Piorno, and J. L. A. Rodrigo, "A link quality estimator for power-efficient communication over on-body channels," in *Proc. IEEE International Conference on Embedded and Ubiquitous Computing (EUC)*, Aug. 2014, pp. 250–257.

[32] M. Vallejo, J. Recas, and J. L. Ayala, "Proactive and reactive transmission power control for energy-efficient on-body communications," *Sensors*, vol. 15, no. 3, pp. 5914–5934, Mar. 2015.

[33] S. Kim, S. Kim, and D. S. Eom, "RSSI/LQI-based transmission power control for body area networks in healthcare environment," *IEEE J. Biomed. Health Inform.*, vol. 17, no. 3, pp. 561–571, May 2013.

[34] L. Zou *et al.*, "Bayesian game based power control scheme for inter-WBAN interference mitigation," in *Proc. IEEE Global Communications Conference (GLOBECOM)*, Dec. 2014, pp. 240–245.

[35] X. Yong *et al.*, "A self-adaptive power control algorithm based on game theory for inter-WBAN interference mitigation," in *Proc. IEEE International Conference on Computer and Communications (ICCC)*, Oct. 2016, pp. 2873–2877.

[36] J. Wang, Y. Sun, and Y. Ji, "QoS-based adaptive power control scheme for co-located WBANs: A cooperative bargaining game theoretic perspective," *Wireless Networks*, pp. 1–11, May 2017.

[37] X. Zhao *et al.*, "QoS-driven power control for inter-WBAN interference mitigation," in *Proc. IEEE Global Communications Conference (GLOBECOM)*, Dec. 2015, pp. 1–6.

[38] H. Moosavi and F. M. Bui, "Optimal relay selection and power control with quality-of-service provisioning in wireless body area networks," *IEEE Trans. Wireless Commun.*, vol. 15, no. 8, pp. 5497–5510, Aug. 2016.

[39] M. Quwaider, J. Rao, and S. Biswas, "Body-posture-based dynamic link power control in wearable sensor networks," *IEEE Commun. Mag.*, vol. 48, no. 7, pp. 134–142, Jul. 2010.

[40] W. Zang and Y. Li, "Motion aware transmission power control scheme in wireless body area network," in *Proc. IEEE Workshop on Signal Processing Systems (SiPS)*, Oct. 2015, pp. 1–5.

[41] W. Zang, S. Zhang, and Y. Li, "An accelerometer-assisted transmission power control solution for energy-efficient communications in WBAN," *IEEE J. Sel. Areas Commun.*, vol. 34, no. 12, pp. 3427–3437, Sep. 2016.

[42] W. Zang and Y. Li, "Gait cycle driven transmission power control scheme for wireless body area network," *IEEE J. Biomed. Health Inform.*, Mar. 2017.

[43] Y. Li *et al.*, "MAPM: Movement-based adaptive prediction mechanism for energy conservation in body sensor networks," in *Proc. IEEE Global Communications Conference (GLOBECOM)*, Dec. 2016, pp. 1–6.

[44] M. Neugebauer, J. Plonnigs, and K. Kabitzsch, "A new beacon order adaptation algorithm for IEEE 802.15.4 networks," in *Proc. European Workshop on Wireless Sensor Networks*, Feb. 2005, pp. 302–311.

[45] B. Gao and C. He, "An individual beacon order adaptation algorithm for IEEE 802.15.4 networks," in *Proc. IEEE International Conference on Communication Systems*, Nov. 2008, pp. 12–16.

[46] A. Barbieri, F. Chiti, and R. Fantacci, "WSN17-2: Proposal of an adaptive MAC protocol for efficient IEEE 802.15.4 low power communications," in *Proc. IEEE Global Communications Conference (GLOBECOM)*, Nov. 2006, pp. 1–5.

[47] H. Rasouli, Y. S. Kavian, and H. F. Rashvand, "ADCA: Adaptive duty cycle algorithm for energy efficient IEEE 802.15.4 beacon-enabled wireless sensor networks," *IEEE Sensors J.*, vol. 14, no. 11, pp. 3893–3902, Aug. 2014.

[48] J. Hurtado-López and E. Casilari, "An adaptive algorithm to optimize the dynamics of IEEE 802.15. 4 networks," in *Proc. International Conference on Mobile Networks and Management*, Sep. 2013, pp. 136–148.

[49] M. Khanafer, M. Guennoun, and H. T. Mouftah, "Adaptive sleeping periods in IEEE 802.15.4 for efficient energy savings: Markov-based theoretical analysis," in *Proc. IEEE International Conference on Communications (ICC)*, Jun. 2011, pp. 1–6.

[50] C. H. S. Oliveira, Y. Ghamri-Doudane, and S. Lohier, "A duty cycle self-adaptation algorithm for the 802.15.4 wireless sensor networks," in *Proc. IEEE Global Information Infrastructure Symposium*, Oct. 2013, pp. 1–7.

[51] A. Farhad, Y. Zia, and F. B. Hussain, "Survey of dynamic super-frame adjustment schemes in beacon-enabled IEEE 802.15.4 networks: An application's perspective," *Wireless Personal Communications*, vol. 91, no. 1, pp. 119–135, Nov. 2016.

[52] A. Farhad *et al.*, "D-MAC: A dynamic MAC algorithm for the body area sensor networks based on ieee 802.15. 4," *International Journal of Computer Science and Network Security (IJCSNS)*, vol. 16, no. 5, p. 29, May 2016.

[53] M. M. Alam *et al.*, "A heuristic self-adaptive medium access control for resource-constrained WBAN systems," *IEEE Access*, vol. 4, pp. 1287–1300, 2016.

[54] H. Alshaheen and H. T. Rizk, "Improving the energy efficiency for a WBSN based on a coordinate duty cycle and network coding," in *Proc. International Wireless Communications and Mobile Computing Conference (IWCMC)*, Jun. 2017, pp. 1215–1220.

[55] M. M. Alam and E. Ben Hamida, "Strategies for optimal MAC parameters tuning in IEEE 802.15.6 wearable wireless sensor networks," *J. Med. Syst.*, vol. 39, no. 9, pp. 1–16, Sep. 2015.

[56] S. J. Marinkovic *et al.*, "Energy-efficient low duty cycle MAC protocol for wireless body area networks," *IEEE Trans. Inf. Technol. Biomed.*, vol. 13, no. 6, pp. 915–925, Nov. 2009.

[57] A. Asadi and V. Mancuso, "A survey on opportunistic scheduling in wireless communications," *IEEE Commun. Surveys Tuts.*, vol. 15, no. 4, pp. 1671–1688, Apr. 2013.

[58] Y. Tselishchev, L. Libman, and A. Boulis, "Reducing transmission losses in body area networks using variable TDMA scheduling," in *Proc. IEEE International Symposium on a World of Wireless, Mobile and Multimedia Networks (WoWMoM)*, Jun. 2011, pp. 1–10.

[59] Y. Tselishchev, A. Boulis, and L. Libman, "Variable scheduling to mitigate channel losses in energy-efficient body area networks," *Sensors*, vol. 12, no. 11, pp. 14 692–14 710, Nov. 2012.

[60] E. N. Gilbert, "Capacity of a burst-noise channel," *Bell Labs Tech. J.*, vol. 39, no. 5, pp. 1253–1265, Sep. 1960.

[61] Y. Zhou *et al.*, "Beacon-based opportunistic scheduling in wireless body area network," in *Proc. IEEE International Conference of the Engineering in Medicine and Biology Society (EMBC)*, Aug. 2016, pp. 4995–4998.

[62] R. Pan *et al.*, "An opportunistic relay protocol with dynamic scheduling in wireless body area sensor network," *IEEE Sensors J.*, vol. 15, no. 7, pp. 3743–3750, Jul. 2015.

[63] Z. Yan, B. Liu, and C. W. Chen, "QoS-driven scheduling approach using optimal slot allocation for wireless body area networks," in *Proc. IEEE International Conference on e-Health Networking, Applications and Services (Healthcom)*, Oct. 2012, pp. 267–272.

[64] B. Liu, Z. Yan, and C. W. Chen, "MAC protocol in wireless body area networks for e-health: Challenges and a context-aware design," *IEEE Wireless Commun.*, vol. 20, no. 4, pp. 64–72, Sep. 2013.

[65] B. Liu, Z. Yan, and C. W. Chen, "Medium access control for wireless body area networks with QoS provisioning and energy efficient design," *IEEE Trans. Mobile Comput.*, vol. 16, no. 2, pp. 422–434, Feb. 2017.

[66] S. Bhandari and S. Moh, "A priority-based adaptive MAC protocol for wireless body area networks," *Sensors*, vol. 16, no. 3, p. 401, Mar. 2016.

[67] A. Sevin, C. Bayilmis, and I. Kirbas, "Design and implementation of a new quality of service-aware cross-layer medium access protocol for wireless body area networks," *Comput. Electr. Eng.*, vol. 56, pp. 145–156, Nov. 2016.

[68] A. K. Subramanian and I. Paramasivam, "PRIN: A priority-based energy efficient MAC protocol for wireless sensor networks varying the sample inter-arrival time," *Wireless Personal Communications*, pp. 1–19, Feb. 2016.

[69] X. Yuan *et al.*, "A token-based dynamic scheduled MAC protocol for health monitoring," *EURASIP Journal on Wireless Communications and Networking*, vol. 2016, no. 1, pp. 1–18, May 2016.

[70] K. S. Prabh and J.-H. Hauer, "Opportunistic packet scheduling in body area networks," in *Proc. European Conference Wireless Sensor Networks (EWSN)*, Feb. 2011, pp. 114–129.

[71] J.-H. Hauer, "Leveraging human mobility for communication in body area networks," *ACM Trans. Sens. Netw.*, vol. 10, no. 3, pp. 1–38, Apr. 2014.

[72] M. Salayma *et al.*, "New dynamic, reliable and energy efficient scheduling for wireless body area networks (WBAN)," in *Proc. IEEE International Conference on Communications (ICC)*, May 2017, pp. 1–6.

[73] K. S. Prabh *et al.*, "A MAC protocol for reliable communication in low power body area networks," *J. Syst. Archit.*, May 2016.

[74] N. Thepvilojanapong *et al.*, "Adaptive channel and time allocation for body area networks," *IET Commun.*, vol. 5, no. 12, pp. 1637–1649, Aug. 2011.

[75] M. J. Ali, H. Moungla, and A. Mehaoua, "Dynamic channel access scheme for interference mitigation in relay-assisted intra-WBANs," in *Proc. International Conference on Protocol Engineering (ICPE) and International Conference on New Technologies of Distributed Systems (NTDS)*, Jul. 2015, pp. 1–6.

[76] P. Tuset-Peiro *et al.*, "LPDQ: A self-scheduled TDMA MAC protocol for one-hop dynamic low-power wireless networks," *Pervasive Mob. Comput.*, vol. 20, pp. 84–99, Jul. 2015.

[77] N. Mouzehkesh *et al.*, "Dynamic backoff scheduling of low data rate applications in wireless body area networks," *Wireless Networks*, vol. 21, no. 8, pp. 2571–2592, Nov. 2015.

[78] K. S. Deepak and A. V. Babu, "Packet size optimization for energy efficient cooperative wireless body area networks," in *Proc. IEEE India Conference (INDICON)*, Dec. 2012, pp. 736–741.

[79] M. S. Mohammadi, Q. Zhang, and E. Dutkiewicz, "Channel-adaptive MAC frame length in wireless body area networks," in *Proc. International Symposium on Wireless Personal Multimedia Communications (WPMC)*, Sep. 2014, pp. 584–588.

[80] S. Moulik, S. Misra, and D. Das, "AT-MAC: Adaptive MAC-frame payload tuning for reliable communication in wireless body area networks," *IEEE Trans. Mobile Comput.*, vol. 16, no. 6, pp. 1516–1529, Jun. 2017.

[81] R. Chai *et al.*, "Network lifetime maximization based joint resource optimization for wireless body area networks," in *Proc. IEEE International Symposium on Personal, Indoor and Mobile Radio Communications (PIMRC)*, Sep. 2014, pp. 1088–1092.

[82] Q. Zhang, M. Chaturvedi, and R. H. Jacobsen, "Performance study of the enhancement schemes for baseline MAC of body area networks," in *Proc. International Symposium on Medical Information and Communication Technology (ISMICT)*, Apr. 2014, pp. 1–5.

[83] Z. Liu *et al.*, "Energy-efficient resource allocation with QoS support in wireless body area networks," in *Proc. IEEE Global Communications Conference (GLOBECOM)*, Dec. 2015, pp. 1–6.

[84] M. Sudjai, L. C. Tran, and F. Safaei, "Adaptive space-time-frequency-coded UWB system for wireless body area network," *EURASIP Journal on Wireless Communications and Networking*, vol. 2015, no. 1, pp. 1–11, Dec. 2015.

[85] M. Sudjai *et al.*, "High-speed adaptive wireless body area networks," *EURASIP Journal on Wireless Communications and Networking*, vol. 2016, no. 269, pp. 1–16, Nov. 2016.

[86] M. Sudjai, L. C. Tran, and F. Safaei, "A BER based adaptive STFC MB-OFDM UWB system for WBAN applications," in *Proc. IEEE International Conference on Communications (ICC)*, Jun. 2014, pp. 5670–5675.

[87] M. Sudjai *et al.*, "Optimal adaptive wireless body area networks for high speed in health services," *Biomed. Tech.*, vol. 59, pp. 750–753, Oct. 2014.

[88] S. Katti *et al.*, "XORs in the air: Practical wireless network coding," *IEEE/ACM Trans. Netw.*, vol. 16, no. 3, pp. 497–510, Jun. 2008.

[89] F. Rossetto and M. Zorzi, "Mixing network coding and cooperation for reliable wireless communications," *IEEE Wireless Commun.*, vol. 18, no. 1, pp. 15–21, Feb. 2011.

[90] A. Argyriou and A. Pandharipande, "Cooperative protocol for analog network coding in distributed wireless networks," *IEEE Trans. Wireless Commun.*, vol. 9, no. 10, pp. 3112–3119, Oct. 2010.

[91] L. C. Tran *et al.*, "Novel receiver for correlated fading multi-antenna physical network coding TWRNs," *Advances in Communication Technology*, vol. 5, pp. 16–25, Dec. 2013.

[92] S. Katti, S. Gollakota, and D. Katabi, "Embracing wireless interference: Analog network coding," *ACM SIGCOMM Computer Communication Review*, vol. 37, no. 4, pp. 397–408, Aug. 2007.

[93] S. Marinkovic and E. Popovici, "Network coding for efficient error recovery in wireless sensor networks for medical applications," in *Proc. International Conference on Emerging Network Intelligence*, Oct. 2009, pp. 15–20.

[94] A. Taparugssanagorn, F. Ono, and R. Kohno, "Network coding for non-invasive wireless body area networks," in *Proc. IEEE International Symposium on Personal, Indoor and Mobile Radio Communications Workshops (PIMRC)*, Sep. 2010, pp. 134–138.

[95] E. Byrne *et al.*, "A graph theoretical approach for network coding in wireless body area networks," in *Proc. IEEE International Symposium on Information Theory Proceedings*, Jul. 2011, pp. 405–409.

[96] E. Byrne and A. Manada, "On coding schemes for wireless body area networks," in *Proc. International Symposium onCommunications and Information Technologies (ISCIT)*, Oct. 2012, pp. 149–154.

[97] K. Yokota, A. Mamada, and H. Morita, "An XOR encoding for wireless body area networks," in *Proc. International Conference on Body Area Networks (BodyNets)*, Oct. 2013, pp. 240–243.

[98] M. A. Razzaque *et al.*, "QoS-aware error recovery in wireless body sensor networks using adaptive network coding," *Sensors*, vol. 15, no. 1, pp. 440–464, Dec. 2015.

[99] Z. J. Haas and T. C. Chen, "Cluster-based cooperative communication with network coding in wireless networks," in *Proc. IEEE Military Communications Conference (MILCOM)*, Oct. 2010, pp. 2082–2089.

[100] G. E. Arrobo and R. D. Gitlin, "Improving the reliability of wireless body area networks," in *Proc. IEEE International Conference of the Engineering in Medicine and Biology Society (EMBC)*, Aug. 2011, pp. 2192–2195.

[101] G. E. Arrobo and R. D. Gitlin, "New approaches to reliable wireless body area networks," in *Proc. IEEE International Conference on Microwaves, Communications, Antennas and Electronic Systems (COMCAS)*, Nov. 2011, pp. 1–6.

[102] G. E. Arrobo and R. D. Gitlin, "Minimizing energy consumption for cooperative network and diversity coded sensor networks," in *Proc. Wireless Telecommunications Symposium*, Apr. 2014, pp. 1–7.

[103] E. Kartsakli *et al.*, "A cloud-assisted random linear network coding medium access control protocol for healthcare applications," *Sensors*, vol. 14, no. 3, pp. 4806–4830, Mar. 2014.

[104] E. Kartsakli *et al.*, "Reliable MAC design for ambient assisted living: Moving the coordination to the cloud," *IEEE Commun. Mag.*, vol. 53, no. 1, pp. 78–86, Jan. 2015.

[105] X. Shi, M. Médard, and D. E. Lucani, "When both transmitting and receiving energies matter: An application of network coding in wireless body area networks," in *Proc. International Conference on Research in Networking*, May 2011, pp. 119–128.

[106] X. Shi, M. Médard, and D. E. Lucani, "Whether and where to code in the wireless packet erasure relay channel," *IEEE J. Sel. Areas Commun.*, vol. 31, no. 8, pp. 1379–1389, Aug. 2013.

[107] S. Movassaghi *et al.*, "An energy efficient network coding approach for wireless body area networks," in *Proc. IEEE Conference on Local Computer Networks (LCN)*, Oct. 2013, pp. 468–475.

[108] G. Angelopoulos *et al.*, "Experimental study of the interplay of channel and network coding in low power sensor applications," in *Proc. IEEE International Conference on Communications (ICC)*, Jun. 2013, pp. 5126–5130.

[109] S. Movassaghi, M. Shirvanimoghaddam, and M. Abolhasan, "A cooperative network coding approach to reliable wireless body area networks with demodulate-and-forward," in *Proc. International Wireless Communications and Mobile Computing Conference (IWCMC)*, Jul. 2013, pp. 394–399.

[110] H. Alshaheen and H. T. Rizk, "Improving the energy efficiency for biosensor nodes in the WBSN bottleneck zone based on a random linear network coding," in *Proc. International Symposium on Medical Information and Communication Technology (ISMICT)*, Feb. 2017, pp. 59–63.

[111] A. S. Lalos *et al.*, "Cooperative compressed sensing schemes for telemonitoring of vital signals in WBANs," in *Proc. IEEE Global Communications Conference (GLOBECOM)*, Dec. 2014, pp. 2387–2392.

[112] A. S. Lalos *et al.*, "RLNC-Aided cooperative compressed sensing for energy efficient vital signal telemonitoring," *IEEE Trans. Wireless Commun.*, vol. PP, no. 99, pp. 1–1, Jul. 2015.

[113] B. Liu, Y. You, and C. W. Chen, "CS-based reliable transmission strategy for wireless body area networks," in *Proc. IEEE China Summit and International Conference on Signal and Information Processing (ChinaSIP)*, Jul. 2015, pp. 448–452.

[114] A. Esfahani *et al.*, "An efficient MAC-based scheme against pollution attacks in XOR network coding-enabled WBANs for remote patient monitoring systems," *EURASIP Journal on Wireless Communications and Networking*, vol. 2016, no. 1, p. 113, Apr. 2016.

[115] D. B. Smith, D. Miniutti, and L. W. Hanlen, "Characterization of the body-area propagation channel for monitoring a subject sleeping," *IEEE Trans. Antennas Propag.*, vol. 59, no. 11, pp. 4388–4392, Nov. 2011.

[116] V. Chaganti, L. Hanlen, and D. Smith, "Are narrowband wireless on-body networks wide-sense stationary?" *IEEE Trans. Wireless Commun.*, vol. 13, no. 5, pp. 2432–2442, May 2014.

[117] M. Lauzier *et al.*, "Full mesh channel measurements on body area networks under walking scenarios," in *Proc. European Conference on Antennas and Propagation (EuCAP)*, Apr. 2013, pp. 3508–3512.

[118] S. L. Cotton and W. G. Scanlon, "A statistical analysis of indoor multipath fading for a narrowband wireless body area network," in *Proc. IEEE International Symposium on Personal, Indoor and Mobile Radio Communications (PIMRC)*, Sep. 2006, pp. 1–5.

[119] A. Fort *et al.*, "Indoor body-area channel model for narrowband communications," *IET Microwaves Antennas Propag.*, vol. 1, no. 6, pp. 1197–1203, Dec. 2007.

[120] V. G. Chaganti, D. B. Smith, and L. W. Hanlen, "Second-order statistics for many-link body area networks," *IEEE Antennas Wireless Propag. Lett.*, vol. 9, pp. 322–325, Apr. 2010.

[121] A. Alomainy and Y. Hao, "Modeling and characterization of biotelemetric radio channel from ingested implants considering organ contents," *IEEE Trans. Antennas Propag.*, vol. 57, no. 4, pp. 999–1005, 2009.

[122] S. Movassaghi *et al.*, "Enabling interference-aware and energy-efficient coexistence of multiple wireless body area networks with unknown dynamics," *IEEE Access*, vol. 4, pp. 2935–2951, 2016.

[123] S. Movassaghi *et al.*, "Self-organization amongst multiple co-existing wireless body area networks," in *Proc. IEEE International Symposium on Personal, Indoor and Mobile Radio Communications (PIMRC)*, Aug. 2015, pp. 1323–1327.

[124] H. Zhang, F. Safaei, and L. C. Tran, "Measurement-based characterizations of on-body channel in the human walking scenario," in *Proc. IEEE Vehicular Technology Conference (VTC2017-Spring)*, Jun. 2017, pp. 1–5.

[125] H. Zhang, F. Safaei, and L. C. Tran, "Joint analog network coding and channel allocation in the walking scenario for WBAN," in *Proc. IEEE Symposium on Computers and Communication (ISCC)*, Jun. 2016, pp. 604–609.

[126] H. Zhang, F. Safaei, and L. C. Tran, "A novel cooperation-based network coding scheme for walking scenarios in WBANs," *Wireless Communications and Mobile Computing*, vol. 2017, pp. 1–20, Sep. 2017.

[127] H. Zhang, F. Safaei, and L. C. Tran, "Channel autocorrelation based dynamic slot scheduling for body area networks," *Submitted to EURASIP Journal on Wireless Communications and Networking*, 2017.

[128] L. Hanlen *et al.*, "Open-source testbed for body area networks: 200 sample/sec, 12 hrs continuous measurement," in *Proc. IEEE International Symposium on Personal, Indoor and Mobile Radio Communications Workshops (PIMRC)*, Sep. 2010, pp. 66–71.

[129] K. Pearson, "Note on regression and inheritance in the case of two parents," *Proc. Roy. Soc. London*, vol. 58, pp. 240–242, Jan. 1895.

[130] J. G. Proakis and M. Salehi, *Digital Communications, 5th ed*. McGraw-Hill, 2007.

[131] J. G. Proakis and M. Salehi, *Fundamentals of communication systems*. Pearson Education, 2007.

[132] D. B. Smith *et al.*, "Temporal correlation of dynamic on-body area radio channel," *Electron. Lett.*, vol. 45, no. 24, pp. 1212–1213, Nov. 2009.

[133] J. N. Laneman, D. N. C. Tse, and G. W. Wornell, "Cooperative diversity in wireless networks: Efficient protocols and outage behavior," *IEEE Trans. Inf. Theory*, vol. 50, no. 12, pp. 3062–3080, Dec. 2004.

[134] L. C. Tran and A. Mertins, "Error performance and energy efficiency analyses of fully cooperative OFDM communication in frequency selective fading," *IET Commun.*, vol. 10, no. 18, pp. 2525–2533, Dec. 2016.

[135] S. Ivanov, D. Botvich, and S. Balasubramaniam, "Cooperative wireless sensor environments supporting body area networks," *IEEE Trans. Consum. Electron.*, vol. 58, no. 2, pp. 284–292, May 2012.

[136] L. C. Tran *et al.*, "Comprehensive performance analysis of fully cooperative communication in WBANs," *IEEE Access*, vol. 4, pp. 8737–8756, Dec. 2016.

[137] Y. Chen *et al.*, "Cooperative communications in ultra-wideband wireless body area networks: Channel modeling and system diversity analysis," *IEEE J. Sel. Areas Commun.*, vol. 27, no. 1, pp. 5–16, Jan. 2009.

[138] H. T. Friis, "A note on a simple transmission formula," *Proc. IRE*, vol. 34, no. 5, pp. 254–256, May 1946.

[139] A. Boulis. (2017). Castalia: A simulator for wireless sensor networks and body area networks, [Online]. Available: `https://github.com/boulis/Castalia/`.

[140] R. D'Errico and L. Ouvry, "Time-variant BAN channel characterization," in *Proc. IEEE International Symposium on Personal, Indoor and Mobile Radio Communications (PIMRC)*, Sep. 2009, pp. 3000–3004.

[141] H. Feng *et al.*, "Prediction-based dynamic relay transmission scheme for wireless body area networks," in *Proc. IEEE International Symposium on Personal, Indoor and Mobile Radio Communications (PIMRC)*, Sep. 2013, pp. 2539–2544.

[142] H. W. Kuhn, "The Hungarian method for the assignment problem," *Nav. Res. Logist.*, vol. 2, no. 1-2, pp. 83–97, Mar. 1955.

[143] Texas Instuments. (2017). 2.4 GHz IEEE 802.15.4/zigbee-ready RF transceiver, [Online]. Available: `http://www.ti.com/lit/ds/symlink/cc2420.pdf`.

[144] D. B. Smith *et al.*, "Propagation models for body-area networks: A survey and new outlook," *IEEE Antennas Propag. Mag.*, vol. 55, no. 5, pp. 97–117, Oct. 2013.

[145] Q. Tang *et al.*, "Communication scheduling to minimize thermal effects of implanted biosensor networks in homogeneous tissue," *IEEE Trans. Biomed. Eng.*, vol. 52, no. 7, pp. 1285–1294, Jul. 2005.

[146] H. Zhang, F. Safaei, and L. C. Tran, "Autocorrelation based transmission power control in WBANs," *Accepted by 12th International Symposium on Medical Information and Communication Technology (ISMICT)*, 2017.

[147] C. Li *et al.*, "A hybrid lifetime extended directional approach for WBANs," *Sensors*, vol. 15, no. 11, pp. 28 005–28 030, Nov. 2015.

[148] O. Omeni *et al.*, "Energy efficient medium access protocol for wireless medical body area sensor networks," *IEEE Trans. Biomed. Circuits Syst.*, vol. 2, no. 4, pp. 251–259, Dec. 2008.

[149] J. K. Sundararajan *et al.*, "Network coding meets TCP," in *Proc. IEEE International Conference on Computer Communications (INFOCOM)*, Apr. 2009, pp. 280–288.